Investigation of Partial Discharge Occurrence and Detectability in High Voltage Power Cable Accessories

Jarot Setyawan

Student Number: 1389947

Delft University of Technology
Faculty of Electrical Engineering
High Voltage Technology and Management
November 2009

Investigation of Partial Discharge Occurrence and Detectability in High Voltage Power Cable Accessories

MSc Graduation thesis of

Jarot Setyawan

Student Number: 1389947

Thesis Committee:

Prof. dr. J.J. Smit

Dr. hab. ir. E. Gulski

Dr. ir. P. Bauer

MSc. Piotr Cichecki

Delft University of Technology
Faculty of Electrical Engineering
Electrical Power Engineering
High Voltage Technology and Management
November 2009

ACKNOWLEDGEMENT

I would like to express my sincere gratitude to all people and institution that have helped me for finishing this master thesis.

Foremost, I would like to gratitude my supervisor, Dr. hab. Ir. E. Gulski, for his excellent guidance during my research. His enthusiasm, continuous support and patience has motivated and helped me during the research and writing of this thesis. My sincere thanks also go to Piotr Cichecki for his advice, guidance and supervision during the project. He was always accessible and willing to help with all measurement problems and stimulating discussions.

Besides my supervisor, I would like to thank the rest of my thesis committee, Prof. J. J. Smit and Dr. ir. P. Bauer, for their availability to take place in the thesis committee. I would also like to thank Prysmian Cables and Systems B.V, especially Riccardo Bodega and Theo J.W.H. Hermans for their help and support in this project. Furthermore I would thank to P.V.M van Nes and B.J. Naagen for their help, ideas and supervision during the long hours measurement in the high-voltage laboratory.

My gratitude goes to PT PLN (Persero) for giving me the opportunity and financial support to study at TU Delft. Special thanks also go to Dr. P.H.F. Morshuis and Mrs. Anita Pharmatrisanti for their help during my study. Furthermore, thanks to all my colleagues in TU Delft, especially all my friends from PT PLN (Persero).

My special thanks go to my parents for their constant support and prayers throughout my life. Furthermore, I have no suitable words to describe my deepest gratefulness to my beautiful wife, Popi Puspitasari, as she is simply perfect with her unconditional love, great understanding, thoughtful support and persistent confidence in me, especially when I encountered difficulties. Finally, I want to express my deepest gratitude for my lovely daughter, Larasati Puspita Setyawan. Leaving her when she was three months old to take this master program was the hardest part of my study period. I owe her much more than two years of playing-time together; it is to her that I dedicated this work.

Jarot Setyawan

ABSTRACT

The use of XLPE insulation for high-voltage power cable is increasing worldwide. Consequently, the number of new installed high-voltage XLPE power cable is also increase in the power network. The new cable systems are installed in the field and inaccurate assembling of cable accessories could result in the presence of defects. The after-laying test is performed in the new cable system to check the quality of cable system installation.

One of the most important applications in the after-laying test is partial discharge measurement due to the characteristic of the XLPE insulation which is very sensitive to the PD activity. Therefore the after-laying test is important to certify a good start of the lifetime of the cable system.

The main problem in off-line PD detection as part of after-laying test is the complexity between PD detection methods, testing voltages and PD occurrence. For that reason, the investigation of the typical installation defects, their related effect and characteristic based on different PD detection methods and different voltage energizing are very important.

In this thesis, three artificial defects that represent different type of PD situation, surface discharge and electrode-bounded cavity, are created in the joint of full scale test set-up of 150 kV transmission power cable systems. Investigation is done by making simulation of electric field distribution profile in order to see the field enhancement due to the presence of defects and then applying a PD measurement by using different energizing and PD detection method to investigate the PD properties and detectability of each defect. In addition, several measurement issues that influence the HF/VHF/UHF un-conventional PD measurement are also investigated in this thesis to provide a better understanding and performance of un-conventional PD detection in after-laying test of HV cable system.

TABLE OF CONTENTS

CHAPTER 1

Introduction

1.1 High Voltage Power Cable Network

The primary purpose of the power system is to provide energy or electrical power from source (power plant) to the consumers in a safe and reliable way at the lowest possible cost. From Figure 1.1 it can be seen that high voltage (HV) transmission is one of the most important part of the system because it delivers almost all powers that generated by power plants. Electric power can be transmitted by overhead power lines or underground power cables.

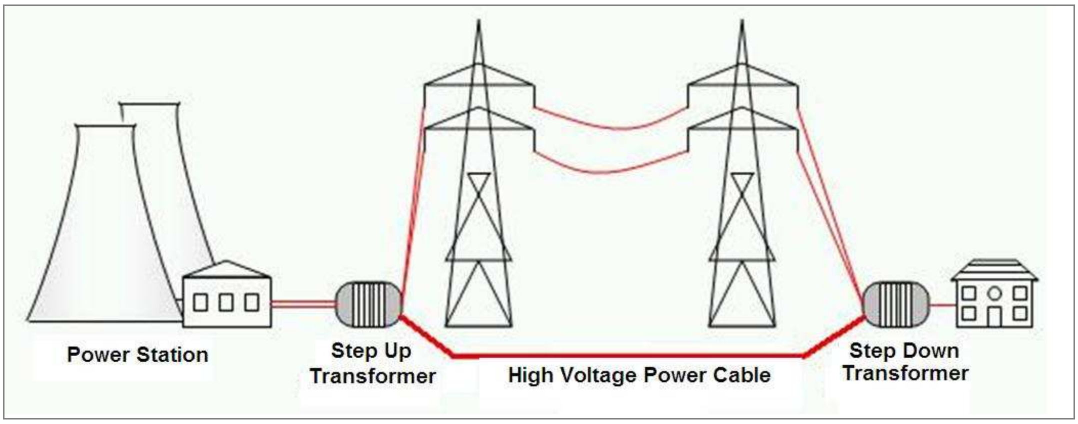

Figure 1.1: HV power cable in an electricity network

Power cable system basically consists of cables themselves and their accessories. Cable accessories consist of joint and termination. Joint is special connection component which used to join two cable ends together while termination is special component to provide the end of a cable. In figure 1.2, a simple representation of cable system is provided.

In recent days, the use of HV power cable is increasing due to its importance based on the following reasons [1]:

- Increasing of population of urban areas in industrialized countries is strongly related to the increasing of energy consumption. The only possibility to transfer the electric power in these areas is by using power cables.

- Power cables solve the environmental problems that are associated with overhead transmission lines.
- Parts of the existing power cable networks have reached the end of their lifetime and need to be replaced with the new ones.
- Many developing countries have changed their power system network to meet the increasing of demand by using power cables.

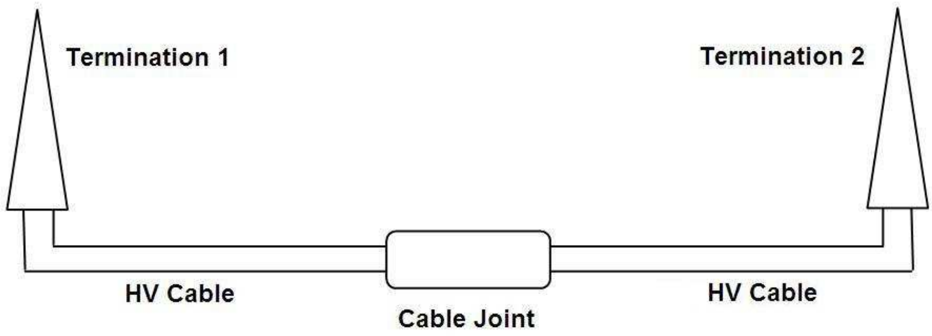

Figure 1.2: Simple representation of cable system

Starting from 1960s, cross-linked polyethylene (XLPE) polymer was used as insulation in high voltage power cables [1]. Nowadays, this type of HV power cables is increasingly applied in the field due to its advantages, e.g. low dielectric losses, suitable for high operating temperature, relatively easy and low cost in manufacturing, simple maintenance, elimination of impregnation and easier to install due its single layer of dielectric. Therefore, 150 kV XLPE power cable is used for the investigation in this thesis.

1.2 After-Laying Test for High Voltage Power Cables

As a consequence of its important function and increasing number of new installed HV power cables, minimizing the failure of HV power cables has become very important. To assure the reliable installation and operation of HV power cables, several quality assurance tests have to be applied start from manufacturing process and completed by after-laying test after installation of HV power cables. After-laying test is applied to check the presence of defects on cable accessories (joints and terminations) during on-site assembling process while the cable part itself can be considered as defect free after it passed the type and routine tests in the factory.

Accessories of HV cable systems are important parts of cable systems in relation to the failure due to the fact that the majority of faults that occur in cable systems are occurring locally in the joints and terminations. The fundamental aspect of after-laying test is to provide non-destructive test by applying a certain electrical stress to the installed cable system to detect defects in the accessories by using partial discharges (PD) measurements. In principle, the after-laying test is applied to verify the quality and reliability of cable system after installation process [2]. There are several factors that can produce defects during the installation of HV power cable:

- Damages that can be generated during transportation, storage and installation of HV cables after the complete factory tests have been applied.
- Imperfect assembling process of cable accessories in the field.

The impact of transportation and assembling process can only be investigated after installation process is complete. If defects are present in the cable accessories, it will generate situation which produce electric field enhancement in the area of the defects and PD activities can occur. PD also can produce insulation degradation that may lead to complete breakdown of the cable insulation. Therefore, PD detection together with after-laying test of HV cable system can be used as an indication of presence of the defects and evaluation the hazardous level of the defects.

1.3 Energizing and Partial Discharge Measurement Methods for After-Laying Test

Nowadays off-line PD measurement is commonly applied for after-laying test of HV cable system. It means that the cable system to be tested is disconnected from power network. Consequently, external voltage source is needed to energize the cable system and to ignite PD activities. Several types of external voltage sources which can be used for off-line PD measurement are [2]:

- Alternating current voltage (AC);
- Damped alternating current voltage (DAC);
- Very low frequency voltage (VLF); only for distribution cables.
- Direct current voltage (DC); only for paper-oil cables.

Application of DC and VLF voltage has several problems and limitations [2]. DC voltage does not represent AC electrical stress and not sensitive to AC insulation problems e.g. partial discharges. Furthermore, the use of DC voltage on polymeric insulation can produce space charge formation that will distort the normal field distribution. In comparison to AC voltage, application of VLF voltage on polymeric insulation shows different PD behaviors (PD inception voltage and PD magnitude). For several reasons mentioned above, AC voltage and damped AC voltage will be used for energizing method of HV cable circuit in this thesis.

Partial discharge detection method can be classified into two techniques: conventional and non-conventional. Conventional PD detection is a standardized method for PD measurement as described in IEC 60270. This method based on measurement of apparent charge displacement q in the leads of the sample. This charge is usually expressed in picocoulombs (pC). Non-conventional PD measurement is based on detection of high frequency PD pulses generated by PD activities. In this thesis, both PD detection methods will be used.

1.4 The Problem Definition

Imperfect installation of HV cable system in the field can generate different typical defects in cable accessories. The systematic description of these defects and its detectability based on different PD detection methods and different voltage energizing are very important. Basically in PD detection we have to deal with two basic aspects. First aspect is measurement process which determined by PD detection methods and testing voltages. The second one is PD physic which is related to PD occurrence. The main problem in off-line PD detection as part of after-laying test is the complexity between PD detection methods, testing voltages and PD occurrence. The systematic relation between these three factors will be investigated in this thesis. Figure 1.3 shows the scheme of PD detection and the external influence factors.

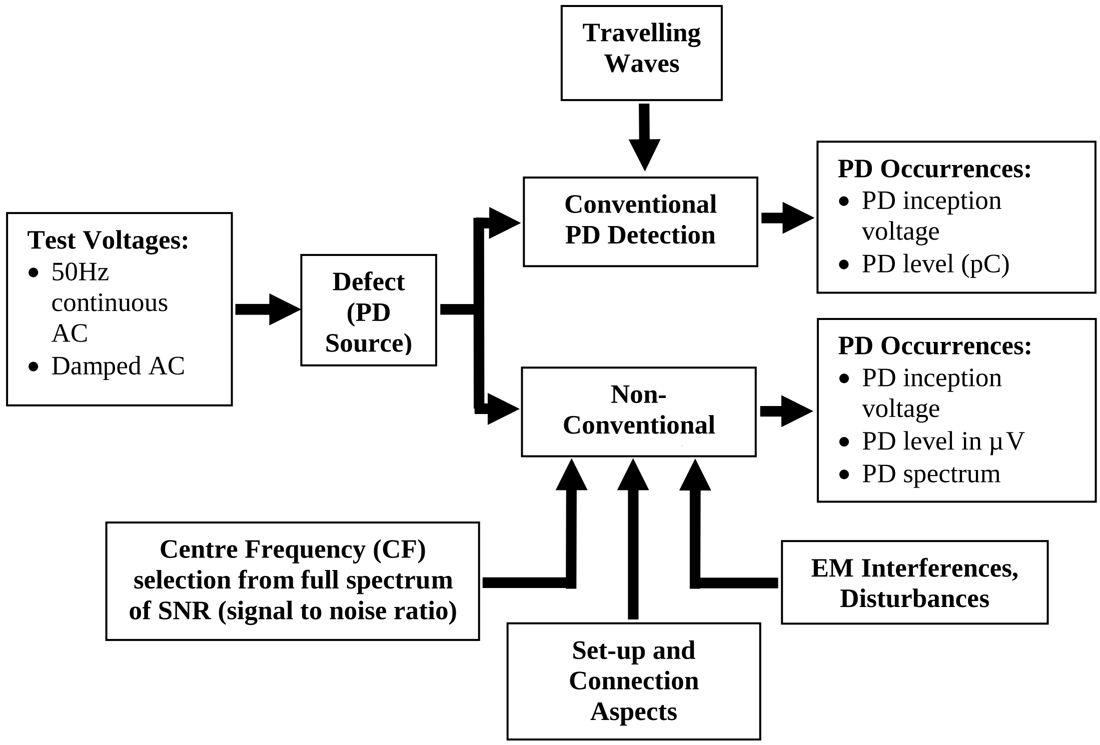

Figure 1.3: Scheme of PD detection and the external influence factors

1.5 Objective of Study

The main objective of this study is to investigate systematical relation between important factors of on-site PD detection for after-laying test of HV cable system. There are several steps have to be taken to fulfill this specified goal:

1. Inventory of about most typical defects that can occur during installation process of HV cable accessories and its electric field enhancement which can result in PD activities.
2. Preparation of full-size artificial models covering the electric field distribution profile and applicability for experimental investigation up to 150 kV will be applied to selected representative defect:
    a) Missing semi-conductive screen in the cable joint;
    b) Extra semi-conductive screen in the cable joint;
    c) Electrode-bounded cavity.

3. Definition of continuous and damped AC voltage sources and conventional and un-conventional PD detection methods.
4. Experimental investigation on (2). Using (3) observation of important parameters:
   a) Those are influence the PD measurement for both methods (conventional and un-conventional);
   b) Those are related to specifics of the PD defects.
5. Evaluation of set-up and connection aspects for the application of on-site PD detection for after-laying test of HV cable system by using un-conventional PD detection method.

1.6 Thesis Layout

This thesis is described in several chapters; Chapter 2 describes HV extruded cable system and its current standard for after-laying test of new installed cable system. Chapter 3 explains the PD occurrence and typical installation defects in extruded power cable system. Chapter 4 describes the experiment test set-up and measurement methods. Chapter 5 presents the results of field plotting simulation and PD measurements for artificial defect 1. Chapter 6 provides the results of field plotting simulation and PD measurements for artificial defect 2. Chapter 7 describes the results of field plotting simulation and PD measurements for artificial defect 3. Chapter 8 represents the investigation of several measurement issues for un-conventional PD measurement. Chapter 9 provides the conclusions of this study and recommendation for future research.

CHAPTER 2

High Voltage Extruded Cable Systems

At the present time, extruded insulation mainly XLPE (cross-linked polyethylene) insulation has mostly replaced the use of impregnated-paper as HV cable insulation due to several advantages of XLPE insulation as already mentioned in section 1.1. In principle, cable system consists of two main components, the cable part and the cable accessories. Single cable accessories are represented by two terminations and depending on the length no joint or one and more joints can be used. In this chapter the XLPE cable system and its related standard for after-laying test will be described.

2.1 Extruded High Voltage Power Cables

The extruded synthetic insulation can be in the form of polyethylene (PE), cross-linked polyethylene (XLPE) or ethylene propylene rubber (EPR). PE is an excellent insulator but it has limitation in operating temperature and thermal reserves in the case of short circuits [1]. EPR also perform as excellent insulator but EPR is limited to the voltage range up to about 150 kV due to its comparatively high dielectric losses [1]. The use XLPE is made by cross-linking the PE polymer chain to form cross-linked polyethylene and the temperature limit is increased. XLPE insulation is mostly used in newly installed extruded insulation high voltage cable in most countries due to its several advantages [1].

High voltage power cable has a common design, independent of its operating voltage and frequency. Basically it consists of the conductor, the insulation, the inner and outer semi-conductive screens, earthed metallic screen and protection sheath that form long concentric cylinder. Figure 2.1 shows a common design of high voltage XLPE cable.

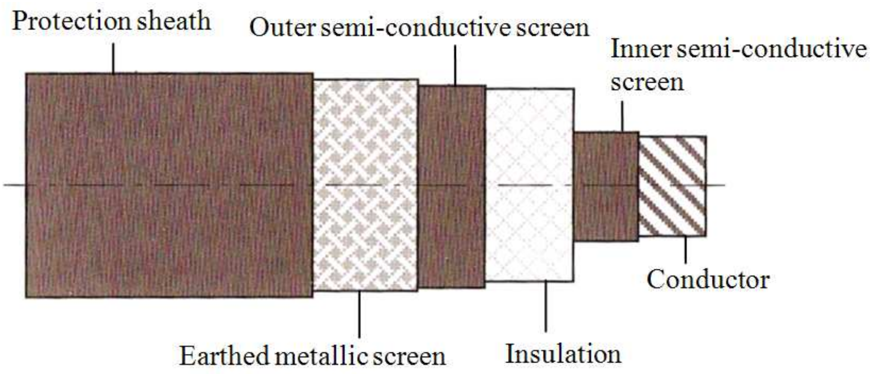

Figure 2.1: Common design elements of high voltage cable [1]

2.1.1 Conductor

The main task of conductor is to transfer the current with the lowest losses. This essential function will strongly determine the material selection and design of the conductor. The conductor also determines the mechanical tensile strength and bending ability of the cable [1]. There are two materials that can fulfil the requirements for conductor, copper (Cu) and aluminium (Al). The advantage of copper is it has approximately 60% lower specific resistance and consequently result in smaller cross section for a given current carrying capacity [1]. Aluminium has advantage in lower density, about three times lower than copper, lead to reduced weight about half for the same cable capacity [1]. The type of conductor used for the investigation in this thesis project is round-massive aluminium.

2.1.2 Insulation layer

Insulation layers are used over the conductor. The insulation is critical part in cable structure due its task to withstand a long term electrical stress during the service life of the cable. When the voltage is applied to the cable, the insulation layer will experience electrical stress according to equation 2.1 [3].

$$E(x) = U/[x.ln(R/r)] \tag{2.1}$$

Where U is the operating voltage, R and r are the external and internal radius of insulation and x is the radius of the insulation where the electrical stress is determined by the equation above.

The use of extruded synthetic insulation in single layer construction is increasing due to its advantages in relatively easy processing and handling of this insulation. This insulation can be selected to have 10% lower dielectric losses than cellulosic paper, higher intrinsic breakdown strength four times as high as impregnated paper insulation [4]. The disadvantage is that a single defect can produce large influence on the whole insulation due to its homogeneity of this type of insulation [4].

2.1.3 Semi-conductive screen

This component also known as field smoothing or field limiting layers. In principle, these layers have two functions [1]:

- Elimination of field concentration from non-homogeneous area that result in electrical stress in cable insulation by providing smooth and homogeneous boundary surface with the insulation.
- Prevention of gaps or voids occurrence that can lead to the interface between conductor-insulation and insulation-earth wires due to mechanical and thermal stress, especially in polymer-insulated cables which have no impregnating medium.

The first function can be fulfilled by using semi-conductive materials that compatible with the insulation and provide smooth and homogeneous interface with the insulation. The second function of semi-conductive screen is provided by using materials that have thermal expansion as close as possible to the insulation material that is used [1]. In the case of XLPE cable, the perfect bond between this semi-conductive layer and the insulation is very important due to the absence of self-healing effect as given for example in multi-layer construction of paper-impregnated insulation in the case of partial discharge occurrence.

2.1.4 Earthed metallic screen

This grounded metallic screen has a function as an electrical shielding for the cable in order to produce free electric field in the surrounding of cable. Moreover, this component has some other following functions [1]:

- Provide a return path for capacitive charging current under operating condition
- Conduction of the earth fault current until the system is switched off
- Protection against accidental contact
- Mechanical protection of insulation while the cable is bending.

2.1.5 Protection sheath

This component has a function to protect the cable from possibility of mechanical damage and corrosion caused by the water. High-density polyethylene (HDPE) is commonly used as a material for this protection sheath because it provides good mechanical protection and excellent resistance to abrasion with low moisture penetration [1].

2.2 High Voltage Cable Accessories

Accessories of HV cable system consist of terminations and joints, also called splices. The function of termination is as an interface between the ends of cable system to other electrical systems while joint is required to connect two or more cable sections with limited length into longer sections of cable. The limitation of individual length of cable section is related to the problem of transportation. Cable drums cannot exceed a specified maximum dimensions to be well transported from cable manufacturer to the site which for XLPE HV class cable it is mostly up to 1 km [1]. Joint can be considered as two terminations connected back-to-back and termination can be regarded as half of a joint [5]. For HV cable systems, these cable accessories are critical components for several reasons [1]:

- The electrical field distribution will completely different than the normal cylindrical electric field distribution in the cable;
- The presence of interface between the cable insulation and the accessories insulation;
- The accessories need to be installed on site where many external factors can influence the installation process.

Without the presence of defects, disruption of the normal radial field distribution in the cable still occurs due to change in the cable geometry in cable accessories. The outer semi-conductive screen is removed to provide a sufficient distance between the conductor and screen to reduce the electrical stress at the cable edge [5]. However, this method results in another electrical stress at the end of semi-conductive screen. Consequently, cable accessories always equipped with field control to manage the electrical stress not being higher than permissible limit for the insulation at all points. The condition of field enhancement in cable end without the presence of field control is shown in figure 2.2.

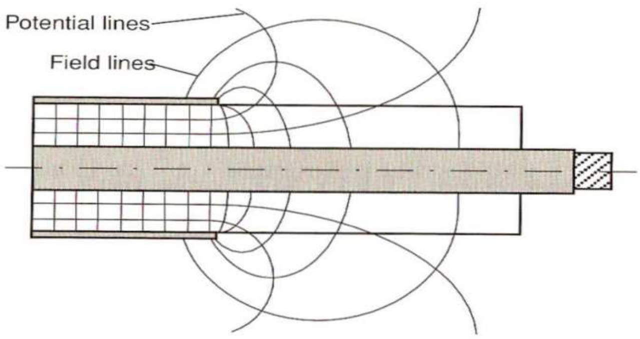

Figure 2.2: Field enhancements in the cable end without field control [1]

Stress cone, which is composed from two components, a control deflector and an elastic insulator, is used both for joint and termination to control the field at the cable end. Additionally, in joint there is another field control in the form of special shape of high voltage electrode in the conductor connection.

The principle of stress cone in accessories is based on the theory of electrode grading. This electrode grading is achieved by lengthening the outer semi-conductive layer and result in gradually reduced of the field concentration [3]. Figure 2.3 shows that the concentration of equipotential lines which result in field concentration is reduced by using the electrode grading. E.g. in click-fit joint, the high voltage electrode is shaped in such way that the field between the high voltage and earth electrodes is gradually cross the interface between two insulations in the joint. Figure 2.4 shows this field grading effect.

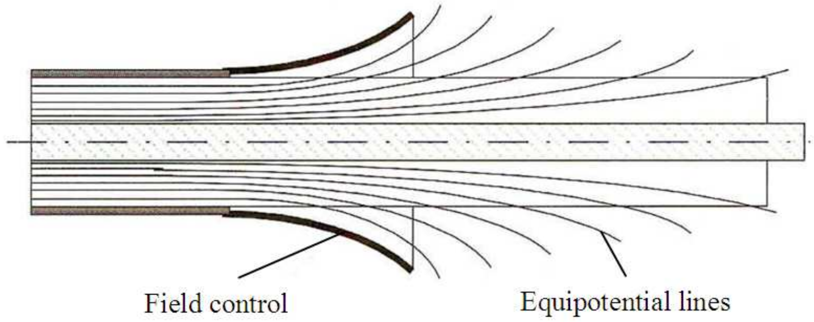

Figure 2.3: Equipotential lines situation in the cable end using field control [1]

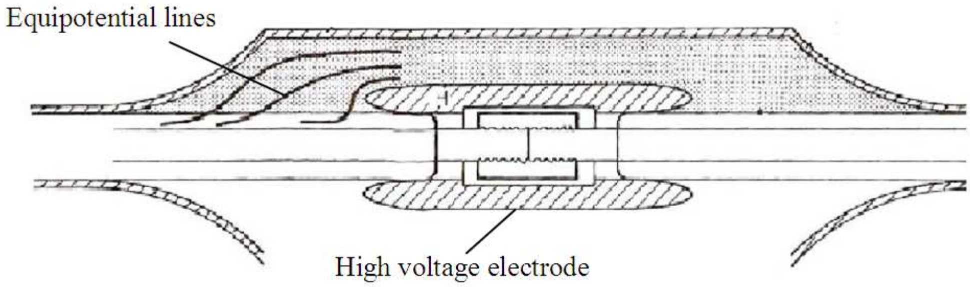

Figure 2.4: Field grading in cable joint [3]

2.3 Current Standards for After-Laying Test of XLPE Cable System

The term *testing* as defined in the international standards means a visual or measured comparison of specified parameters or requirements with the actual value of a product [1]. After-laying test represents the final test before operation of the new installed cable system. The main purpose of this test is to detect the presence of defects that can be generated during transportation, assembling and installation of cable accessories on site.

Regarding the after-laying test of XLPE power cables, there are two international standards for a guideline of the test which consist of:

- IEC 60840; Power cables with extruded insulation and their accessories for rated voltages above 30 kV (U_m = 36 kV) up to 150 kV (U_m = 170 kV) Test methods and requirements.
- IEC 62067; Power cables with extruded insulation and their accessories for rated voltages above 150 kV (U_m = 170 kV) up to 500 kV (U_m = 550 kV) - Test methods and requirements.

Determining the level of test voltage and its duration in after-laying test is important factor otherwise there will be overstress on the cable system. Based on Cigré Investigation about the test effectiveness performed by WG21-09 in 1987/1988, the cable system start from 50 kV to 150 kV should be tested on-site at least with the voltage level $2.5U_0$ for 15 minutes [6]. The after-laying test will be called successful if the new installed cable system survives during high voltage application without any breakdown in the cable part and cable accessories. The practical guidelines for this testing will be adjusted depend on previous Cigré Investigation, the experience and regional conditions. Table 2.1 shows standards of after installation testing in several countries.

Table 2.1

Current Practice for After-Laying Testing [6]

Country	**Voltage**	**Times (minutes)**
The Netherlands	$2.5U_0$	10
Germany	$2.5U_0$	30
Belgium	$2.0U_0$	15 – 30
South Africa	$1.7U_0$	
Switzerland	$1.7U_0$ - $2.5U_0$	
United Kingdom	$1.7U_0$ - $2.0U_0$ $2.5U_0$	60 10

Furthermore, in 1997, Cigré published its official recommendation regarding the after-laying test, which is for 60-110 kV circuit is $2U_0$ in 60 min and for 130-150 kV circuits $1.7U_0$ in 60 min [7].

Although the cable system is assembled from PD-tested components, there is still opportunity of creating defects due to improper assembling process on-site. These defects mostly result in field enhancement in cable accessories. The detection, localization and recognition of these defects are very important in order to avoid future failure in cable system. These function cannot be fulfilled by using withstand voltage testing only. Furthermore, there is a contrary between the importance of getting sufficient confidence about the proper installation of cable system and the reduction of testing voltage level due to avoid overstressing in cable system. The extension of after-laying test with PD measurement could be the solution for these problems.

PD measurement has been accepted as an effective method for identifying and localization of defects in sensitive, accurate and non-destructive technique for extruded high voltage cables and their accessories [8]. Therefore, it would be very reasonable to combine withstand test with diagnostic measurement in the form of PD testing after on-site installation of HV cable in order to detect any problems that can be generated during transportation, laying and assembling of accessories. At this moment, PD measurements are not mentioned in the after-laying test standards of HV cable. There are two recommendations for PD detection in power cable systems which consist of:

- IEEE Std 400.3™-2006; Guide for Partial Discharge Testing of Shielded Power Cable Systems in a Field Environment;
- CIGRÉ Technical Brochure No.182; Partial Discharge Detection in installed HV extruded cable systems; CIGRÉ WG 21.16, April 2001.

Regarding the PD measurement which in principle can be divided into two methods, conventional and un-conventional PD detection, the standardization is only related to the conventional PD detection. Therefore, investigation about typical defects in HV cable installation and their characteristic and detectable with PD measurement for both methods, conventional and un-conventional, will become very important.

2.4 Conclusion

1. Cable accessories represent critical parts in cable system. On-site assembling of cable accessories may generate defects and these defects mostly result in field enhancement and generate PD activities.
2. The detection and recognition of these defects in after-laying test of HV cable system, with non-destructive cable test system is very important to prevent future failure during cable system operation.
3. Extension of current after-laying test standard with PD measurement which has been accepted as an effective method for identifying and localization of defects in sensitive, accurate and non-destructive technique for extruded high voltage cables and their accessories can be a solution for this problem.

CHAPTER 3

Partial Discharges and Typical Installation Defects for Extruded High Voltage Power Cable Systems

The term *partial discharge* as defined in the IEC 60270 standard means a localized electrical discharge that only partially bridges the insulation between conductors and which may or may not occur adjacent to a conductor. Improper assembling of cable accessories on-site can produce defects that result in PD activities. Therefore, the understanding and detection of these defects by means of PD measurement will be very important to prevent a failure in cable system operation.

3.1 Partial Discharges in High Voltage Cable System

3.1.1 Partial Discharge Occurrence

Partial discharge occurs from electrical breakdown of defect in the insulation medium or in the surface of insulation medium when the applied electric field is higher than a dielectric strength of insulation medium. PD occurs in insulation system of HV cable due to in-homogeneity of electric field distribution as a result of the presence of the defects. The power cable with extruded insulation is very sensitive to the presence of PD due to the absence of liquid impregnating medium that can extinguish any partial discharges and the barrier effect from multi-layer insulation system in paper-oil power cable. Consequently, the newly-installed extruded insulation power cable needs a completely free from PD which is verified by means of after-laying test.

In principle, there are three types of PD-related failure that can occur in power cable system. These partial discharges can be classified depend on the origin or location that result in field enhancement situation and produce partial discharge activities in cable systems. These types of PD are:

- Discharge result from internal cavity in the insulation media.
- Surface discharge along interfaces.
- Discharge in the form of electrical treeing in insulation.

Figure 3.1 shows the three types of condition in power cable system that can result in discharge activities.

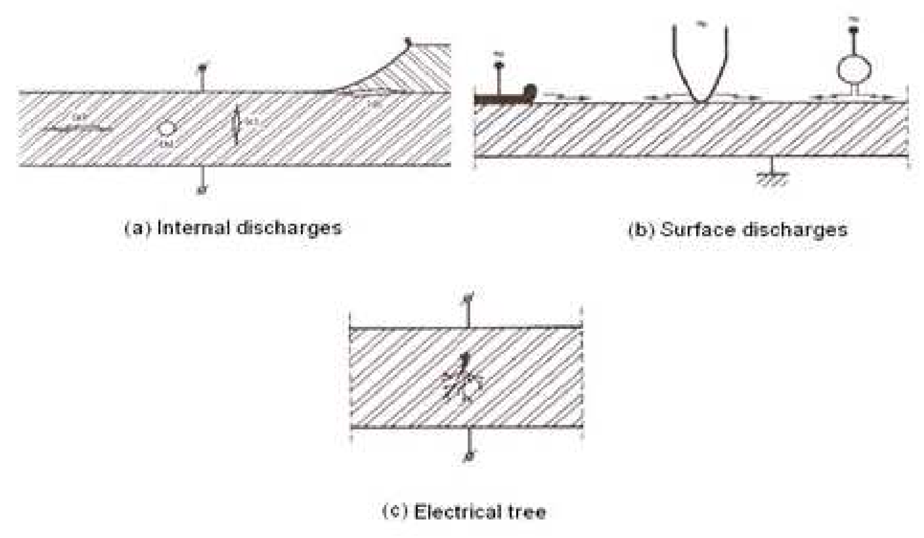

Figure 3.1: Types of PD-related failure that can occur in power cable system [9].

a. Internal cavity

Internal cavity frequently occurs in the form of spherical or elliptical gas-filled cavity. If the voltage is applied to the insulation system, the electric field in the cavity will be higher than the surrounding insulation medium due to the lower dielectric constant of the gas inside the cavity than the dielectric constant of the insulation medium. The shape and location of the cavity will also determine the electric field enhancement in the cavity. If the cavity is perpendicular to the field directions, the field enhancement in the cavity will be ε times the normal electric field in the dielectric, where ε is the permittivity of the insulation material. There are several typical possibilities for the type of this cavity as depicted in Figure 3.2. A flat cavity (the length of cavity is higher than its height) consists of dielectric-bounded cavity and electrode-bounded cavity. Dielectric-bounded cavity represents a cavity which has two dielectric walls as shown in Figure 3.2 (a), while electrode-bounded cavity represents a cavity that has one dielectric and one electrode wall as shown in Figure 3.2 (b). The electrode-bounded cavity can present in the area between insulation and semi-conductive screen often in the form of flat cavity (the length of cavity is higher than its height). This cavity is situated in a tangential field direction and also produces substantial field concentrations after breakdown occurs. When the cavity is spherical as shown in

Figure 3.2 (c), the electric field will enhance to $3\varepsilon/(1+2\varepsilon)$ times the normal field and will become 1.5 times if the ε is high. If the cavity is narrow and parallel to electric field direction as shown in Figure 3.2 (d), the stress in cavity tends to be equal with electric field in dielectric; however this cavity represents a more critical case because it bridges a larger part of the insulation [3] and produces substantial field concentrations after breakdown occurs.

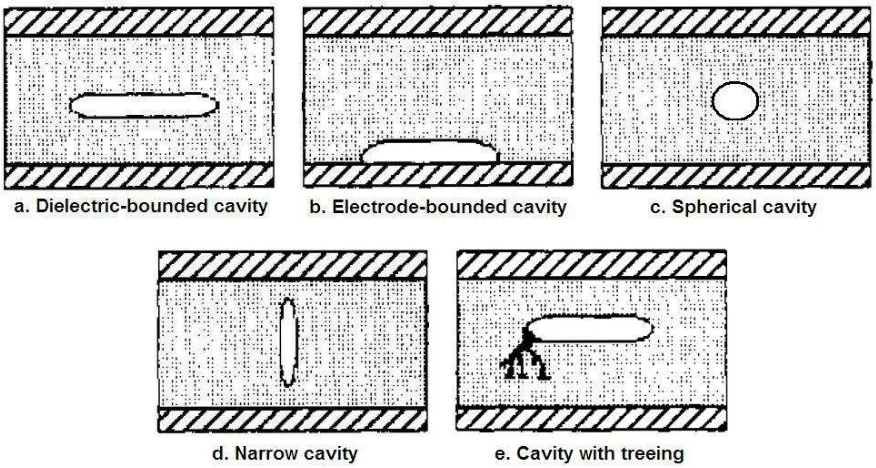

Figure 3.2: Typical case of cavities in insulation material [10].

The gas inside the cavity will breakdown when the field enhancement is higher than the breakdown strength of the gas in the cavity, and discharge will occur in cavity. The breakdown strength of the gas inside the cavity can be derived from the Paschen curve as shown in Figure 3.3. According to this curve, the breakdown strength is determined by the size of cavity, the type and pressure of the gas inside the cavity. The presence of cavity in insulation can result in complete breakdown of the material due to degradation of material which depends on field strength, type of insulation material and PD magnitude [10]. This degradation process starts with the erosion of the wall of cavity then followed by pit formation at the edge of cavity and results in high electric field enhancement. If the field exceeds the breakdown strength of material then the breakdown of the material in the edge area of the cavity will occur which lead to the start of the electrical treeing as shown in Figure 3.2 (e).

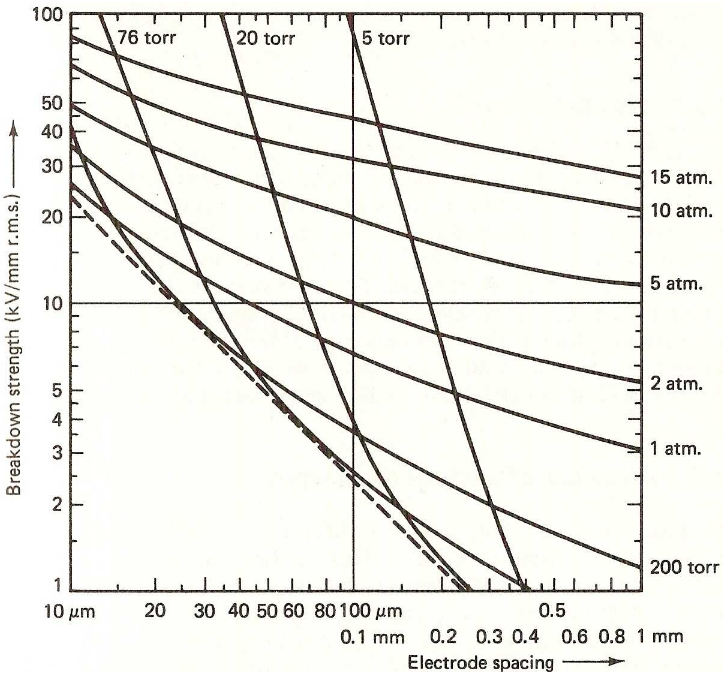

Figure 3.3: Breakdown strength of air inside the cavity as a function of electrode distance and air pressure [9].

b. Surface discharge

Surface discharge occurs in the interface of two insulation materials where substantial high tangential field strength is present. Surface discharge can be initiated when there is a high enough of stress component in parallel with the insulation surface to cause discharges [9]. Surface discharges are often occurred in cable accessories due to missing outer semi-conductive screen or incompletely removed of outer semi-conductive screen in the area after the stress cone. The surface discharges will occur as a result in field enhancement in the edge of the semi-conductive screen. The inception voltage of this type of discharge for the edge of plane-plane configuration is relatively low; depend on the thickness and permittivity of insulation material and also the sharpness of the electrode edge [9].

c. Electrical tree discharge

Electrical treeing in extruded dielectric cable insulation represents a tree-like path of electrical deterioration through the dielectric body. The radial growth of treeing is in line with the electric field lines and when it bridges the electrodes the complete breakdown in the insulation will occurs. Even though extruded insulation has intrinsic electrical strength many times higher than electrical stresses that probably occur in actual operation, the electrical treeing can occurs in much lower stress than intrinsic strength of insulation material. The reason is the presence of the defects in the insulation material that result in electric field enhancement and produce PD in the form of electrical trees. Treeing can be initiated from sharp point in the electrodes or by erosion of the edge of internal cavity in the insulation [10]. Electrical trees can also result from the conversion of water trees. The cable accessories which exposed to high moisture condition are susceptible for moisture penetration that can result in generation and development of water trees. Water trees result in local stress enhancement that can be converted to initiation of electrical trees. The electrical tree discharges form a special case of internal discharge due to its characteristic that very unstable and the trees may grow rapidly [9] and usually consists of many branches. Electrical tree normally produce higher PD magnitude than in the case of PD from cavity [11]. Furthermore, once this electrical tree has been initiated, the fast complete breakdown of cable insulation may occur.

3.1.2 Partial Discharge Recurrence Pulses

The understanding of PD process is important for the detection and measurement of the PD pulses created by PD activities. For describing the PD process, a well-known a-b-c circuit is used. This electrical model can be used to describe the PD recurrence process of three types of PD which mentioned in section 3.1.1. The a-b-c circuit is shown in Figure 3.4. The capacitance *c* represents the capacitance of the defect. The capacitance of the dielectric in series with the defect is represented by capacitance *b* and the sound part of the dielectric is represented by capacitance *a*.

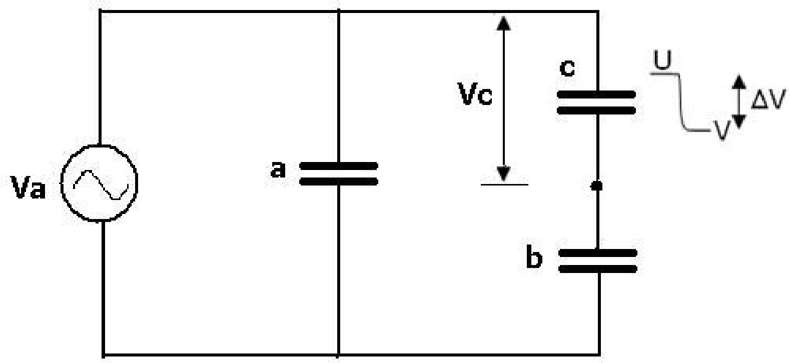

Figure 3.4: The a-b-c equivalent circuit for describing PD recurrence process [9]

The recurrence process of PD pulses is shown in Figure 3.5. The high voltage applied to the insulation system is v_a and the voltage across the defect is v_c. A discharge will occurs in the defect when the voltage v_c reaches the breakdown voltage U^+, the voltage v_c then drops to V^+ and the current impulse i is produced. The voltage drop ΔV takes place in extremely short time compared to the duration of 50 Hz sine wave so this can be regarded as a step function [9].

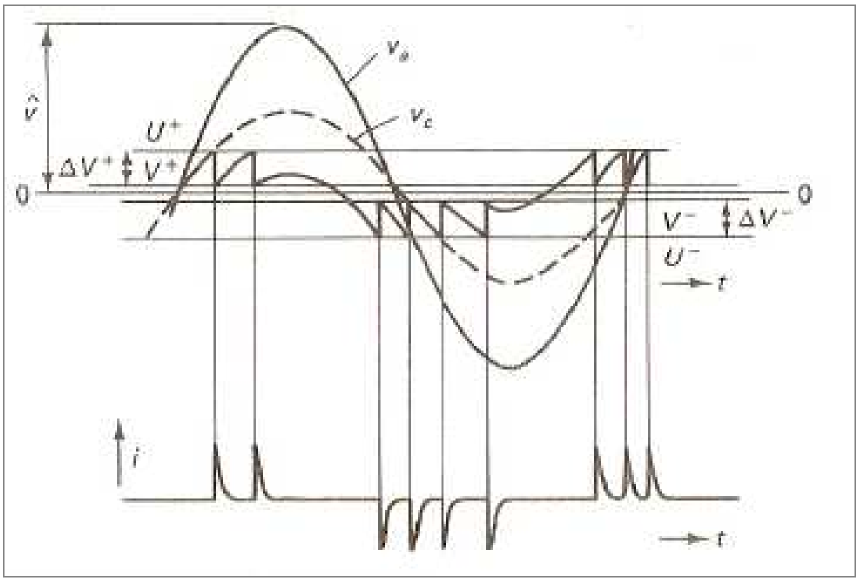

Figure 3.5: The principle of PD pulses occurrence for a-b-c circuit [9]

After the discharge has occurred, the voltage v_c increases again and when this voltage reaches U^+ a new discharge will occur. This process will happen several times until the voltage v_a decreases and the voltage v_c reaches U^- and a new discharge occurs. It can be seen that recurrence discharges and current impulses will occur when the AC voltage is applied to the dielectric system which contain of defect.

The charge q_1, which is transferred in defect c when the PD occurs, will be equal to:

$$q_1 \cong (b + c)\Delta V \tag{3.1}$$

The degradation of the dielectric due to PD activity is certainly related to this charge. However, this charge quantity cannot be measured with discharge detector in practical situation. The value that can be measured is the charge displacement q in the leads to the sample; this charge quantity is expressed in picocoulombs (pC) and equal to:

$$q = b\Delta V \tag{3.2}$$

This charge displacement is related to the discharge in the defect, however this quantity is not directly represent the charge transfer in the defect. There are several reasons that make the charge displacement quantity q are reasonable for the PD measurements [12]:

- The discharge magnitude q is proportional to the energy dissipation in the partial discharge.
- The discharge magnitude q is proportional to the size of the defect.
- This transfer of charge q can be measured by electrical PD detector.
- The order of discharge magnitude q in powers of ten can be used to determine the harmfulness of discharge.

The collapse time of voltage pulse caused by the discharge process is determined by the type of defects that produce PD pulses. For internal cavity, the voltage pulses collapse in a time of at most few nanoseconds, consequently the resulting voltage pulses that travel in both directions from the PD source will have pulse width in nanoseconds region. For surface discharge, the voltage pulse from the PD source will have pulse width in some tens nanoseconds, therefore resulting pulses from PD process will have corresponding frequency up to few hundreds of MHz or 1 GHz [13]. Furthermore, this high frequency component of PD pulses will attenuate due to losses in semiconducting shields in XPLE power cable. As a result of this attenuation, the magnitude of PD pulses will decrease and their width will increase as a function of propagation distance [13].

3.2 Typical Installation Defects in HV Power Cable System

The presence of defects in cable system represents weak points in cable system operation. In the case of newly installed HV cable system, all cable parts are considered as PD-free components as they have passed the type and routine test in the cable factory. However, there is still a risk of the presence of defects in the newly installed HV cable system. These defects can be a result of improper on-site assembling (poor workmanship) process of the cable accessories or hidden defects in the design of cable accessory [14]. The human influences and on-site external environmental factors in assembling of the cable accessories also increase the risk of the presence of the defects. Once the defects have created, there will be a possibility of the breakdown in the mid-long term operation of the cable system due to the non-homogeneities in electric field distribution. The resulting risk for the short-long term behaviour of the insulation system is depend on the type, form, size and location of the defect. Therefore understanding of these typical installation defects and their related effects in newly installed HV cable system is very important. There are several typical defects of HV cable system that can occur due to the on-site installation of HV cable system which consist of:

- Sharp point or protrusion.
- Missing semi-conductive screen.
- Remaining semi-conductive screen in the cable joint.
- Conductive particle on the insulation material.
- Improper positioning of cable accessory.

3.2.1 Sharp Points or Protrusions

The sharp point or protrusion in insulation system always results in concentration of field lines in the tip of the sharp point/protrusion and result in high local electric field enhancement in that area. The presence of metallic protrusion in polymeric accessories may produce an intrinsic breakdown of a small part of the insulation [14]. The electric field enhancement caused by the protrusion is strongly determined by the shape of the protrusion, in the form of ratio of height (h) to width (b) as shown in Figure 3.6.

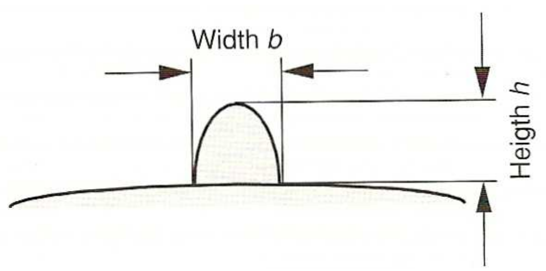

Figure 3.6: Idealized semi-elliptical protrusion [1]

The greater the ratio h/b, there will be higher electric field enhancement. The situation is relatively uncritical when $h/b \leq 1$ due to less magnification of electric field [1]. The presence of protrusions on the semi-conductive screen as shown in Figure 3.7 is of the most critical case due to unfavourable situation where they are pointed and in the radial direction [1]. This situation can lead to theoretically infinite electric field enhancement. The cable dielectric in the area of the greatest electric field enhancement will be electrically overstressed and degradation process of insulation starts. As a result from this, the insulation material is locally separated and forms a hollow channel [1]. Furthermore gas discharges occur in this channel and result in further erosion of insulation material due to the growth of the channel. Consequently internal partial discharge caused by this type of defect usually lead to complete breakdown in the insulation, with a process known as erosion breakdown [1].

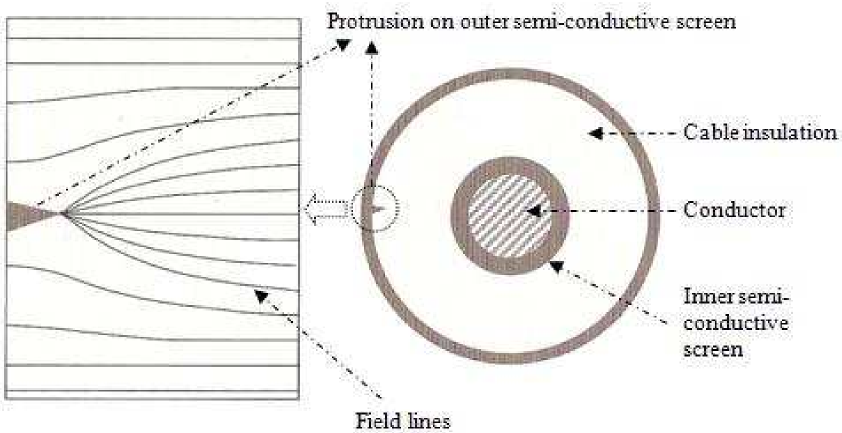

Figure 3.7: Semi-conductive screen protrusion that results in stress concentration at the tip of the protrusion.

3.2.2 Missing Semi-conductive Screen

The presence of missing outer semi-conductive screen in cable accessory will result in an electric field enhancement that occurs in the edge of removed semi-conductive screen. This situation causes surface discharge that takes place at the edge of outer semi-conductive screen over the XLPE insulation surface. The missing semi-conductive screen which occurs in the area close to the cable joint can be seen in Figure 3.8.

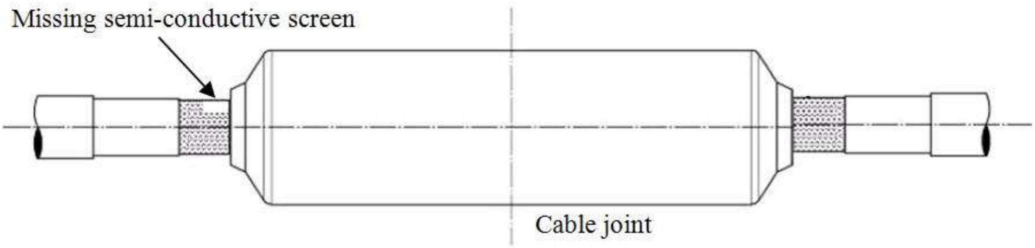

Figure 3.8: Missing semi-conductive screen in the cable joint

The surface discharge at the interface between air and XLPE insulation can cause a degradation process in the XLPE insulation. This degradation process is related to the chemical changes of the polymeric surface that result in the formation of crystals on the surface of the polymer insulation [14]. Field intensification will occurs at the cluster of crystals and result in increasing of PD activities. After long time treeing process will start and result in erosion of the surface of insulation material.

3.2.3 Remaining Semi-conductive Screen in the Cable Joint

As already described in the section 2.2 the cable accessories always equipped with the control deflector to avoid field concentration in the end of power cable. This control deflector represents the extension of the outer semi-conductive screen at the cable end. For this purpose, the outer semi-conductive screen on the cable end has to be peeled for the connection between the end of outer semi-conductive screen of the cable and the control deflector in the cable accessories. Improper peeling process can result in the remaining semi-conductive screen which is placed on the interface between cable insulation and accessory insulation. This interface represents the weak spot in accessories construction where the tangential field on that interface must be kept as low as possible [3]. This situation is shown in Figure 3.9.

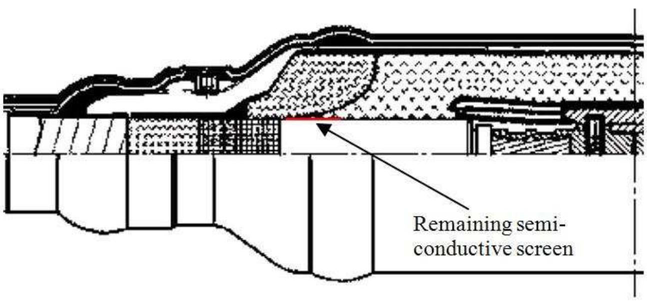

Figure 3.9: The remaining semi-conductive screen on the boundary between cable insulation and joint insulation

This unnecessary extension of the semi-conductive screen in the cable accessory will produce electric field enhancement in the edge of the semi-conductive screen that can result in PD activity at the boundaries between cable insulation and accessory insulation. Furthermore, the deterioration process of the cable insulation and accessory insulation will occur.

3.2.4 Conductive Particles on The Insulation Material

The on-site installation process of cable accessory can result in the presence of contamination of impurities on the surface of insulation material in the cable accessories. These contaminations are usually in the form of conductive particles [14]. These conductive particles can be metal, moisture or semi-conductive impurities and these unwanted particles are present on the interface between cable insulation and accessories insulation. The AC surface discharge is strongly influenced by the condition of the dielectric surface [15], therefore the presence of conductive particles that decreases the resistivity of the insulation surface is very detrimental which is related to the surface discharge degradation process along the interface of the cable insulation.

3.2.5 Improper Positioning of Cable Accessory

As described in section 3.2.3, the outer semi-conductive screen on the cable end must be removed for a certain length for the installation of accessory on XLPE cables as shown in Figure 3.10. For optimal field distribution in the cable accessory the positioning of the cable accessory and the cable end must be accurate that result in proper connection between the end of outer semi-conductive screen and the control deflector in the cable accessory. Improper positioning of the cable accessory will result in field enhancement at the end of outer semi-conductive screen of the cable end.

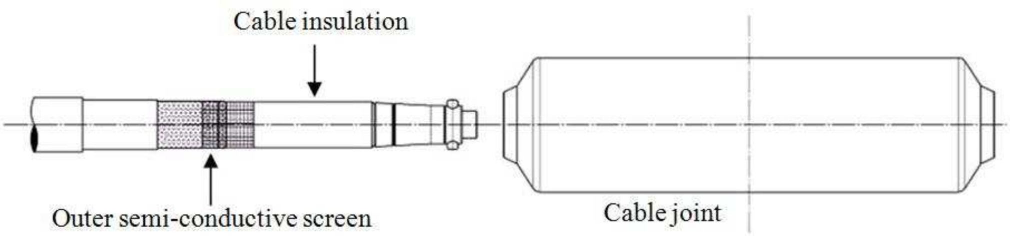

Figure 3.10: Cable end preparation with removed outer semi-conductive screen

There are two possibilities of this improper positioning of cable accessory. The first defect condition occurs if the outer semi-conductive screen is removed too far that results in a gap between the end of outer semi-conductive screen and the control deflector. The field concentration at the end of outer semi-conductive screen will cause surface discharges on the surface of the cable insulation. The second defect will occur if the removal of outer semi-conductive screen is not long enough which result in extra outer semi-conductive screen below the control deflector. Similar to the first condition, the field enhancement and surface discharges can occur in the edge of semi-conductive screen which placed on the boundary between cable insulation and accessory insulation. Consequently, the insulation degradation of cable and accessory can occur due to surface discharge activities.

3.3 Artificial Defects for the Investigation

For the investigation purpose there are three artificial defects which applied in the cable joint. These defects are the missing of outer semi-conductive screen, extra semi-conductive screen in the joint and the electrode-bounded cavity. These three artificial defects represent the different case of PD occurrences. The first and second artificial defect represents the surface discharge along the interface of insulation material. This type of PD can result in failure of cable system even if the extruded insulation is totally immune to PD-induced electrical tree initiation [13]. The third artificial defect represents the case of electrode-bounded cavity between the outer semi-conductive screen and the cable insulation. Investigation is done by modelling the defect by Ansoft field plotting program to get an electric field behaviour in the cable system due to the presence of defect and then applying two different AC voltages to energize the test set-up which consist of these three defects in order to generate PD activities and then two PD detection methods are used for the measurement.

3.3.1 Missing Semi-Conductive Screen in the Cable Joint

This artificial defect is created by removing the outer semi-conductive screen of the cable in the small area before entering the joint. Figure 3.11 shows a cable cross-section with an artificial defect which is placed on the area close to the cable joint.

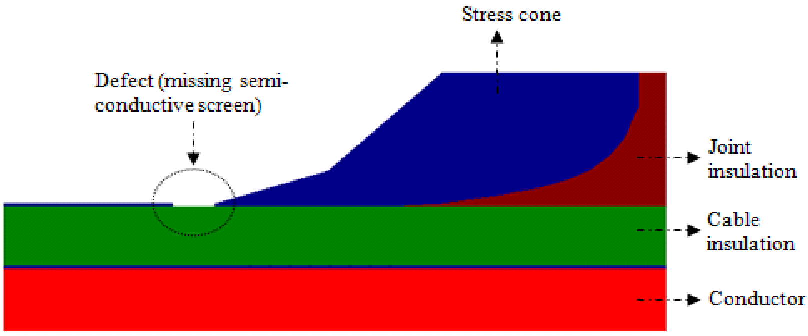

Figure 3.11: Schematic drawing for missing outer semi-conductive screen

This artificial defect represents the case of surface discharge. As described in section 3.2.2, this type of defect will produce electric field enhancement in the edge of semi-conductive screen and result in surface discharges on the surface of cable insulation. The effect of different sizes of the defect as shown in Figure 3.12 is investigated by using Ansoft field plotting simulation program and then different PD measurement methods are applied to the test set-up to investigate the PD behaviour of this type of defect.

Figure 3.12: Three sizes of missing semi-conductive screen on cable joint

3.3.2 Extra Semi-conductive Screen in the Cable Joint

The second artificial defect for the investigation is extra semi-conductive screen in the cable joint that represent the case of improper positioning of cable joint. This defect can result from the miscalculation in the length of removed semi-conductive screen in the cable end preparation for cable joint as depicted in Figure 3.13. This defect is made by lengthening the end of semi-conductive screen in the cable end by painting with the semi-conductive varnish. Figure 3.14 shows a schematic drawing of cable cross-section which consists of the artificial defect.

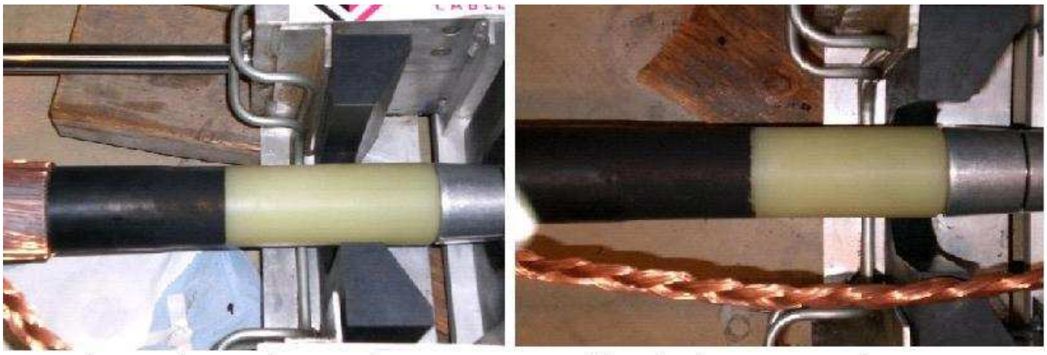

Figure 3.13: Extra semi-conductive screen in cable joint

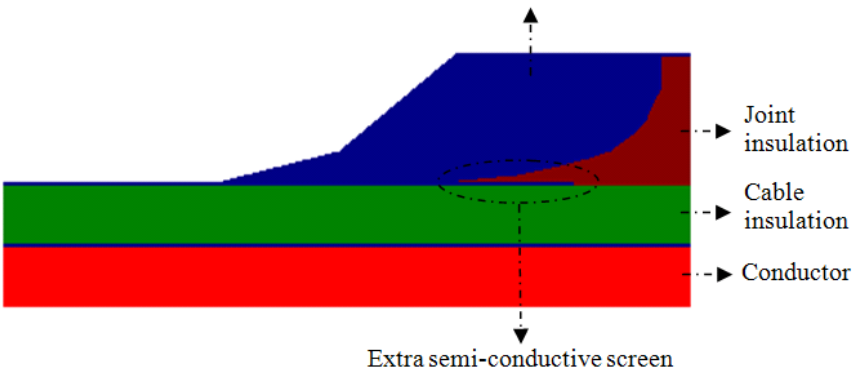

Figure 3.14: Schematic drawing for extra semi-conductive screen in cable joint

This extra semi-conductive screen is situated on the boundary between the cable insulation and the accessory insulation. Similar to the first defect, the electric field enhancement occurs at the end of the extra semi-conductive screen and probably results in the PD activity on the boundary of the insulation. Field plotting simulation is applied to see the effect of different size of the defect in the electric field enhancement and two PD measurement methods on the critical size of defect are applied to investigate the PD occurrence for this artificial defect.

3.3.3 Electrode-bounded Cavity between Cable Insulation and Outer Semi-conductive Screen

The last artificial defect for the investigation is electrode-bounded cavity between the cable insulation and outer semi-conductive screen. This defect may occur due to poor contact between cable insulation and semi-conductive screen. The process of creating this artificial defect is shown in Figure 3.13. The process starts by removing small part of outer semi-conductive screen on the area close to the cable joint and then making a small scratch on that area and finally covering the area with copper tape. Figure 3.14 shows a schematic drawing of cable cross-section which consists of the artificial defect.

Figure 3.15: Process of making electrode-bounded cavity defect

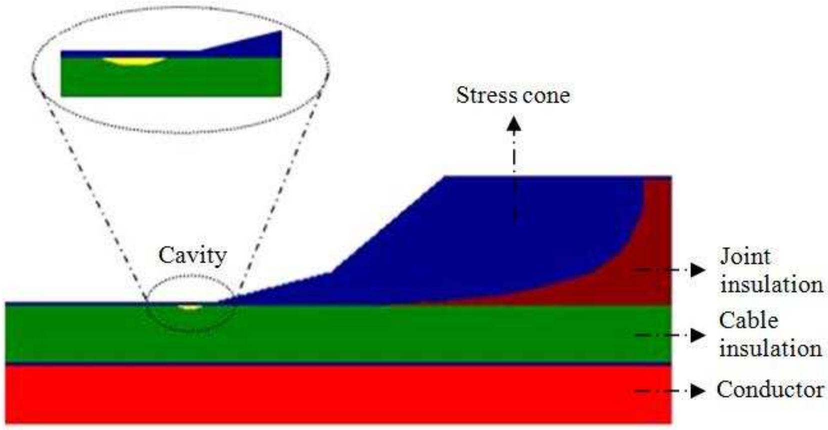

Figure 3.16: Schematic drawing of electrode-bounded cavity defect

As already described in the section 3.1.1, the electric field enhancement will occur in the electrode-bounded cavity which filled by air. PD will occur if this electric field enhancement exceeds the breakdown strength of air inside the cavity. Field plotting simulation and two PD measurement methods are applied to the test set-up which consists of this artificial defect to see the electric field enhancement and PD properties.

3.4 Conclusion

1. The presence of defect in power cable system can result in non-homogeneities of electric field distribution. If the electric field enhancement caused by the defect is higher than the breakdown strength of insulation medium then PD activities occur in the power cable system.

2. The power cable system with extruded insulation is very sensitive to the presence of PD activities thus the newly-installed extruded insulation power cable needs to be completely free from PD activity which is verified by means of after-laying test.

3. The improper on-site installation of the cable accessories can produce defects in the cable system that can result in the cable system failure in short-long operation time span.

4. Three artificial defects that represent different types of installation defects are applied to the test set-up and investigation is done by modelling the defect with Ansoft field plotting program to get the electric field behaviour and then applying two different PD measurement methods to get the PD properties for each defect.

CHAPTER 4

Experimental Test Set-up and Measurement Methods

Regarding this project investigation, a full scale test set-up of transmission power cable system was built in high voltage laboratory of TU Delft. Several methods for setup energizing and detection of PD will be used for investigation of artificial installation defects. In this chapter the experiment test set-up and measurement methods for energizing and PD detection will be described.

4.1 Description of Test Set-up

The test set-up consists of 100 meter of 150 kV cable type EYLKrvlwd 87/150 kV 1x1200 which divided into two sections by using one click-fit joint and ended by two outdoor type terminations. The distance between termination 1 and joint is 90m while between joint and termination 2 is 10m. The whole components in the cable system are provided by Prysmian Cables and Systems B.V, Netherlands. The test set-up is shown in Figure 4.1.

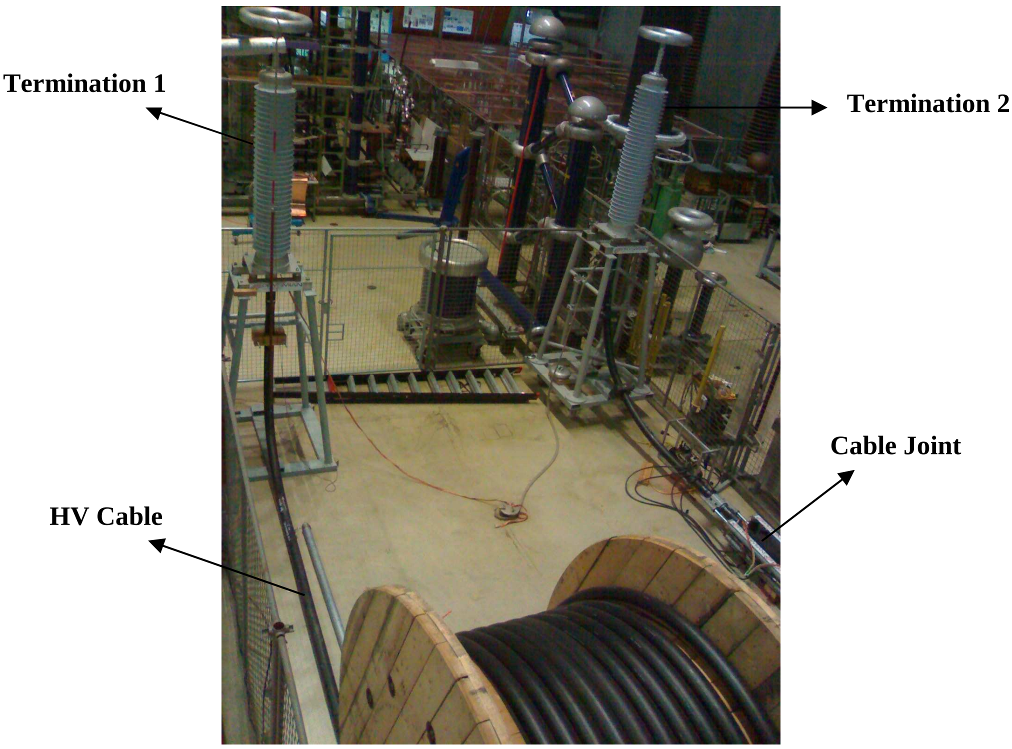

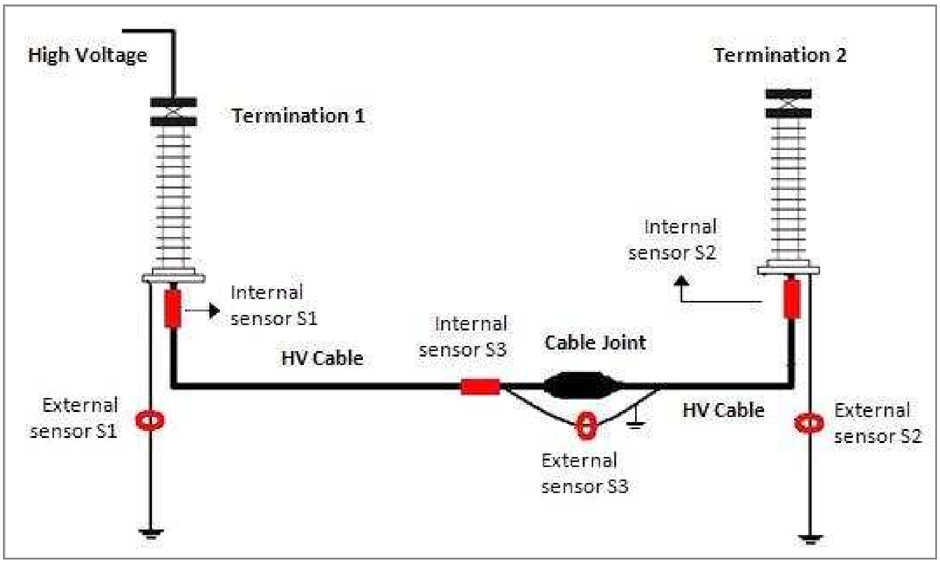

Figure 4.1: Test set-up configurations

A type of termination that is used for the test set-up is OTC-170-X. This termination is designed to terminate an extruded high voltage cable in outdoor conditions under the heaviest pollution conditions. It consists of two main parts, an insulator and a cable end. The schematic drawing of this type of termination is shown in Figure 4.2.

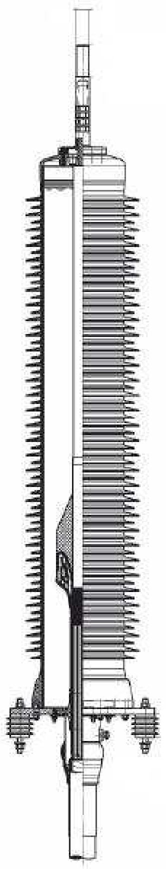

Figure 4.2: Termination type OTC-170-X

A pre-molded click-fit joint type CFJ-170A is used for this project. This joint type is designed to connect two extruded high voltage cables of the same construction. It consists of two main components, click-fit joint insulator and click-fit plug. Figure 4.3 shows the drawing of this type of joint.

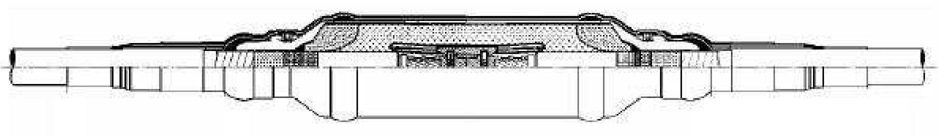

Figure 4.3: Cable joint type CFJ-170

Regarding the un-conventional PD detection, inductive sensor will be used for the PD detection purposes. There are three internal sensors installed in the accessories. The external sensors are connected to the grounding of terminations and joint.

4.2 Energizing Methods

In order to generate PD activities in the cable system which already installed with artificial defect, a HV stress needs to be applied in the test set-up. There are two HV energizing methods that are applied for this project. 50Hz AC energizing method is applied for two PD measurement methods, conventional IEC 60270 and un-conventional while damped 400 Hz Damped AC (DAC) energizing method is used for conventional IEC 60270 PD detection.

4.2.1 50Hz AC energizing

In this method, the test set-up is energized by 50Hz AC voltage from step-up transformer. The high voltage side of the transformer is connected to the test set-up through the termination 1 as depicted in Figure 4.1. Furthermore the test object is connected in parallel to PD detection methods, conventional or un-conventional PD detection. The principle of this energizing method is shown in Figure 4.4 and depicted more detail for both PD detection methods in Figure 4.8 and 4.10.

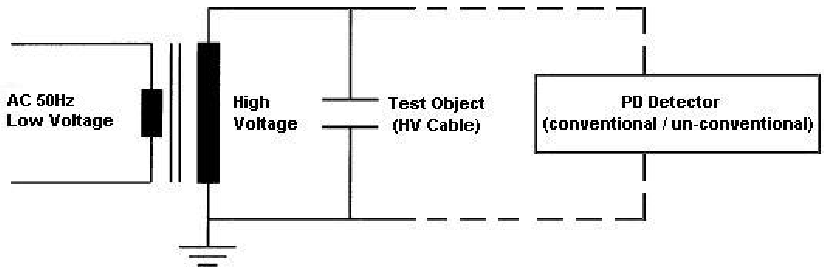

Figure 4.4: AC 50Hz energizing circuit

4.2.2 Damped AC (DAC) Energizing

The second energizing method that is used for detection of PD activities in the test set-up is damped AC (DAC) voltage. This energizing method is recognized as cost-effective voltage withstand test for polymeric insulated HV cables [16]. The DAC voltage provides convenient solution for problem related with 50Hz AC energizing method, which is not practically and economically used in on-site testing due to heavy weight and high power requirement [17]. DAC voltage method reduces the need of power requirement on-site by loading the test object, which is HV cable, by using a DC supply after which the cable is discharged through an inductor [14] by closing a solid-state switch S and create a series resonant circuit. The equivalent circuit for DAC voltage in PD measurement application is shown in Figure 4.5. The detail descriptions of the application of DAC voltage in Oscillating Wave Test System (OWTS) is described in section 4.3.1.b.

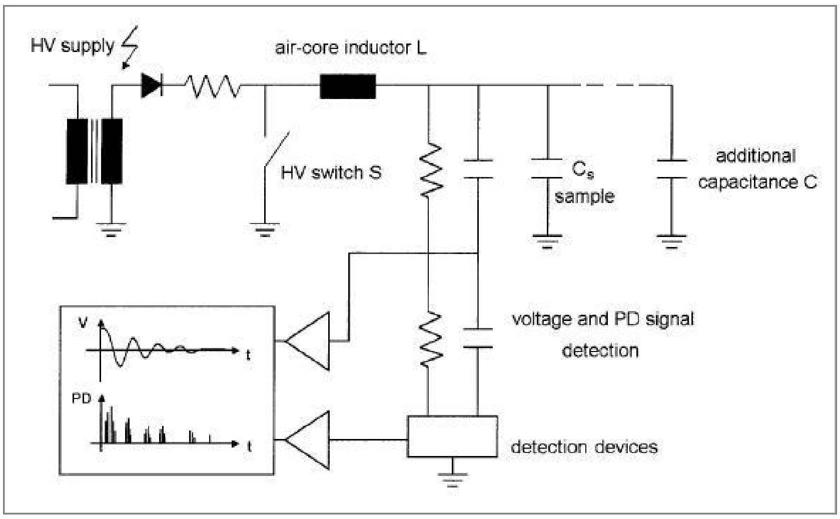

Figure 4.5: Equivalent circuit for DAC voltage application [18]

4.3 Partial Discharge Detection Methods

Partial discharge is small electric pulse that is generated from electrical breakdown of the defect in the insulation medium or in the surface of insulation medium when the applied electric field is higher than a certain critical value. In principle, there are two methods available for detection of partial discharges, conventional IEC 60270 and un-conventional PD detection.

4.3.1 Conventional PD detection method (IEC 60270)

Conventional PD detection method is standardized method based on international standard IEC 60270. Partial discharges that occur in the test object will produce current or voltage pulses. This method based on measurement of the charge displacement q, expressed in picocoulombs (pC), from the pulses which generated from partial discharge. This charge displacement is related to the discharge in the defect due to two reasons mentioned in section 3.1.2.

Measuring equipment for conventional detection consists of coupling device, transmission system and measuring instrument [19]. The most commonly used measuring equipment in practice is a straight PD detection shown in Figure 4.6.

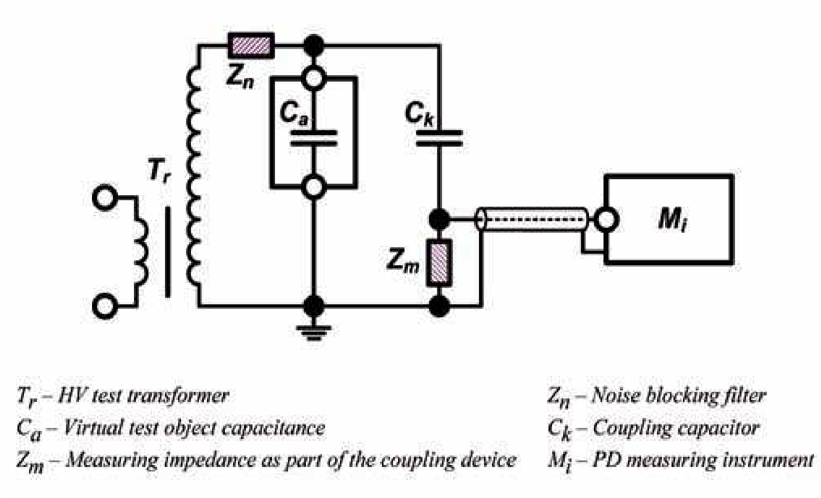

Figure 4.6: PD measuring instrument according to IEC 60270 [20]

This straight PD detection system usually consists of test object C_a which assumed to be capacitive load, a coupling capacitor C_k, impedance or filter Z_n to reduce background noise from high voltage supply, measuring impedance Z_m and PD measuring instrument M_i. The coupling capacitor is directly connected to the high voltage terminal of test object and provides a closed path for the PD current.

Based on IEC 60270, there are two types of measuring instrument suitable for PD detection in HV cable which consists of:

- Wide-band PD instrument. This instrument characterized by the fixed value of transfer impedance between lower and upper limit of frequencies, f_1 and f_2. The spectral density of PD pulse in this range of frequency is nearly constant. The PD pulses captured from the terminals of the test object are quasi-integrated and results in the output of the PD instrument and the reading of the peak level indicator will be proportional to the apparent charge [20]. Apparent charge q and the polarity of PD current can be determined from the response of its instrument.
- Wide-band PD instrument with active integrator. This instrument consists of wide-band amplifier and electronic integrator. The response of the electronic integrator to a PD pulse is a voltage signal that increase with the instantaneous value of total charge. The final amplitude of the signal is consequently proportional to the total charge.

Currently the PD pulse detection and processing are applied by using advanced digital PD measurements. By using digital PD measurements, there are several quantities related to PD can be recorded and evaluated, i.e. time instant of PD occurrence (t_i), apparent charge at t_i (q), test voltage magnitude at t_i (u_i) and phase angle at t_i (ψ_i) [20].

Calibration of PD measuring instrument is important factor in order to ensure that the PD measuring system is able to measure the PD magnitude properly. Calibration is done by injecting a short duration current pulse of known charge from the calibrator to the terminal of test object while the measuring system is de-energized. Equivalent circuit for calibration is shown in Figure 4.7.

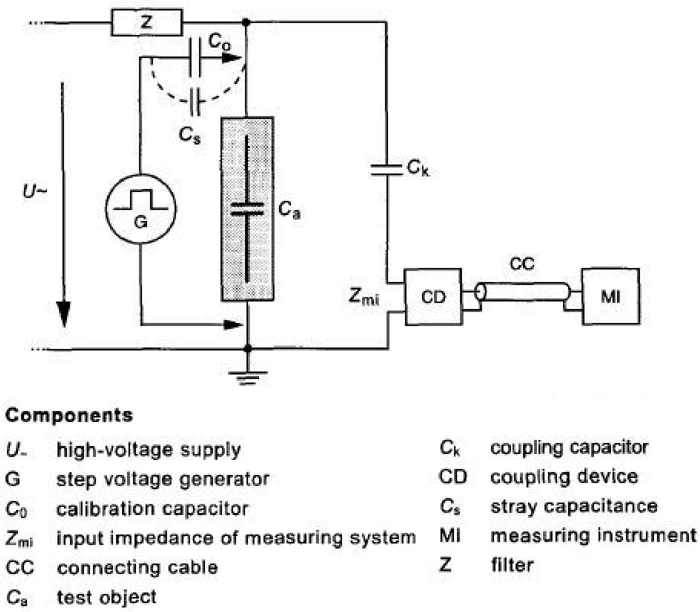

Figure 4.7: Equivalent circuit for calibration [19]

Based on two different energizing methods, there are two conventional PD detection systems will be used in this thesis, 50Hz AC conventional PD detection by using TE 571 digital PD detector and 400Hz DAC conventional PD detection by using oscillating wave test system (OWTS) HV150. Both methods are in compliance with IEC 60270 standard.

a. PD detection by using TE 571 PD Detector

In this PD measurement, 50Hz continuous AC voltage is used as an energizing method. The equivalent circuit for this PD detection is shown in Figure 4.8. This PD detection consists of several important components: test transformer, voltage regulator, digital universal measuring instrument DMI 551, coupling capacitor AKV 572 and PD detector TE 571. By using this PD detection scheme, several important parameters of PD occurrence can be obtained such as:

- PD inception voltage (PDIV)
- PD magnitude in *pC* at PDIV
- PD magnitude as a function of voltage applied
- PD pattern

PD measurement is applied in 2 minutes for each level of test voltages. During this period three quantities are recorded: the number of PD pulses, the maximum value of

PD magnitudes and the average value of PD magnitudes [10]. These three quantities are plotted as a function of phase angle of sinusoidal AC voltage.

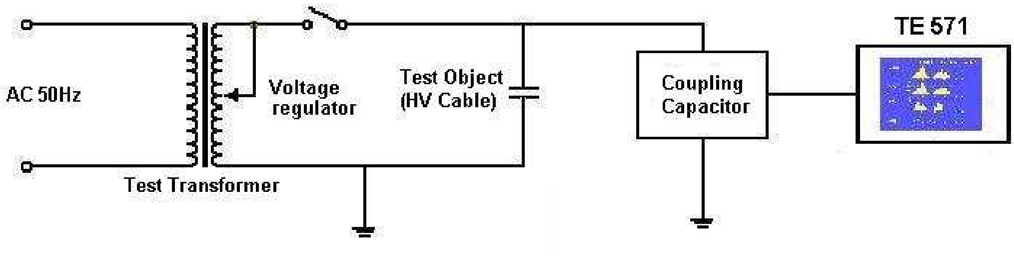

Figure 4.8: Equivalent circuit for PD detection using TE 571

b. PD detection by using OWTS HV150

As already mentioned in section 4.2.2, the use of conventional test transformer as an energizing equipment is not convenient method for on-site testing due to logistical and economical aspects. In the other hand, the other energizing methods like DC voltage and VLF voltage is considered not suitable for testing of HV XLPE cable. Damped AC (DAC) voltage provides solution for these problems. Regarding DAC voltage energizing method which compliance with IEC 60270, the OWTS HV150 will be used for energizing and PD detection for the test object.

The OWTS HV150 can provide PD diagnosis and dielectric losses measurements in HV power cable system. PD diagnostic consists of identification, evaluation and localization of PD activities in cable system. Basically the system consists of several components:

- Computer installed with OWTS software for controlling the measurement process and analyzing the data of PD measurements;
- HV source and an electronic switch to generate damped AC voltage;
- Resonance inductor;
- HV divider and coupling capacitor together with PD measuring system and analyzer.

The test set-up for PD detection by using OWTS HV150 is shown in Figure 4.9.

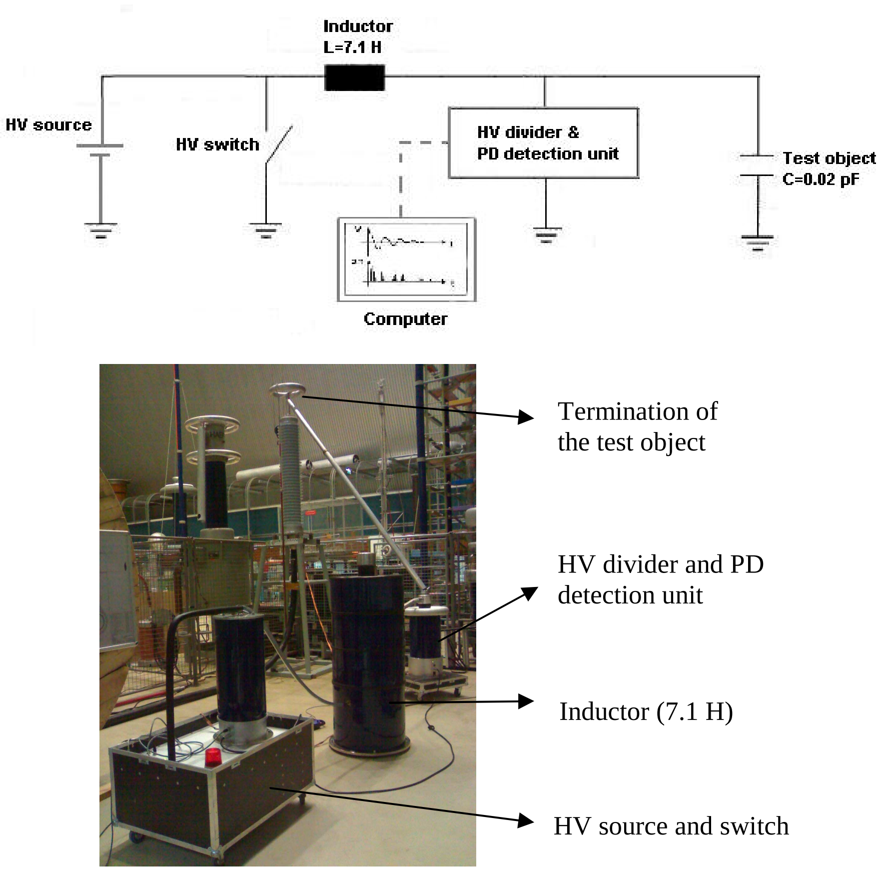

Figure 4.9: Measurement set-up for PD detection using OWTS HV150

The measurement starts by charging the test object, the HV cable system, to a certain value of test voltage U_{test} by using growing DC voltage. The time needed to charge the test object is determined by using [14]:

$$t_{ch} = \frac{U_{test}\,C}{I_{load}} \tag{4.1}$$

Where C is the capacitance of the test object and I_{load} is maximum load current of DC supply. Afterwards, the system is short circuited by electronic switch and the series connection between test object and resonance inductor is created and results in sinusoidal damped AC voltage. The frequency of this damped AC voltage is approximately equal to the resonant frequency if the test circuit [21]. The resonant frequency f_{res}, which is depend on the capacitance of test object C and the resonance inductance L, can be determined by using [14]:

$$f_{res} = \frac{1}{2\pi\sqrt{LC}} \tag{3.2}$$

The use of DAC voltage with frequency up to 500 MHz in laboratory and field measurement shows that there is no fundamental different in PD occurrence (PD inception voltage and PD level) [22]. Since 2004 this method has been applied for PD diagnosis on HV power cable up to 250 kV [21].

4.3.2 Un-conventional PD detection method

Conventional PD detection based on IEC 60270 has been used many years as a standardized method for PD measurement. However, this method has a limitation when used in the field measurement due to relatively high level of ambient noise. Therefore, Un-conventional PD detection is used to provide result with suppressed noise or high signal-to-noise ratio. Basically there two main methods available for un-conventional PD detection method, the High Frequency/Very High Frequency/Ultra High Frequency (HF/VHF/UHF) and acoustic method. Furthermore, HF/VHF/UHF method will be used for investigation of un-conventional PD detection in this thesis. HF/VHF/UHF method is based on the detection of high frequency signal generated from PD activities. In relation to PD detection in accessories of high voltage power cable, the important frequency range lies between 3 MHz $\leq f \leq$ 500 MHz [23]. PD measuring equipment for un-conventional PD detection can be divided into several important sections: PD sensors, triggering parts, spectrum analyzer and computer equipped with PD software analysis. The PD detection system for un-conventional method is depicted in Figure 4.10.

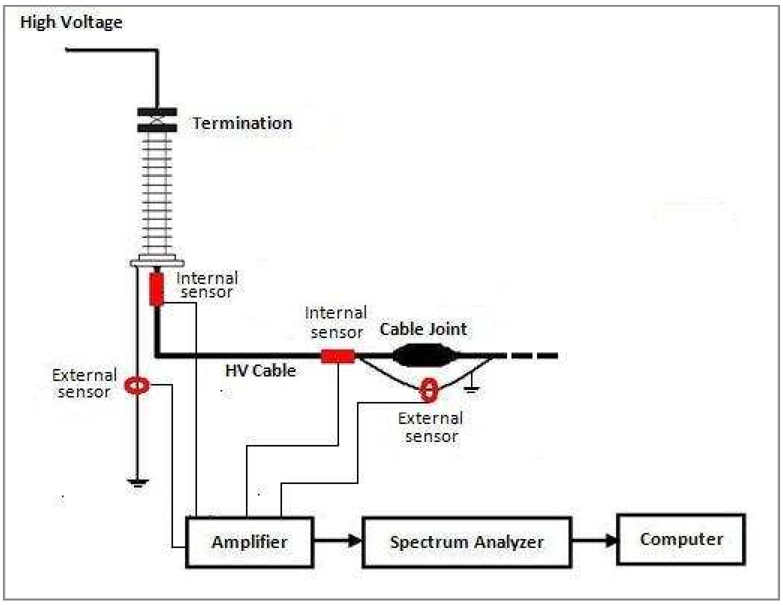

Figure 4.10: Un-conventional PD detection system

PD sensors work based on detection of high frequency current pulses that occur during PD in the cable system. The PD pulses occur in very short time, the width and rise time of the pulses are in the nanoseconds region. Consequently, PD pulses with energy frequency up to hundred MHz are generated [24]. These PD pulses will travel through the cable earth conductor and finally can be recorded by the sensors. For un-conventional PD detection, internal and external capacitive and inductive sensor can be used. Internal inductive sensors can be placed in the cable accessories without disturbing the cable insulation because they placed on the top of earth screen of cable. However, this type of sensors has to be already installed in manufacture of the cable accessories [24]. The external inductive sensors are placed around the ground connections of cable accessories. In real situation they can be placed at the earthing flange of termination or link boxes. These types of sensor mostly used in practice due to the advantage that these sensor do not disrupt the normal configuration of the accessories and cable part. Figure 3.11 shows the picture of internal and external sensor used for PD detection.

(a) (b)

Figure 4.11: Internal (a) and external (b) sensor at cable accessories

The PD signal from sensor then transferred through coaxial cable and amplifier to the spectrum analyzer. There two operation modes of spectrum analyzer that can be utilized for PD detection, “full span” and “zero span” mode [24]. In the first mode, the full spectrum of amplitude of the signal and noise are plotted in the frequency domain from e.g. 0-500 MHz. Full spectrum of noise is obtained by disconnecting the test set-up from HV energizing and then the amplitude of noise is measured for certain frequency step, e.g. 3 MHz, start from 0 MHz up to 500 MHz. By using this full spectrum of signal and noise, several centre frequencies which have high signal-to-noise ratio can be selected. The example of selection suitable frequency ranges which have good noise suppression for un-conventional PD measurement is shown in Figure 4.12.

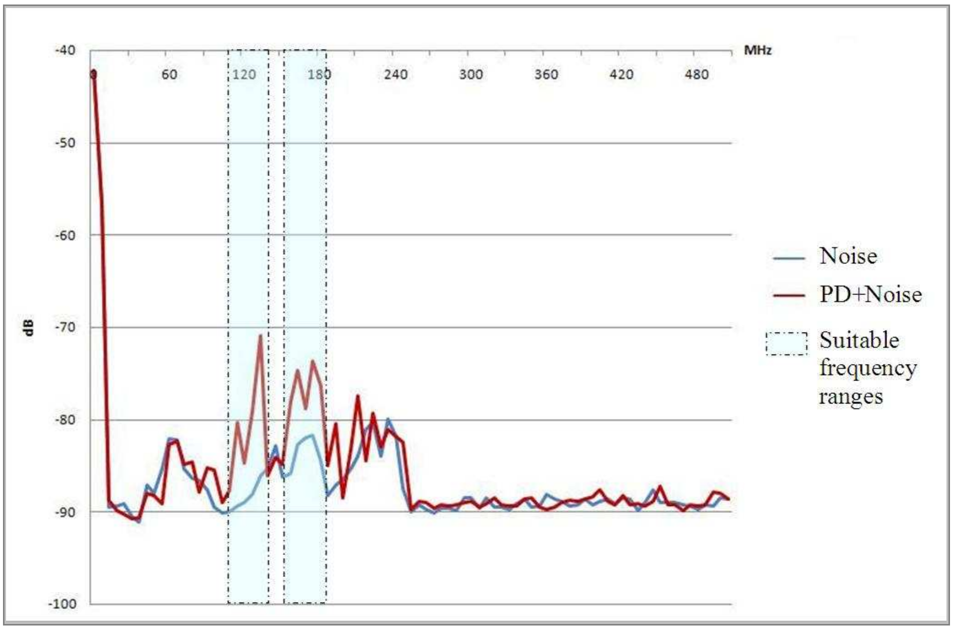

Figure 4.12: Selection of suitable frequency ranges from full spectrum of PD and noise

In the second mode of operation, the signal is shown in time domain at selected centre of frequencies with certain selected value of bandwidth. It means that the spectrum analyzer works as band-pass filter that work only at small range of frequency determined by the bandwidth and blocks unwanted frequency components outside the bandwidth. These centre frequencies, which have high signal-to-ratio, are chosen from the full spectrum in the first mode. In combination with triggering at the frequency of energizing voltage, the phase-resolved PD pattern, in terms of Volts (*V/mV*), can be obtained similar to the conventional PD detection.

By using a computer which already installed with PD software and connected to the spectrum analyzer, two operation modes of spectrum analyzer can be performed on the computer. For "zero span" mode, several repeated recordings of the period of the exciting voltage can be performed (called sweeps) and saved. Furthermore, the amplitude and number of PD pulses as a function of phase (phase-resolved pattern) can be performed and this pattern will be useful to recognize the type of defect in the cable system.

However, calibration on this PD detection method cannot be applied as in conventional PD detection which described in the IEC 60270 standard due to several reasons related with high-frequency behavior of the sensors and the type and routing of the measurement cables [25].

4.4 Conclusion

1. The test set-up for the investigation consists of 100m transmission power cable which divided into two sections by one click-fit joint and ended by two terminations.

2. There are two high-voltage energizing methods available for the on-site PD measurements on HV power cable which consist of 50Hz AC continuous and Damped AC (DAC) voltages.

3. Two different PD detection methods, conventional and un-conventional, are used for investigation. Conventional IEC 60270 PD detection is applied by using TE 571 PD detector and OWTS HV150 while un-conventional PD detection is performed by using HF/VHF/UHF method.

CHAPTER 5

Field Plotting Simulation and Experiment Results for Missing Semi-Conductive Screen Defect

The first artificial defect which is used for the investigation is missing semi-conductive screen on the area close to the cable joint as shown in Figure 3.12. For further discussion this artificial defect is regarded as defect 1. This chapter describes the result of field plotting simulation for different size of defect 1 and the PD measurement results by using different PD detection and energizing methods.

5.1 Field Plotting Simulation Results for Defect 1

For investigating the electrostatic problem due to the presence of artificial defect in the cable system, the Ansoft version 9.0 of Maxwell 2D Student Version (SV) is used. This program can be used for analyzing the electromagnetic fields in cross-section of structure by using Finite Element Analysis (FEA) to solve two-dimensional (2D) electromagnetic problems. The cross-section of cable part as shown in Figure 5.1 is modelled in the RZ plane which means that the cross-section of the structure is rotating around an axis of symmetry in the cross-section.

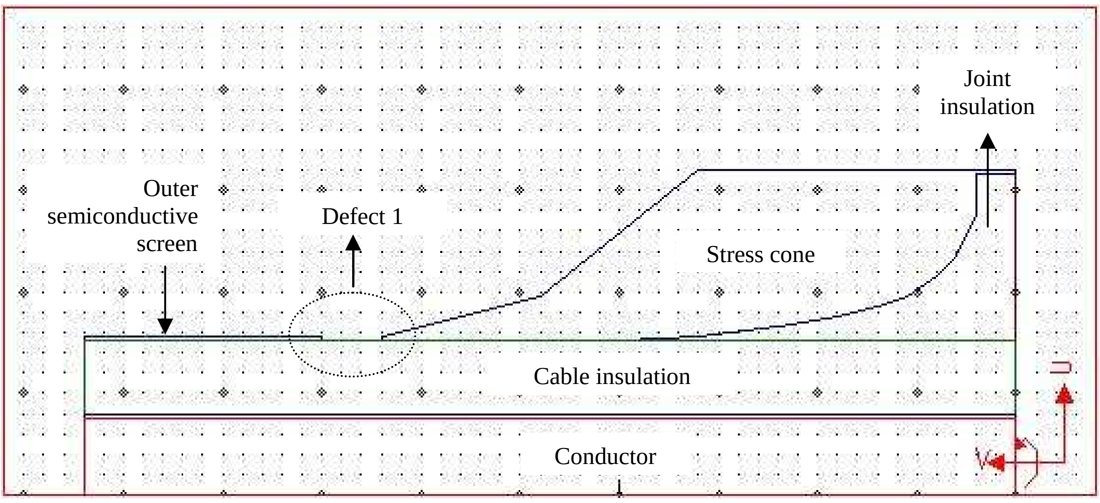

Figure 5.1: The cross-section of cable part which consist of defect 1

Furthermore, after being modelled, all objects in the cross-section model have to be assigned for their material properties which consist of:

- The high-voltage conductor is assumed as perfect conductor with the infinite conductivity.
- The inner and outer semi-conductive screen is assumed as material with the conductivity 10^{-5} siemens/meter.
- The cable insulation is assumed as material with the relative permittivity (ε) 2.25
- The joint insulation is assumed as material with the relative permittivity (ε) 3.
- The background is modelled as air with the relative permittivity (ε) 1.

Investigation the effect of the presence of the defect 1 in electric field behaviour is applied by making a field plotting simulation for normal situation without the presence of defect and the situation with the presence of three sizes of defect as shown in Figure 3.12.

5.1.1 Electric Field Behaviour without Defect 1

Theoretically, the electric field behaviour in the cable system follows the equation (2.1) and the highest electric stress will be located in the area close to the high-voltage conductor while the lower stress will be located in area close to the outer semi-conductive screen. The field plotting result for simulation without the defect at voltage applied 28 kV_{peak} is shown in Figure 5.2. The voltage 28 kV_{peak} is the PD inception voltage (PDIV) for defect 1 size 15mm by using TE 571 PD detector. Therefore this voltage level is used for the stress level in the simulation for normal situation and different size of defect 1.

From the result of normal situation it can be shown that the electric field in the area close to the outer semi-conductive screen where the defect 1 will be created is up to 1.16 kV/mm. Figure 5.3 and 5.4 show the electric field behaviour for voltage applied $1U_0$ (122.5 kV_{peak}) and $1.7U_0$ (208.2 kV_{peak}). When the defect presents in the form of missing outer semi-conductive screen, the electric field distribution changes and the field enhancement occurs in the edge of removed semi-conductive screen and results in the surface discharge occurrence.

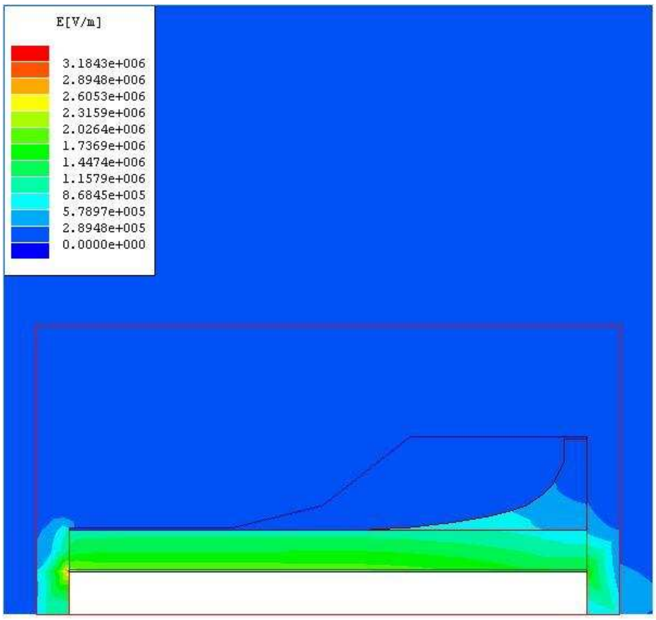

Figure 5.2: Electric field plotting for condition without defect at 28 kV_{peak}

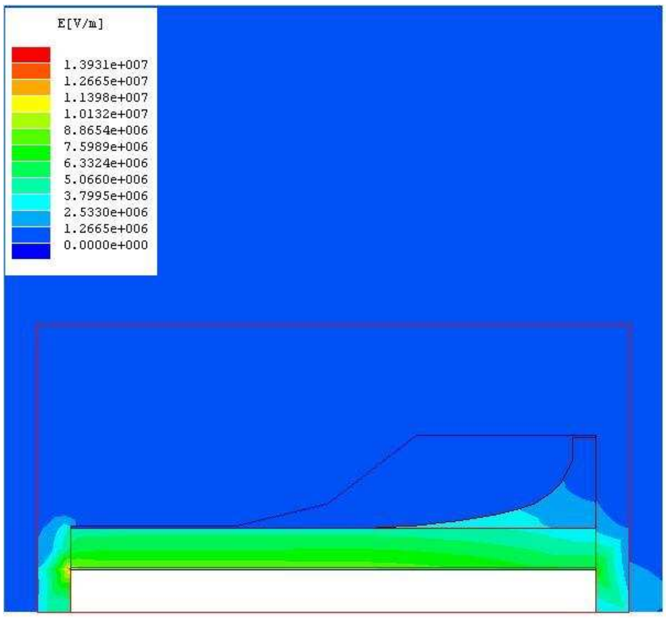

Figure 5.3: Electric field plotting for condition without defect at U_0 (122.5 kV_{peak})

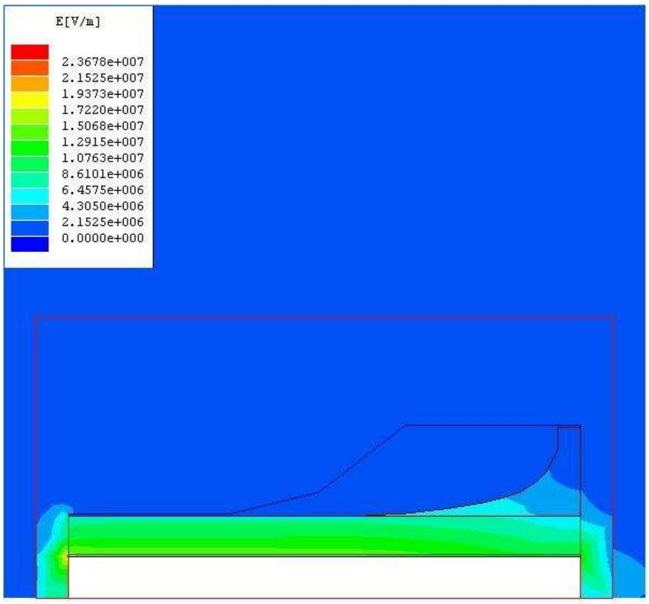

Figure 5.4: Electric field plotting for condition without defect at 1.7U_0 (208.2 kV_{peak})

5.1.2 Electric Field Behaviour for Defect 1 Size 15mm

First size for defect 1 is 15mm of missing outer semi-conductive screen. The presence of this defect disturbs the normal electric field behaviour in the cable system and result in field enhancement at the edge of outer semi-conductive screen as shown in Figure 5.5.

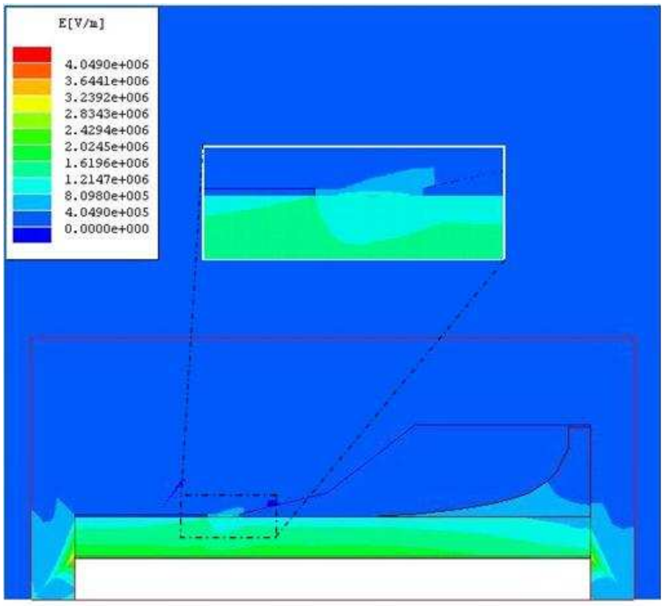

Figure 5.5: Electric field plotting for defect 1 size 15mm at 28 kV_{peak}

It can be seen from the simulation result that the presence of removed semi-conductive screen results in field enhancement up to 1.62 kV/mm for the voltage stress 28 kV_{peak}. Figure 5.6 and 5.7 show the electric field behaviour for voltage applied $1U_0$ (122.5 kV_{peak}) and $1.7U_0$ (208.2 kV_{peak}).

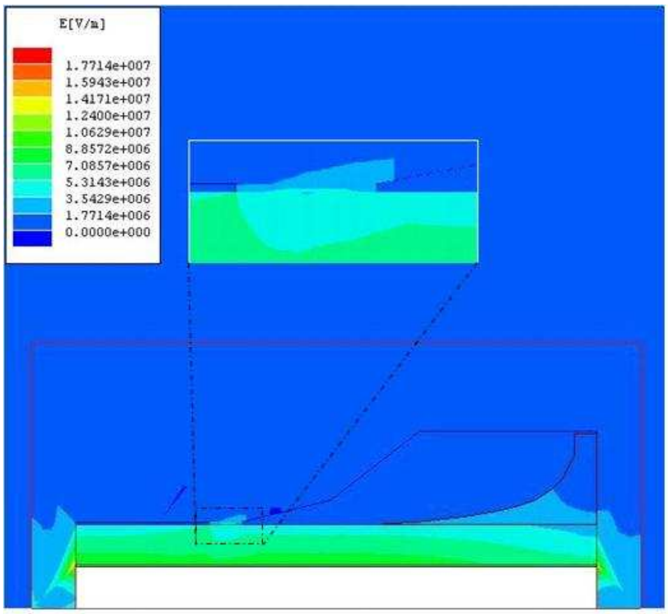

Figure 5.6: Electric field plotting for defect 1 size 15mm at U_0 (122.5 kV_{peak})

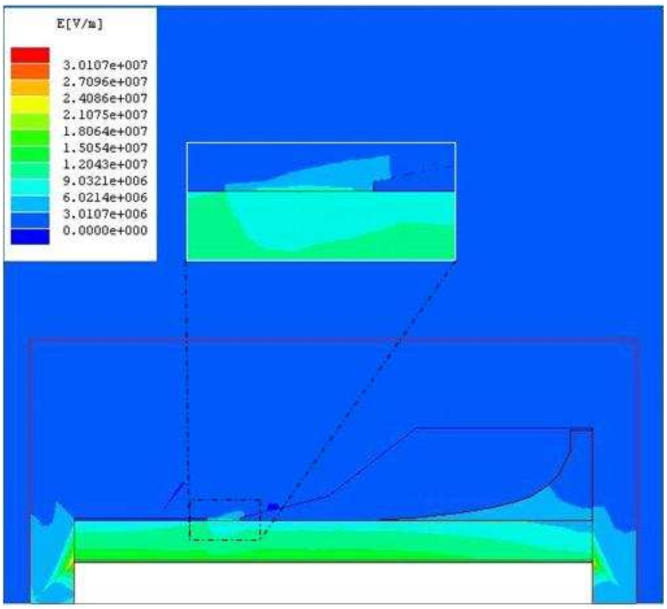

Figure 5.7: Electric field plotting for defect 1 size 15mm at $1.7U_0$ (208.2 kV_{peak})

5.1.3 Electric Field Behaviour for Defect 1 Size 10mm

The effect of different size of defect 1 is investigated by reducing the size of defect 1 from 15mm to 10mm. The simulation result for voltage stress 28 kV_{peak} is shown in Figure 5.8.

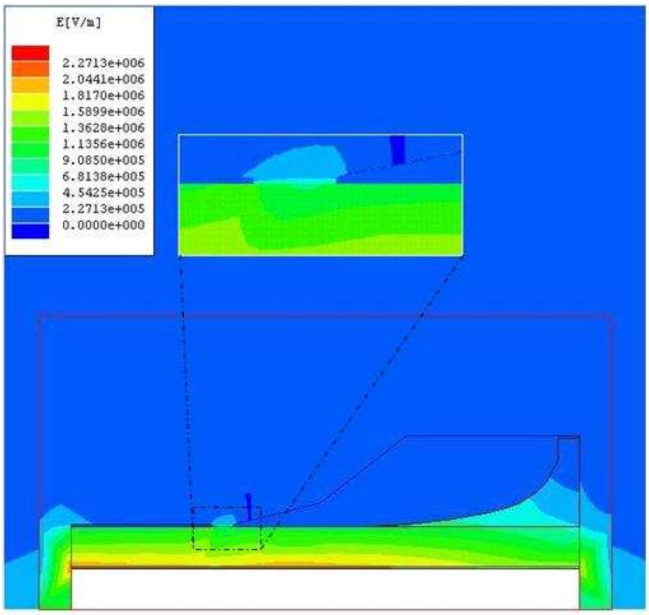

Figure 5.8: Electric field plotting for defect 1 size 10mm at 28 kV_{peak}

The simulation result shows that at smaller size of defect 1, the field concentration no longer occurs at the edge of semi-conductive screen. However, the electric field at the edge of semi-conductive screen (1.36 kV/mm) is higher than normal condition. Figure 5.9 and 5.10 show the electric field behaviour for voltage applied $1U_0$ (122.5 kV_{peak}) and $1.7U_0$ (208.2 kV_{peak}).

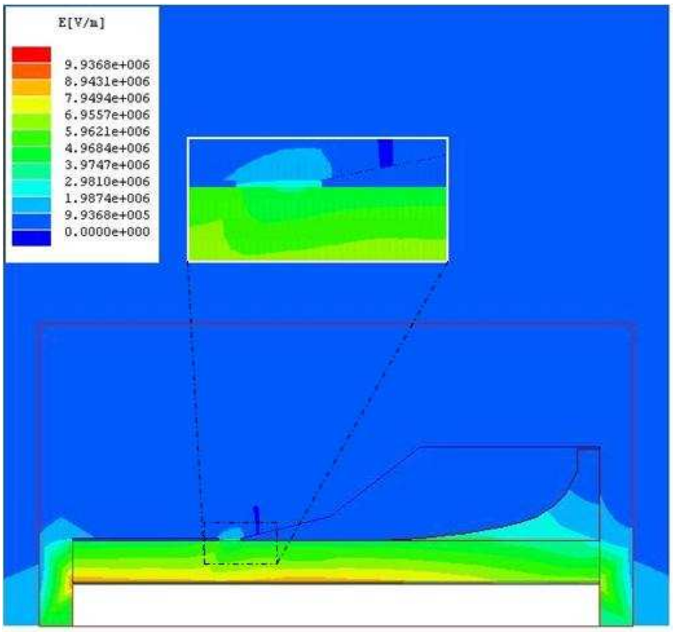

Figure 5.9: Electric field plotting for defect 1 size 10mm at U_0 (122.5 kV_{peak})

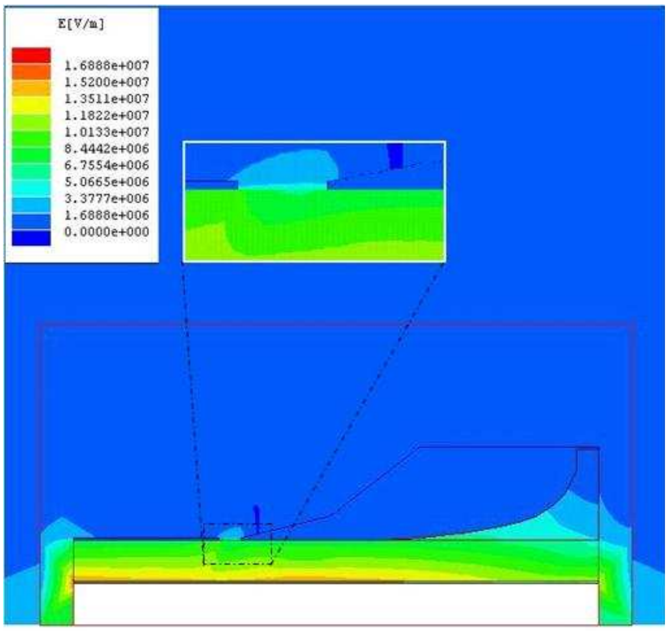

Figure 5.10: Electric field plotting for defect 1 10mm at 1.7U_0 (208.2 kV_{peak})

5.1.4 Electric Field Behaviour for Defect 1 Size 5mm

The last size of defect 1 to be investigated is 5mm. Figure 5.11 shows the simulation result for this size of defect 1 with the same voltage applied (28 kV_{peak}).

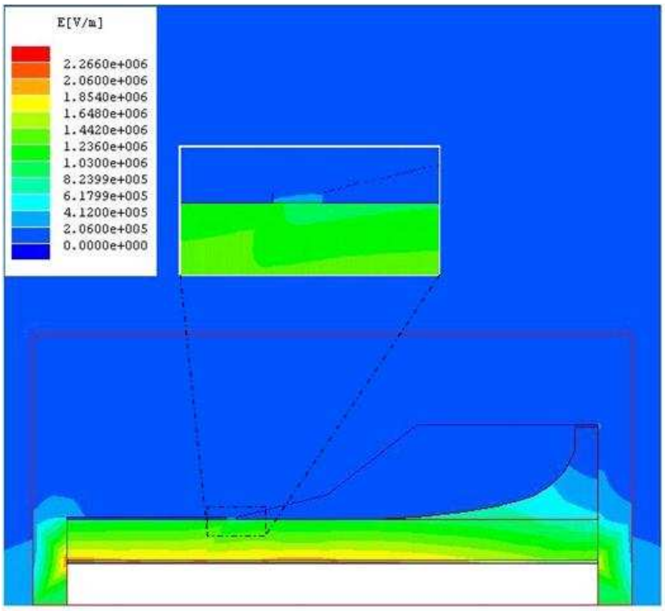

Figure 5.11: Electric field plotting for defect 1 size 5mm at 28 kV_{peak}

It can be seen from the simulation result that at defect 1 size 5mm the electric field distribution is relatively similar to the previous size of defect where there is no field concentration at the edge of semi-conductive screen. The electric field stress at the edge of semi-conductive screen (1.24 kV/mm) is lower than the previous size but still higher than the normal situation. Figure 5.12 and 5.13 show the electric field behaviour for voltage applied $1U_0$ (122.5 kV_{peak}) and $1.7U_0$ (208.2 kV_{peak}).

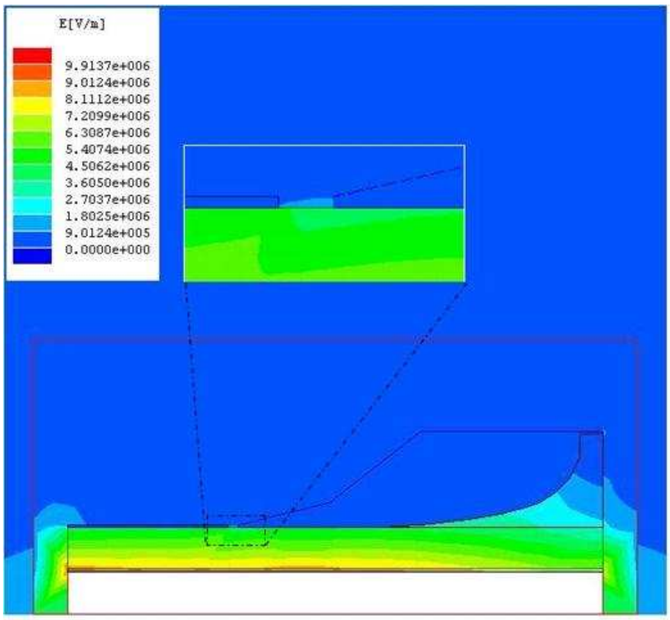

Figure 5.12: Electric field plotting for defect 1 size 5mm at U_0 (122.5 kV_{peak})

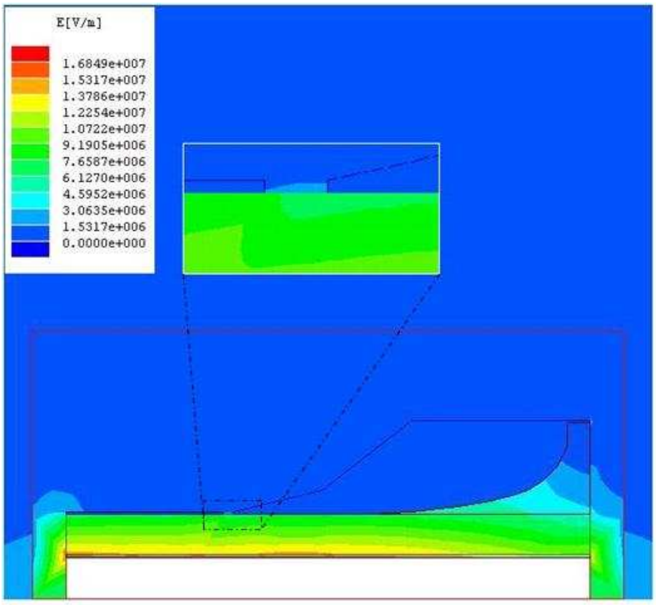

Figure 5.13: Electric field plotting for defect 1 size 5mm at 1.7U_0 (208.2 kV_{peak})

5.1.5 Comparison of Simulation Result for Three Sizes of Defect 1

From the simulation results of defect 1 with the different size, it can be seen that by applying the same voltage stress, the electric field enhancement at the edge of outer semi-conductive screen will decrease with the size of the defect. Table 5.1 shows the result of simulation for different size of defect 1 at several values of voltage stress.

Table 5.1

Electric Field for Different Situation of Defect 1 at Different Voltage Stress

Voltage Stress (kVpeak)	Electric Field (kV/mm) for Each Condition			
	No defect	Defect 5mm	Defect 10mm	Defect 15mm
28	1.16	1.24	1.36	1.62
60	2.49	2.66	2.91	3.47
122.5 (U_0)	5.06	5.41	5.96	7.09
208.2 (1.7U_0)	8.61	9.19	10.13	12.04

In order to the see the increase of electric field in the cable system as a function of applied voltage, a plot of electric field (kV/mm) for each condition of cable system as a function of stress voltage applied up to $1.7U_0$ is shown in Figure 5.14.

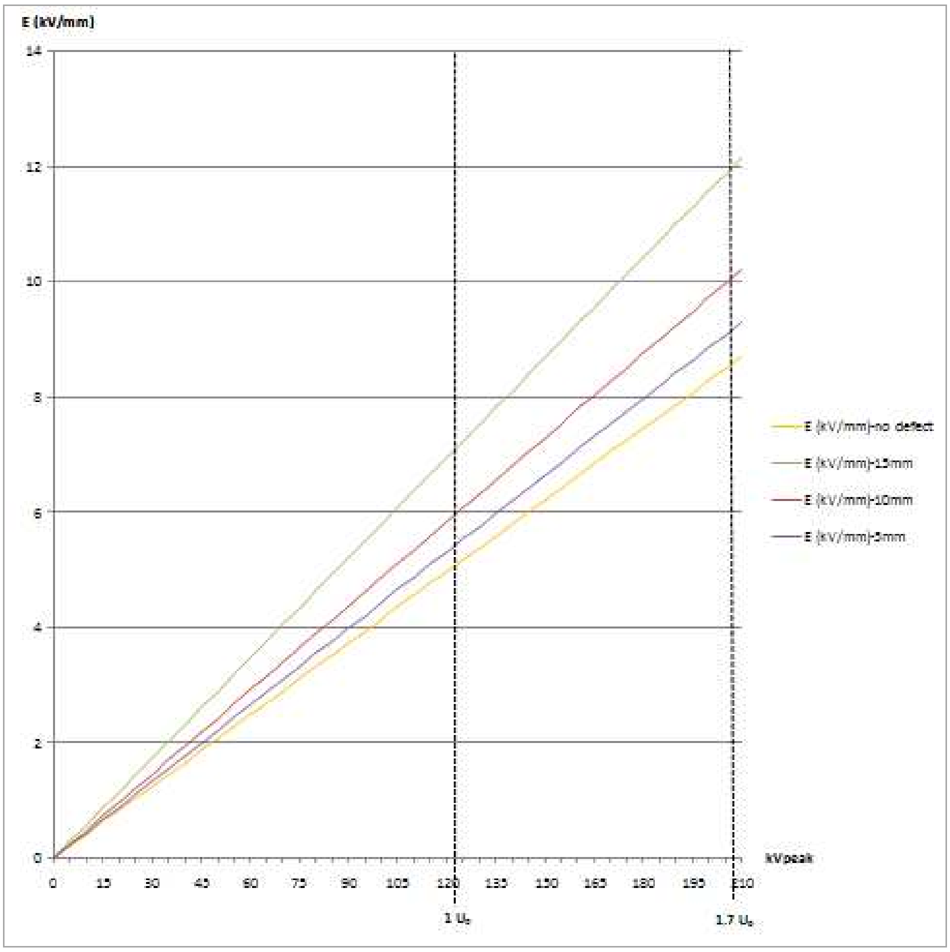

Figure 5.14: Plot of electric field as a function voltage applied for defect 1

It can be seen from this plot that the defect 1 size 15mm produces much higher electric field enhancement than in the case of 10mm and 5mm due to the presence of field concentration at the edge of semi-conductive screen as discussed in section 5.1.2. However, at lower voltage stress there are small differences in the field enhancement for different size of defect 1 therefore the PDIV for different size of defect 1 will probably occur at relatively the same voltage stress. The increase of electric field as function of voltage applied is steeper for the bigger size of defect 1.

5.2 Measurement Results by Using 50Hz AC Energizing and Conventional IEC 60270 PD Detection

PD measurements on cable system which consists of defect 1 are performed with the test set-up as shown in Figure 4.8. Calibration is applied to the test set-up regarding PD measurement in *pC* as described in IEC 60270 standard. Before applying the voltage, the noise level is measured and it was about 5 pC. Measurement is done by slowly increasing the voltage start from 0 kV to get the PD inception voltage (PDIV) and then PD measurement is applied at several levels of voltage with 2 minutes duration for each voltage up to 60 kV_{peak}. The voltage applied was limited to 60 kV_{peak} due to the current limitation in the transformer feeding cables. Plot of PD magnitude in pC as a function of voltage applied up to 60 kV_{peak} is shown in Figure 5.15.

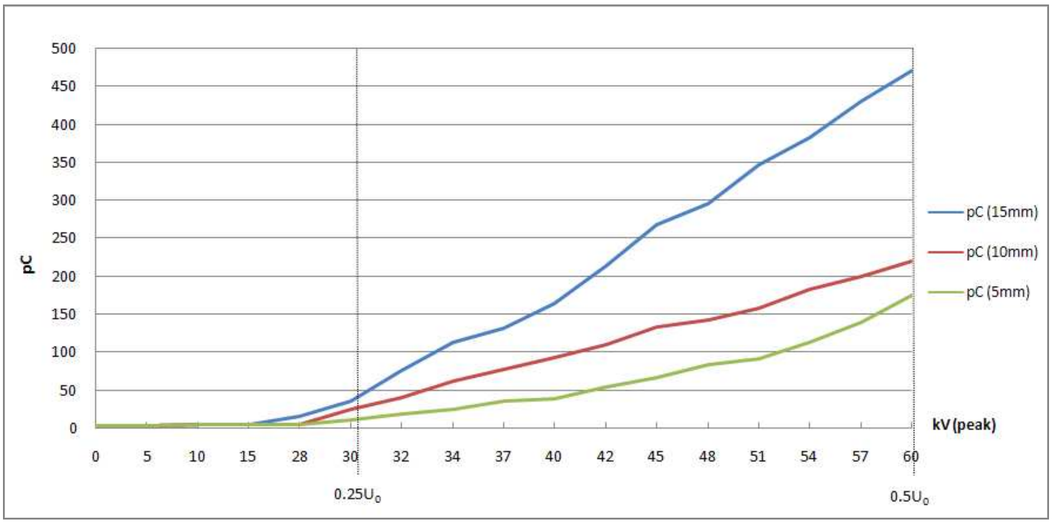

Figure 5.15: PD magnitude – voltage applied for 3 sizes of defect 1

The PDIV for three sizes of defect 1 size was 28 kV_{peak} for 15mm, 30 kV_{peak} for 10mm and 31 kV_{peak} for 5mm. Therefore, it can be concluded that changing the size of defect 1 does not give significant change in PDIV and the Figure 5.15 shows that the increase of PD amplitude as a function of voltage is steeper for the bigger size of defect 1. These occurrences confirm the result of electric field – voltage applied plotting simulation by using Ansoft.

PD phase-resolved patterns for different sizes of defect are obtained by measuring at certain level of voltage for 2 minutes duration. Figure 5.16 until 5.18 show PD phase-resolved patterns which observed at PDIV and 60 kV_{peak} for three sizes of defect 1.

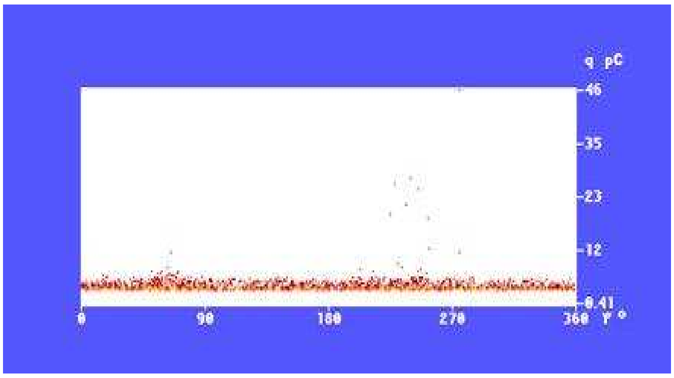

Figure 5.16: PD pattern at 28 kVpeak (PDIV) for defect 1 size 15mm

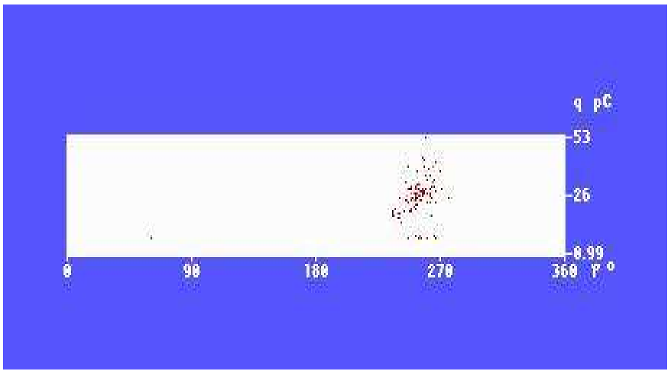

Figure 5.17: PD pattern at 30 kVpeak (PDIV) for defect 1 size 10mm

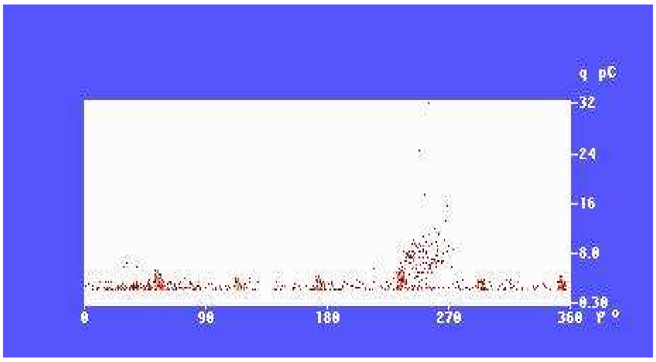

Figure 5.18: PD pattern at 31 kVpeak (PDIV) for defect 1 size 5mm

PD phase-resolved patterns for three sizes of defect 1 show that at PDIV, the asymmetric PD phase-resolved patterns occur at negative half period of the 50Hz AC voltage cycle. Figure 5.19 – 5.20 show PD phase-resolved patterns for three sizes of defect 1 which observed at 60 kV_{peak}.

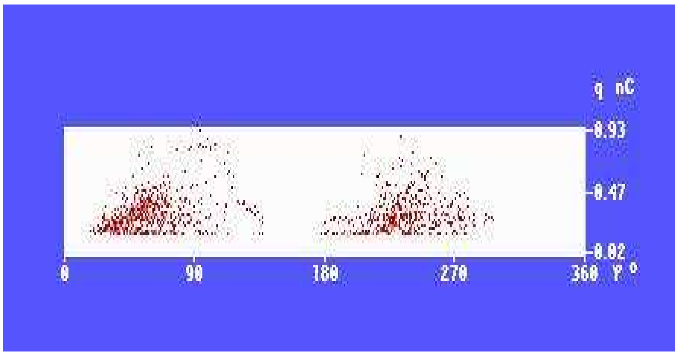

Figure 5.19: PD pattern at 60 kV_{peak} for defect 1 size 15mm

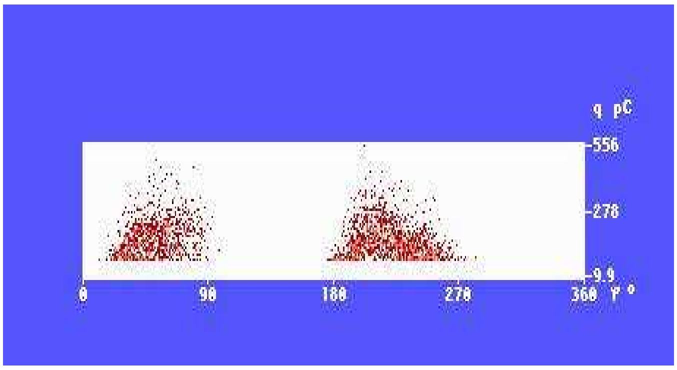

Figure 5.20: PD pattern at 60 kV_{peak} for defect 1 size 10mm

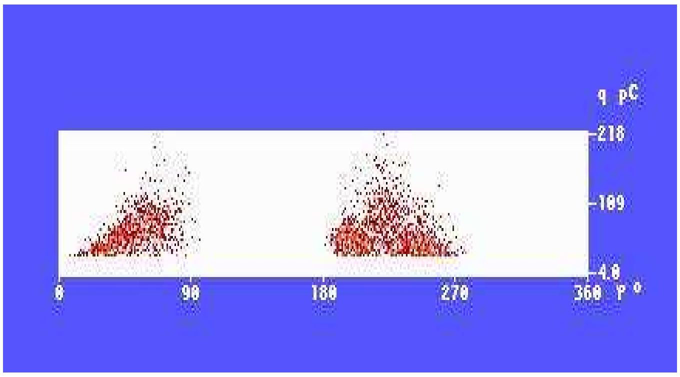

Figure 5.21: PD pattern at 60 kV_{peak} for defect 1 size 5mm

It can be seen from Figure 5.19 – 5.21 that at higher voltage the PD phase-resolved patterns for defect 1 become symmetrical, occur at both positive and negative period of the 50Hz AC voltage cycle.

5.3 Measurement Results by Using 400Hz DAC Energizing and Conventional IEC 60270 PD Detection

PD measurements by using OWTS HV150 are performed by using test set-up as depicted in Figure 4.9. The capacitance of the test object in the form of 100m cable is 0.02 µF. By using fixed inductance 7.1 H, the resonant frequency of the test circuit according to equation 3.2 will be around 422Hz. PD measurements only applied to two sizes of defect 1, 15mm and 5mm. Calibration as described in IEC 60270 standard is applied to the test circuit before PD measurement. Before applying the voltage, the noise level is measured and reached 15 pC. Figure 5.22 and 5.23 show the PD measurement at PDIV for 15mm and 5mm of defect 1.

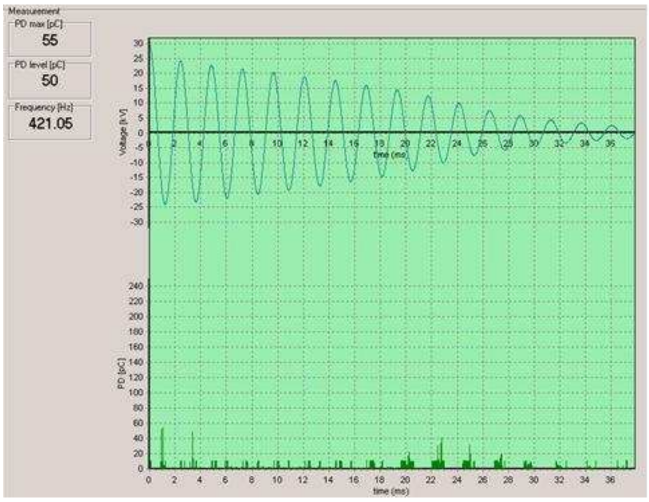

Figure 5.22: PD measurement on defect 1 size 15mm 25 kVpeak (PDIV)

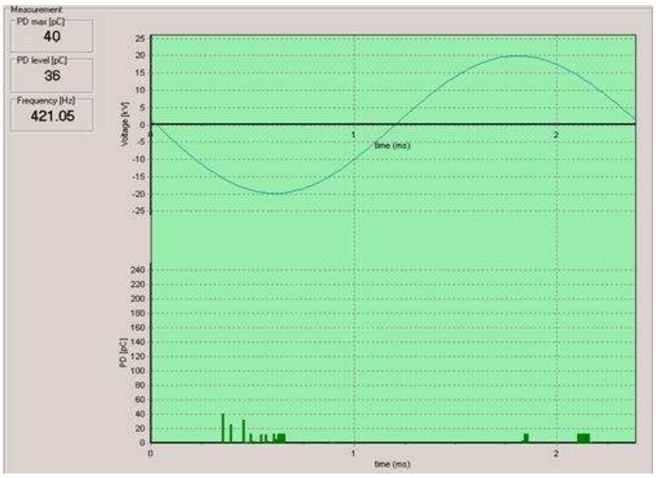

Figure 5.23: PD measurement on defect 1 size 5mm at 25 kVpeak (PDIV)

For both sizes of defect 1, PDIV occurs at the same voltage level, 25 kV_{peak} and PD magnitude is higher at the bigger size of defect 1. This occurrence confirms the result of Ansoft simulation where the size of defect 1 does not give significant influence on PDIV and the field enhancement is higher at bigger size of defect 1. The results of PD measurement on 60 kV_{peak} are shown in Figure 5.24 and 5.25.

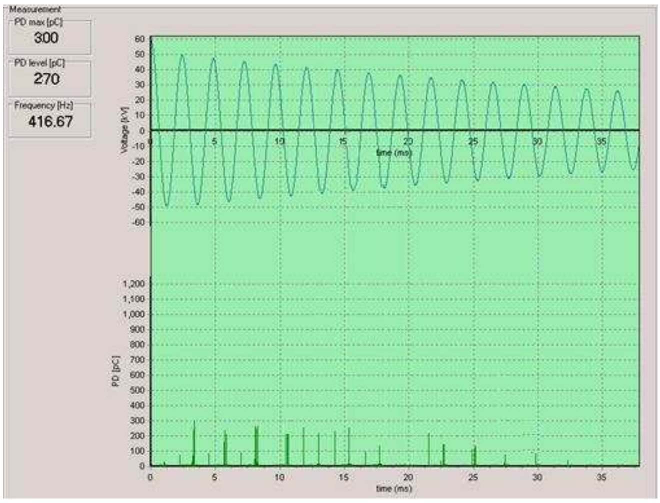

Figure 5.24: PD measurement on 15mm defect 1 at 60 kVpeak

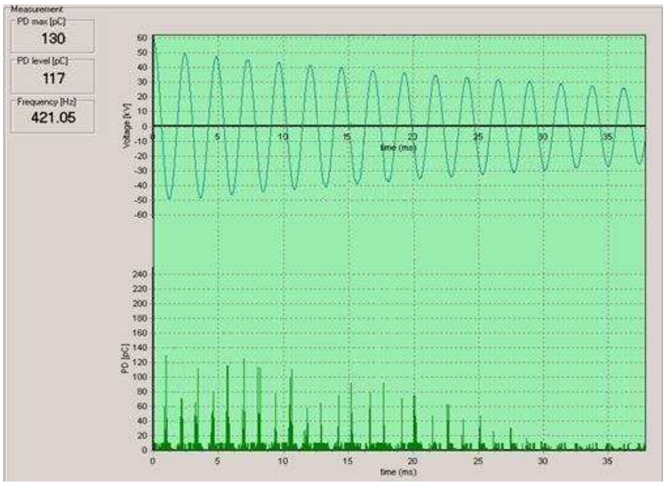

Figure 5.25: PD measurement on 5mm defect 1 at 60 kV_{peak}

Furthermore, plot of PD amplitude as a function of voltage applied up to 60 kV_{peak} as shown in Figure 5.26 is made to see the effect of different size of defect 1 in PD amplitude as a function of applied voltage.

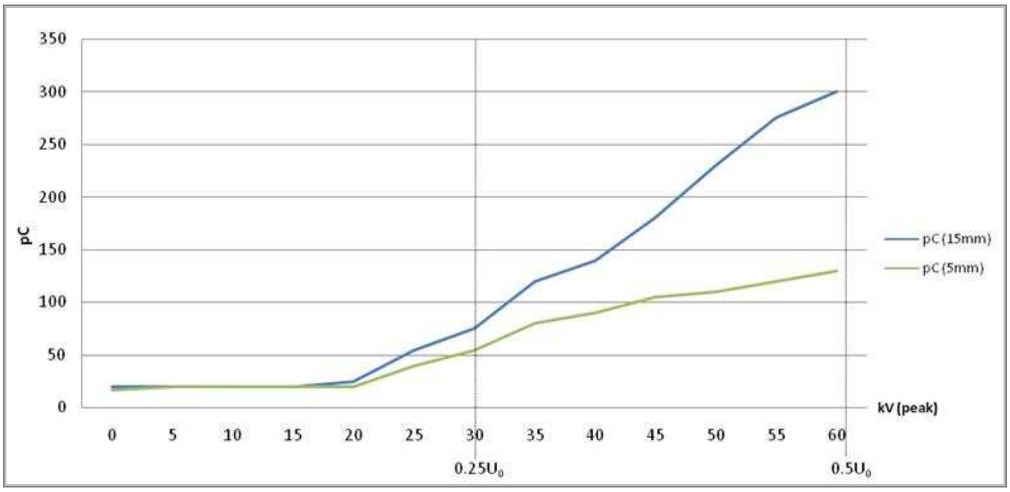

Figure 5.26: Plot of PD amplitude as a function of voltage applied

It can be seen from Figure 5.26 that the increase of PD amplitude as a function of voltage applied is steeper for the bigger size of defect 1.

5.4 Measurement Results by Using 50Hz AC Energizing and Un-Conventional PD Detection

Un-conventional PD measurement has different application than conventional PD measurement as described in section 4.3.2. The measurement set-up is shown in Figure 4.10. PD detection and measurement are applied to six sensor positions in the cable accessories. The selection of centre frequency (CF) for noise suppression is very important, therefore “full span” of background noise and PD pulses from the artificial defect 1 that detected by sensors will be compared up to 500MHz. Un-conventional PD measurement was only applied to one size of defect 1 which is 15mm. Figure 5.27 – 5.32 show full spectra of background noise and signal up to 500 MHz. These spectra are obtained by making a single sweep of frequency spectrum from 0 MHz – 3 GHz of noise and PD signal. PD signal is obtained by applying 50 Hz AC voltage 60 kV_{peak} to the termination 1.

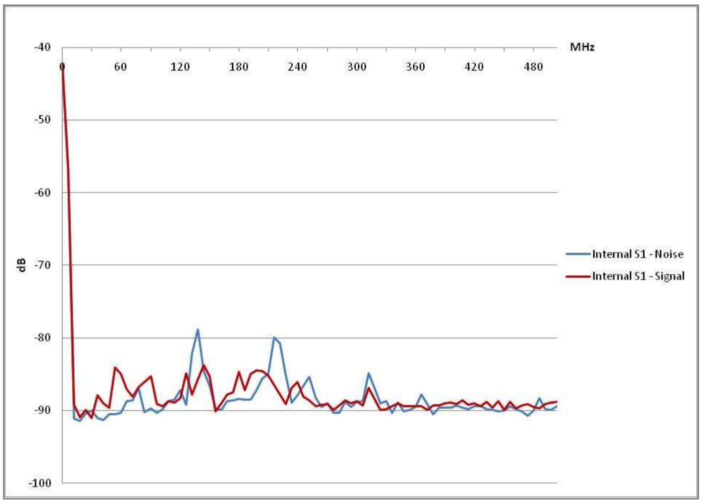

Figure 5.27: Full spectra for internal sensor S1 (at termination 1)

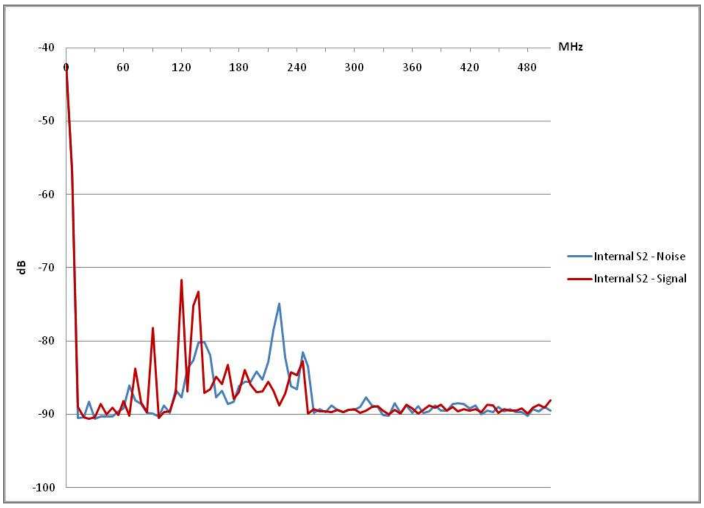

Figure 5.28: Full spectra for internal sensor S2 (at termination 2)

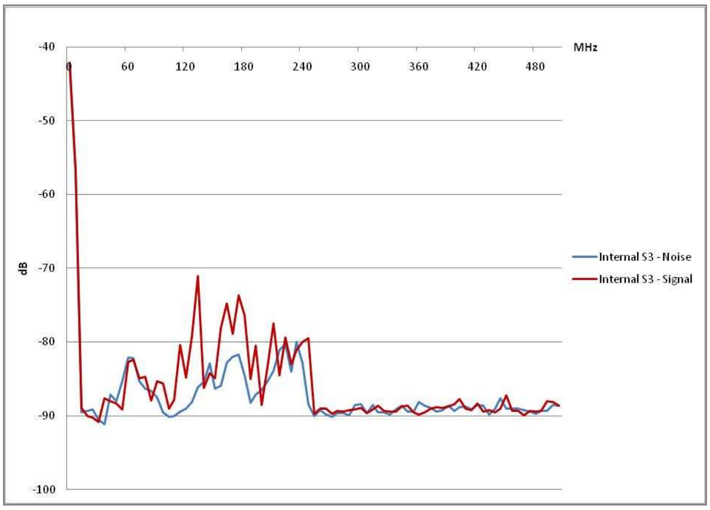

Figure 5.29: Full spectra for internal sensor S3 (at joint)

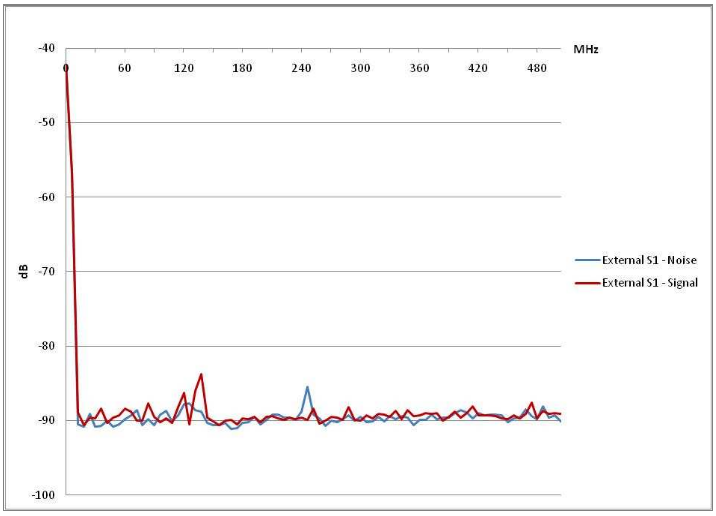

Figure 5.30: Full spectra for external sensor S1 (at termination 1)

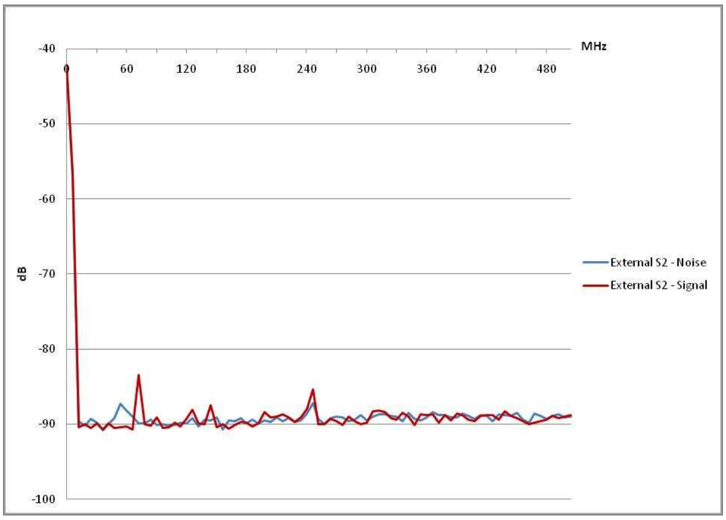

Figure 5.31: Full spectra for external sensor S2 (at termination 2)

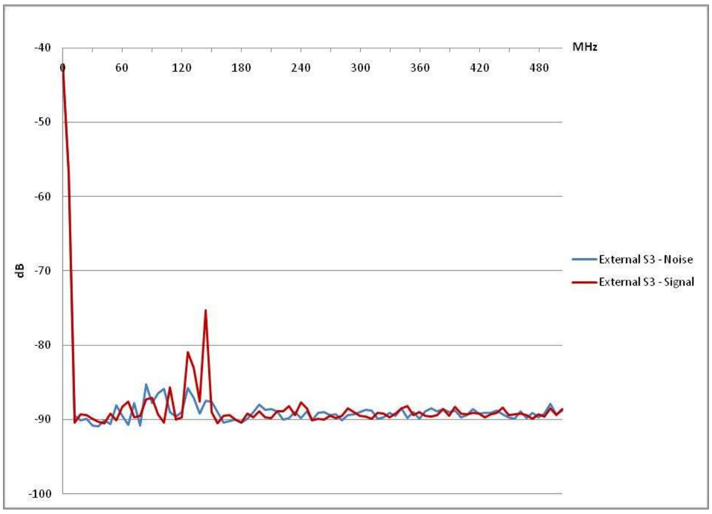

Figure 5.32: Full spectra for external sensor S3 (at joint)

It can be seen from the full spectra of noise and signal that internal sensors show higher sensitivity than external ones. Based on these full spectra three selected frequencies are selected for each sensor and PD patterns are obtained by measuring with 500 sweeps at 60 kV_{peak}. Figure 5.33 shows PD patterns for sensor S1 which placed at termination 1 (approximately 90m from the defect 1).

Internal ***External***

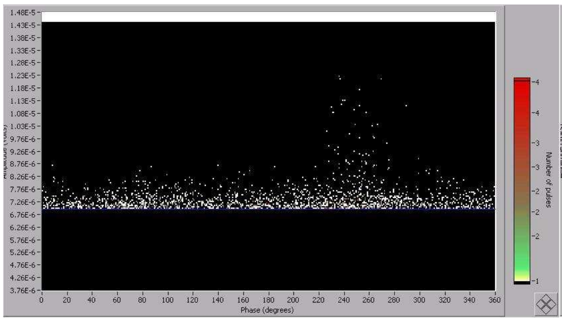

36 MHz

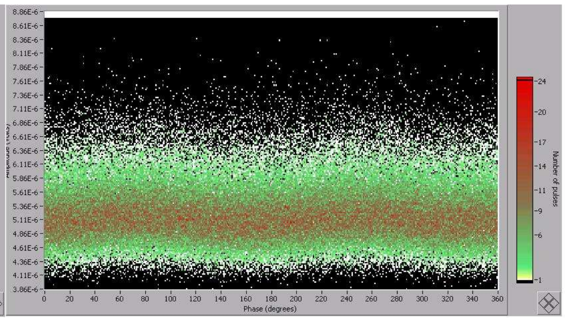

36 MHz

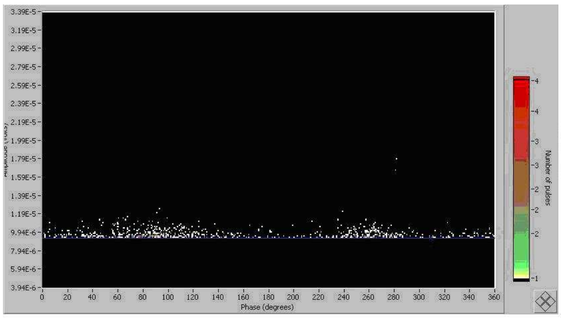

126 MHz

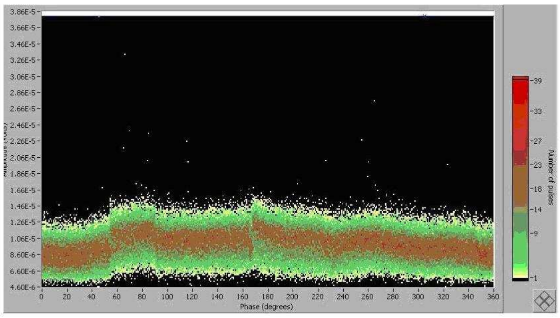

132 MHz

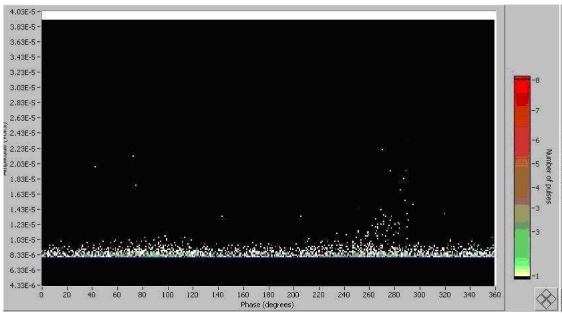

243 MHz

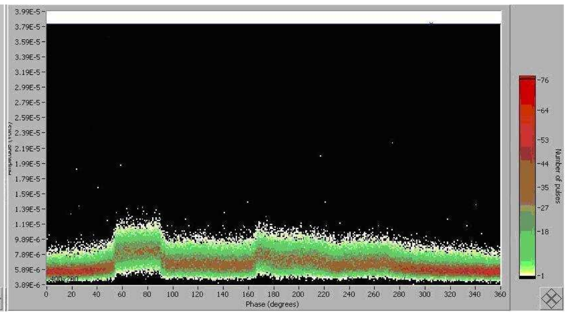

138 MHz

Figure 5.33: PD patterns for sensor S1 (at termination 1) at 60 kV_{peak}

It can be seen that the internal sensors S1 show higher sensitivity than the external sensors. The PD patterns show less PD pulses are measured due to large attenuation of the high frequency PD pulses in distance of 90m. Figure 5.34 shows PD patterns for sensor S2 at termination 2 (approximately 10m from the artificial defect 1).

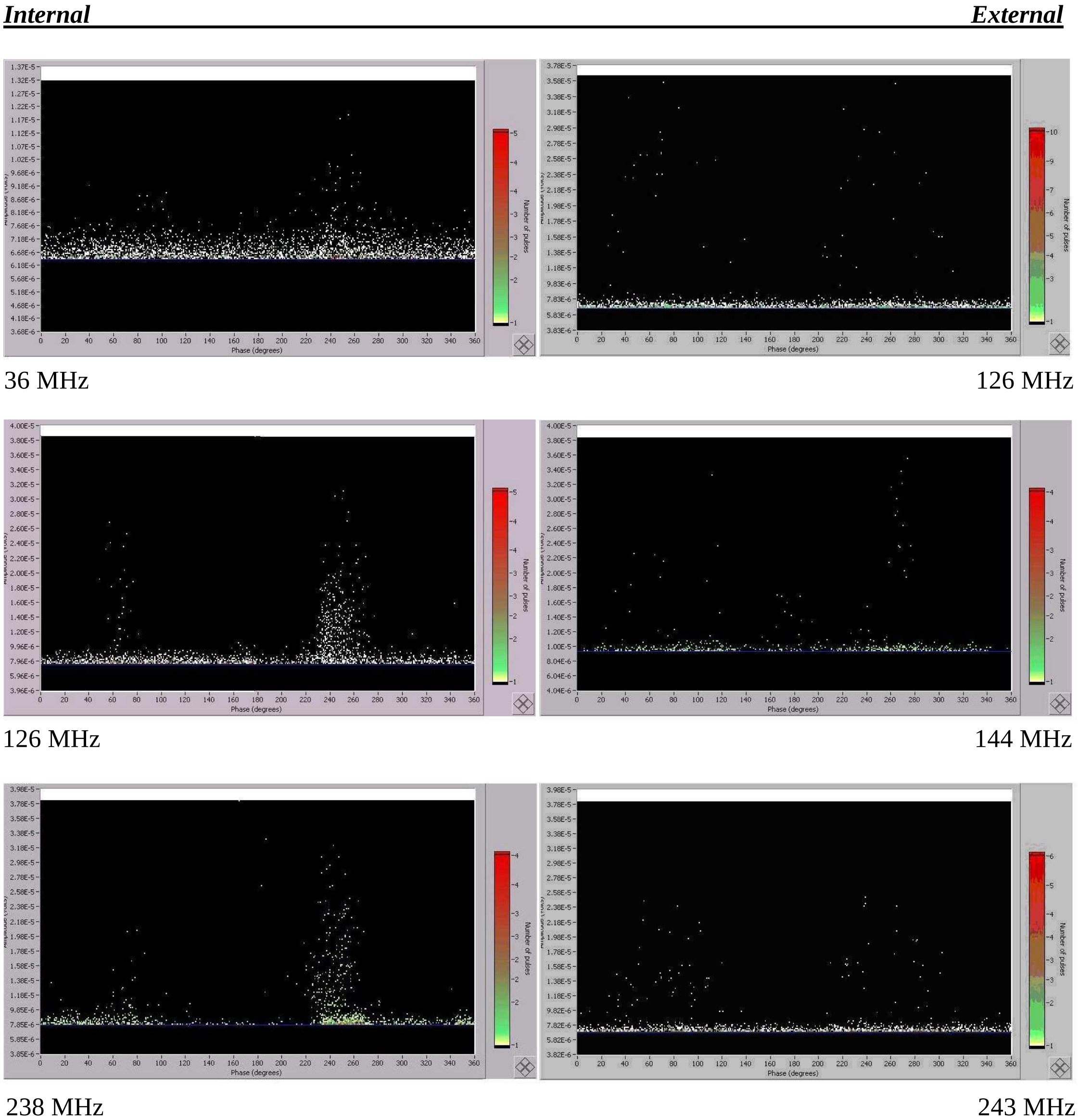

Figure 5.34: PD patterns for sensor S2 (at termination 2) at 60 kVpeak

Similar to the sensor S1, the internal sensors S2 which placed at the termination 2 show higher sensitivity than the external sensors. The PD patterns from sensors S2 show more PD pulses are recorded due to the shorter distance from the artificial defect 1 that results in less attenuation. Figure 5.35 shows results of PD patterns for sensor S3 which located close to the joint.

Internal ***External***

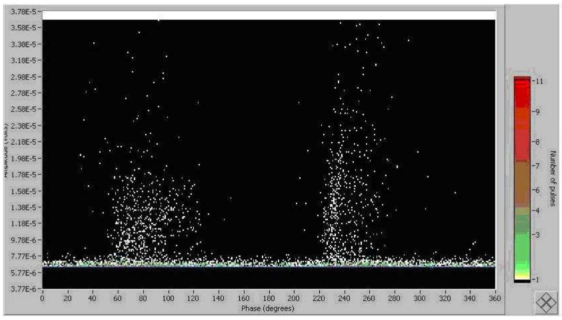

36 MHz

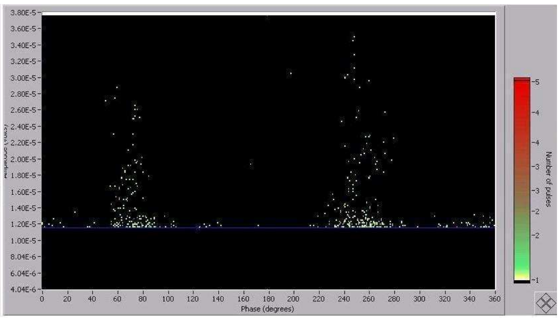

126 MHz

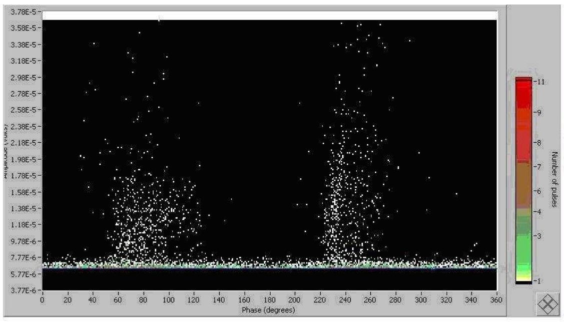

126 MHz

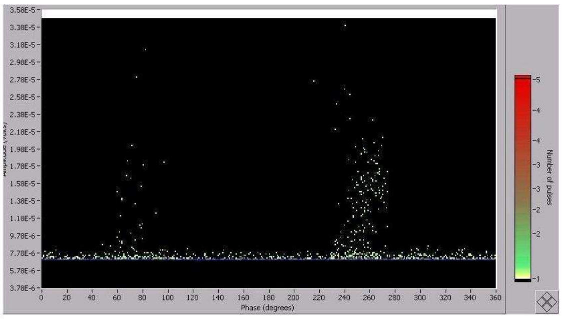

132 MHz

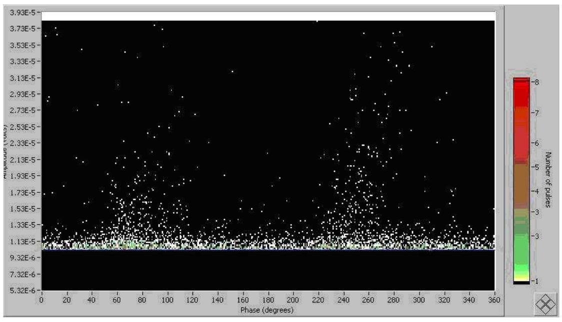

243 MHz

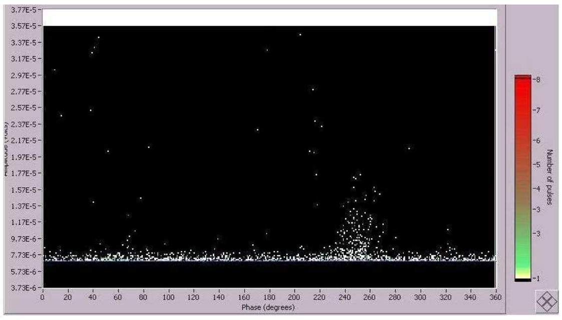

243 MHz

Figure 5.35: PD patterns for sensor S3 (at joint) at 60 kVpeak

Sensor S3 which is located at the joint shows well-defined PD patterns due to close distance between the sensor and the PD source that result in less attenuation of PD pulses. This occurrence related to the large attenuation of the high frequency PD pulses with the distance; therefore in the after-laying test where the main interest is the cable accessory, the sensor should be placed as close as possible to the accessories. Figure 5.36 – 5.38 show the measurement result at lower voltage stress (35 kV_{peak}) for the three centre frequency selection for each sensor.

Internal ***External***

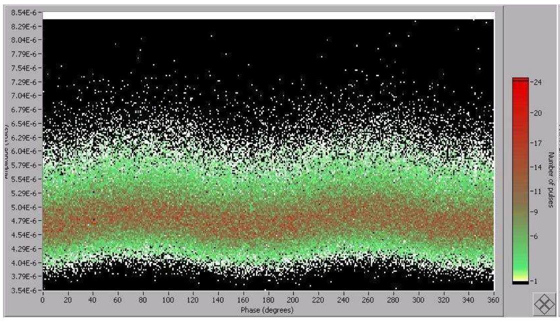
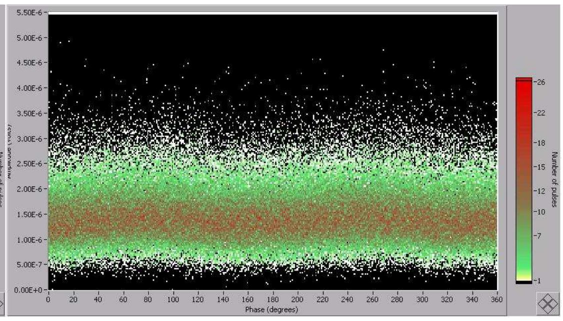

36 MHz 36 MHz

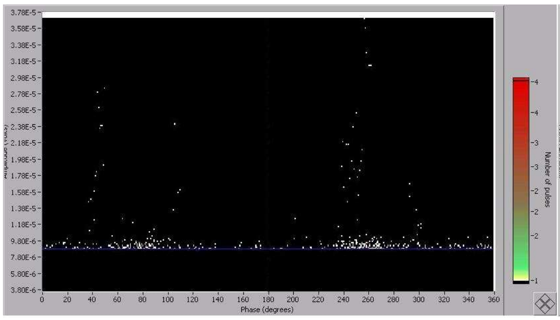
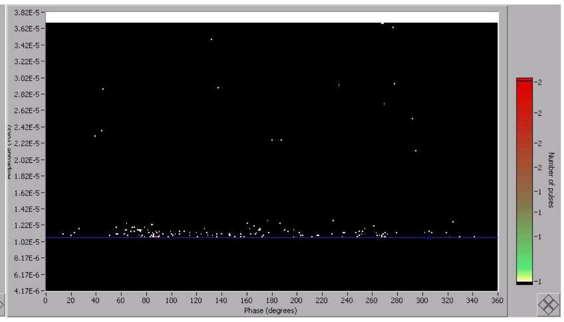

126 MHz 126 MHz

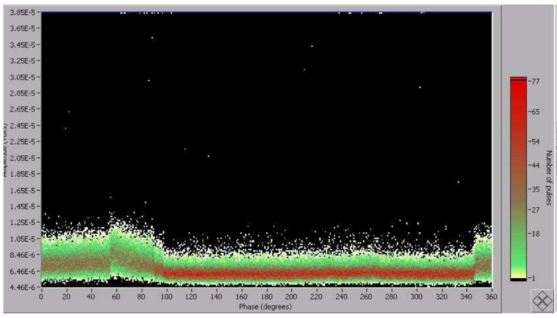
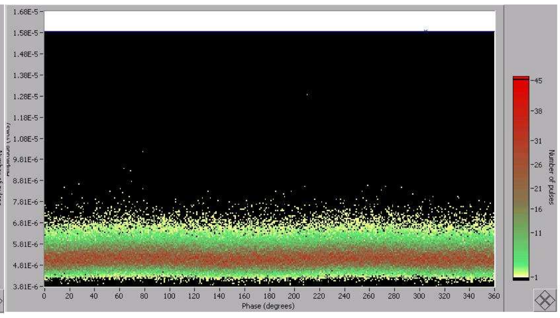

243 MHz 243 MHz

Figure 5.36: PD patterns for sensor S1 (at termination 1) at 35 kVpeak

Internal ***External***

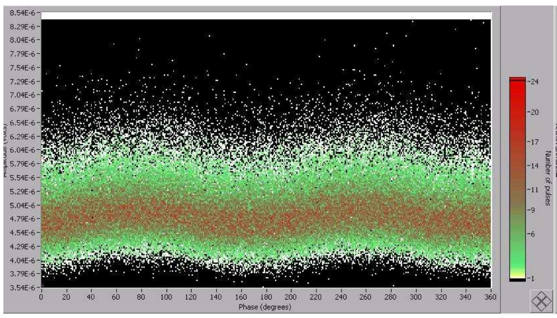
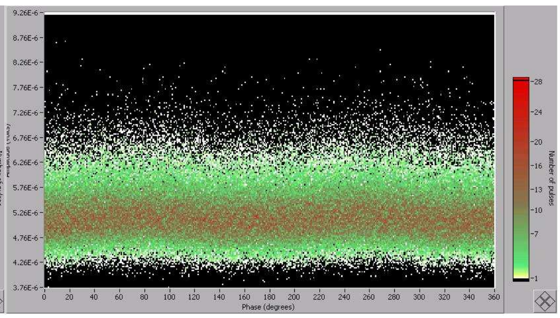

36 MHz 36 MHz

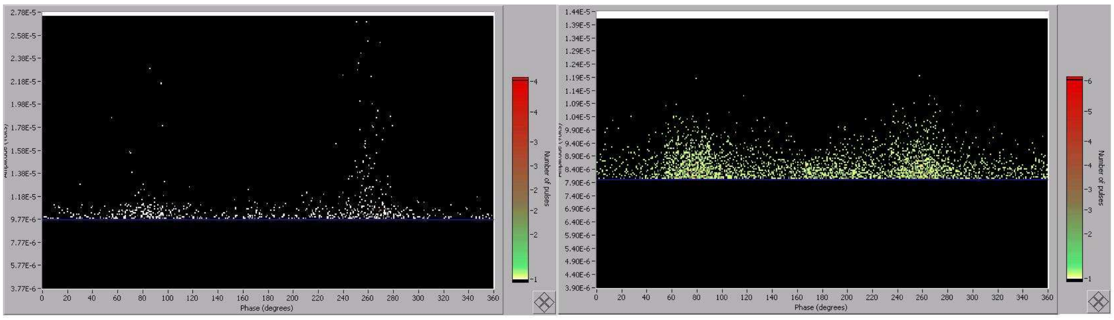

126 MHz 126 MHz

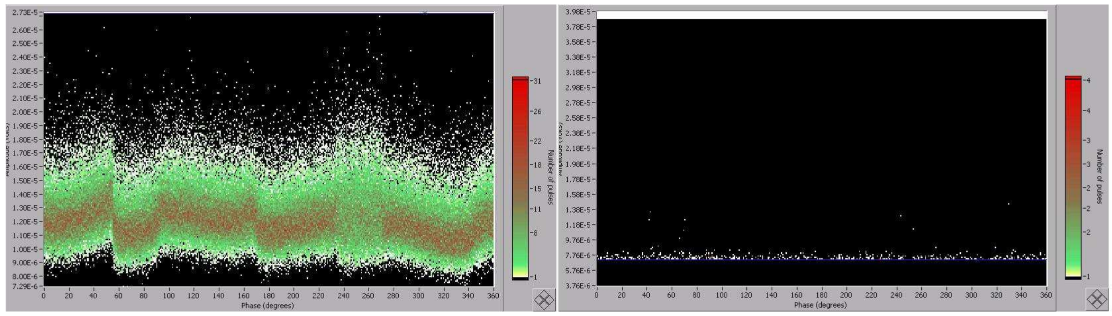

243 MHz 243 MHz

Figure 5.37: PD patterns for sensor S2 (at termination 2) at 35 kVpeak

Internal ***External***

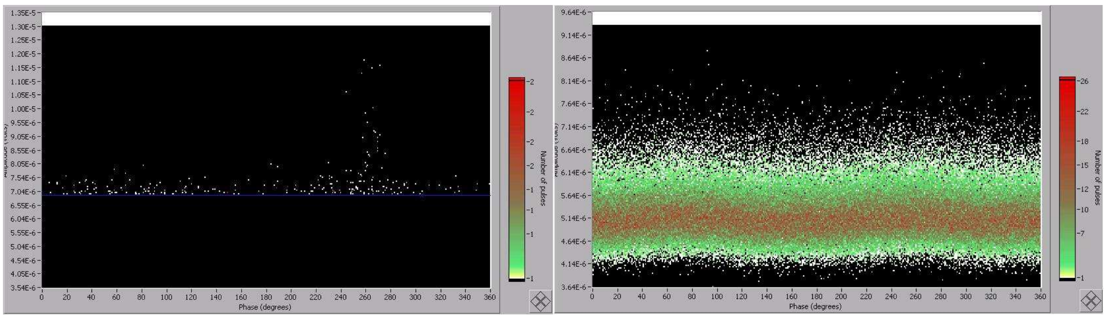

36 MHz 36 MHz

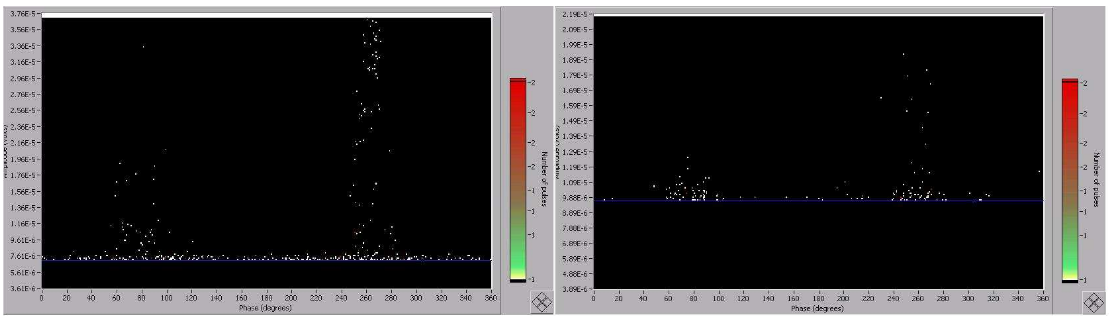

126 MHz 126 MHz

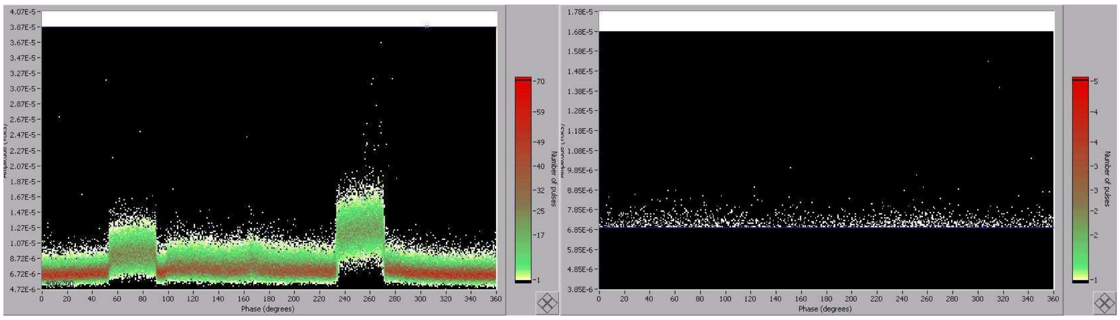

243 MHz 243 MHz

Figure 5.38: PD patterns for sensor S3 (at joint) at 35 kV_{peak}

By applying lower voltage stress, the sensitivity of un-conventional method is decreased due to less PD occurs and only internal sensor S2 and S3 which placed relatively close to the defect source can measured and obtained PD patterns. It can be seen from Figure 5.37 – 5.38 that PD pattern obtained from un-conventional measurement with lower voltage applied (35 kV_{peak}) especially for internal sensor S2 and S3 show similar patterns with PD patterns obtained by using TE 571 PD detector at low voltage stress which is asymmetric and occurred at negative half of the 50Hz AC voltage cycle.

5.5 Conclusion

1. The field plotting simulation shows that by applying the same voltage stress, the electric field enhancement will decrease with the size of the defect 1 and the increase of electric field as function of voltage applied is steeper for the bigger size of defect 1.

2. PD measurements by using 50Hz AC energizing and conventional IEC 60270 PD detection show that changing the size of defect 1 does not give significant change in PDIV and the increase of PD amplitude as a function of voltage is steeper for the bigger size of defect 1.

3. PD measurements by using 50Hz AC energizing and conventional IEC 60270 PD detection show that at low voltage, the asymmetric PD phase-resolved patterns occur at negative half of the 50Hz AC voltage cycle while at higher voltage the PD phase-resolved patterns for defect 1 become symmetrical, occur at both positive and negative period of the 50Hz AC voltage cycle.

4. PD measurements by using 400Hz DAC energizing and conventional IEC 60270 PD detection show that the size of defect does not give significant influence on PDIV and the increase of PD amplitude as a function of voltage applied is steeper for the bigger size of defect 1. The first visible PD pulses occur a negative half of DAC voltage.

5. PD measurements by using 50Hz AC energizing and un-conventional PD detection show that the internal sensors have higher sensitivity than external ones. Well-defined PD patterns are obtained if the positions of sensors are close to the PD source due to less attenuation of high frequency PD pulses. In case of the after-laying test where the main interest is at cable accessories due to the possible presence of installation defects, the sensor should be placed as close as possible to the cable accessories.

6. For un-conventional method, at lower voltage stress around PDIV, PD pattern only obtained from internal sensors which placed relatively close to the defect source. PD patterns obtained from un-conventional method shows similar result with PD patterns obtained from conventional method by using TE 571 PD detector for both lower and higher voltage applied.

Field Plotting Simulation and Experiment Results for Extra Semi-conductive Screen Defect

The second artificial defect used for the investigation is extra semi-conductive screen in the cable joint as shown in Figure 3.13. This artificial defect is considered as defect 2 for further discussion. This chapter describes the effect of the defect 2 and its size in the field enhancement inside the cable system and PD occurrence due to the presence of this defect. PD measurement results by using different energizing and PD detection methods for the critical size of defect 2 are presented in this chapter.

6.1 Field Plotting Simulation Results for Defect 2

As in the case of defect 1, the Ansoft version 9.0 of Maxwell 2D Student Version (SV) is used to simulate the electrostatic field behaviour due to the presence of defect 2 in the cable system. Figure 6.1 shows the cross-section of cable part consists of defect 2 which modelled in the RZ plane similar to the simulation of defect 1.

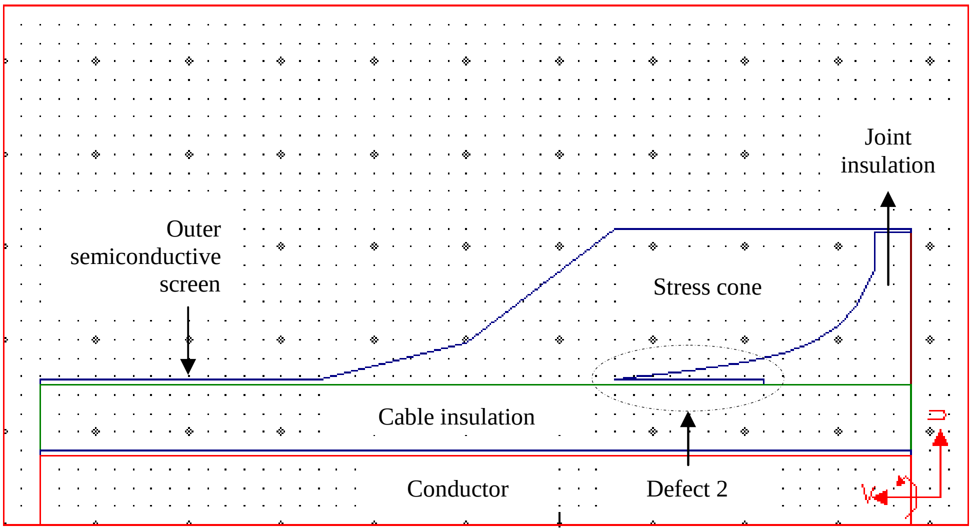

Figure 6.1: The cross-section of cable part which consist of defect 2

Material properties which are used in simulation of defect 1 are also used for modelling the defect 2. The defect 2 is assumed has a thickness of 1.1mm and 40mm length.

Investigation the effect of electric field behaviour in the cable system due to the presence of the defect 2 and its size is applied by making a comparison of electric field plotting for normal situation without the defect 2 and the situation with the presence of defect 2 for several sizes.

6.1.1 Electric Field Behaviour without Defect 2

The radial electric field behaviour in the cable system is not uniformly distributed which is determined by the equation (2.1) where the highest electric field presents at the area close to the high-voltage conductor while the lower electric field occurs at area close to the outer semi-conductive screen of the cable.

In order to see the effect of defect 2 in the cable joint, the comparison of of normal situation without defect 2 and condition with the defect 2 for several voltage stresses are made. Figure 6.2 – 6.4 show the result of electric field plotting simulation for normal condition for voltage stress 30 kV_{peak}, 122.5 kV_{peak} ($1U_0$) and 208.2 kV_{peak} ($1.7U_0$).

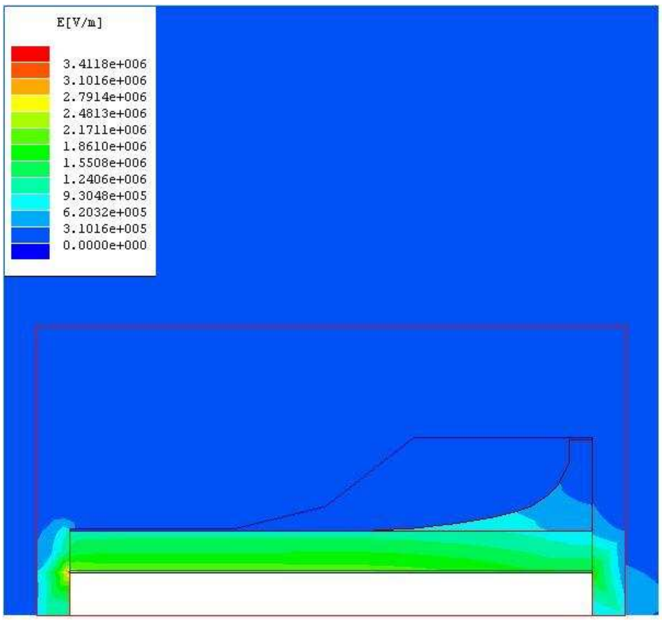

Figure 6.2: Electric field plotting for condition without defect 2 at 30 kV_{peak}

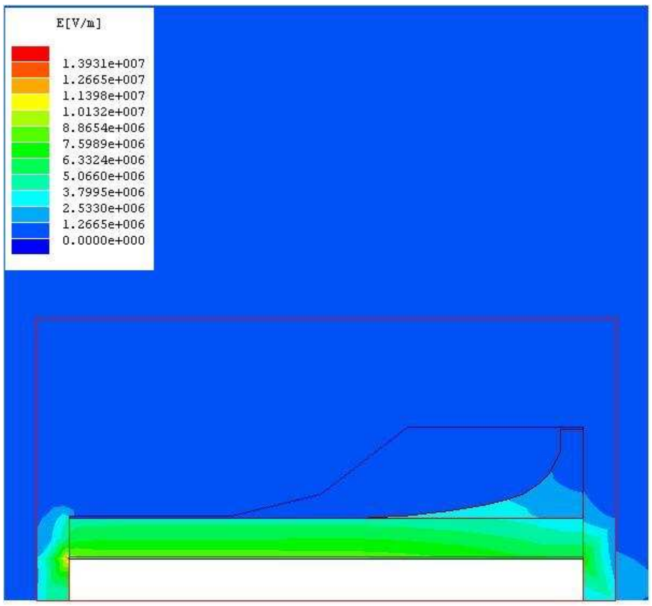

Figure 6.3: Electric field plotting for condition without defect 2 at U_0 (122.5 kV_{peak})

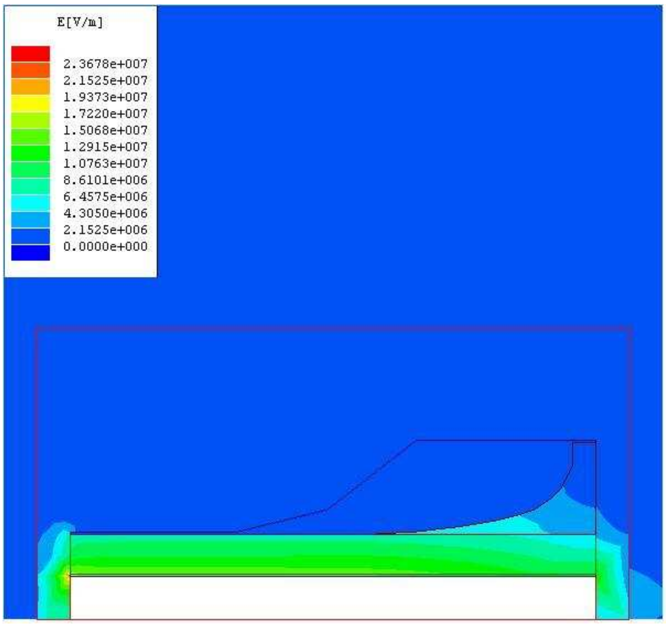

Figure 6.4: Electric field plotting for condition without defect 2 at $1.7U_0$ (208.2 kV_{peak})

It can be seen from the simulation for normal situation that the electric field in the area where the defect 2 will be presented are quite low. The electric field for normal situation at 30 kV_{peak}, 122.5 kV_{peak} and 208.2 kV_{peak} are approximately 1.24 kV/mm, 5.06 kV/mm and 8.61 kV/mm respectively. The presence of defect 2 in the form of extra semi-conductive screen at the boundary between cable insulation and joint insulation will change the electric field distribution and results in the field enhancement at the end of the defect 2, similar to the defect 1. In order to see the effect of the size of defect 2, several simulations at different size of defect 2 are applied.

6.1.2 Electric Field Behaviour for Defect 2 Size 10mm

As described in chapter 3, the presence of extra semi-conductive screen in the cable joint changes the normal electric field and result in the field enhancement at the edge of extra semi-conductive screen. First size of defect 2 to be simulated is 10mm and the starting point of this defect is at the transition point between the end of semi-conductive screen and the start of stress cone. The result of electric field plotting simulation for voltage stress 30 kV_{peak} is shown in Figure 6.5.

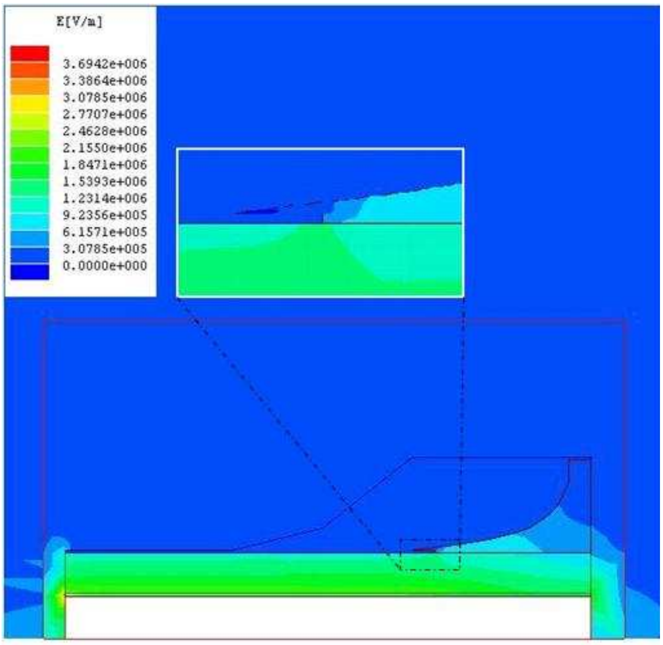

Figure 6.5: Electric field plotting for defect 2 size 10mm at 30 kV_{peak}

The simulation results shows that the presence of defect 2 changes the normal electric field distribution in the cable joint and field concentration occurs at the edge of extra semi-conductive screen and reached 1.54 kV/mm. Figure 6.6 and 6.7 show the electric field behaviour for voltage applied $1U_0$ (122.5 kV_{peak}) and $1.7U_0$ (208.2 kV_{peak}).

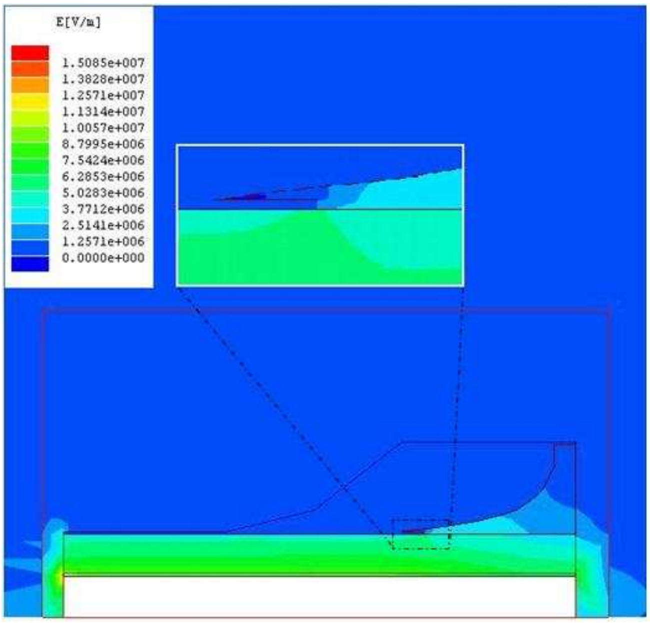

Figure 6.6: Electric field plotting for defect 2 size 10mm at U_0 (122.5 kV_{peak})

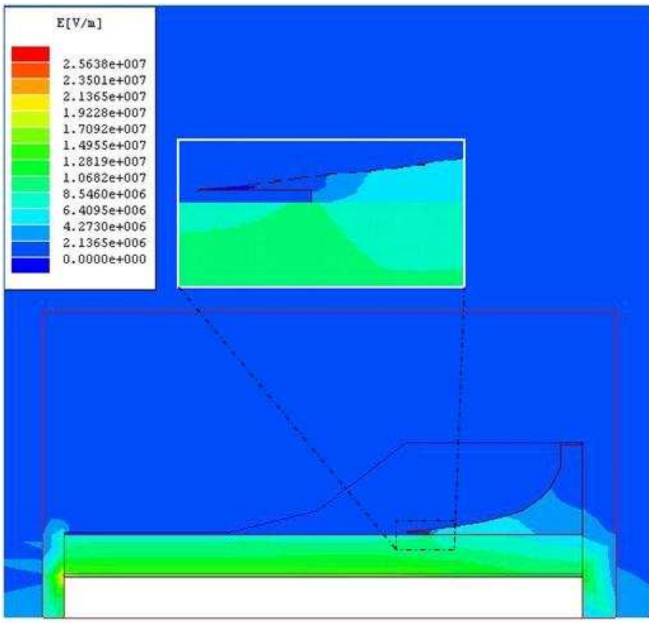

Figure 6.7: Electric field plotting for defect 2 size 10mm at $1.7U_0$ (208.2 kV_{peak})

6.1.3 Electric Field Behaviour for Defect 2 Size 20mm

The effect of different size of defect 2 is investigated by increasing the size of defect 2 from 10mm to 20mm. The simulation result for defect 2 size 20mm at voltage stress 30 kV_{peak} is shown in Figure 6.8.

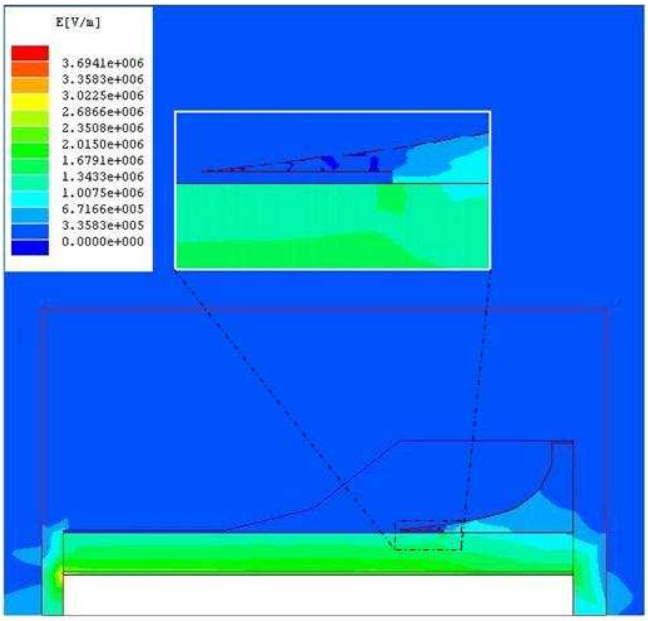

Figure 6.8: Electric field plotting for defect 2 size 20mm at 30 kV_{peak}

The simulation result shows that the longer size of defect 2 produces higher field enhancement at the edge of semi-conductive screen which reached 1.68 kV/mm for voltage stress 30 kV_{peak}. Figure 6.9 and 6.10 show the electric field behaviour for voltage stress $1U_0$ (122.5 kV_{peak}) and $1.7U_0$ (208.2 kV_{peak}).

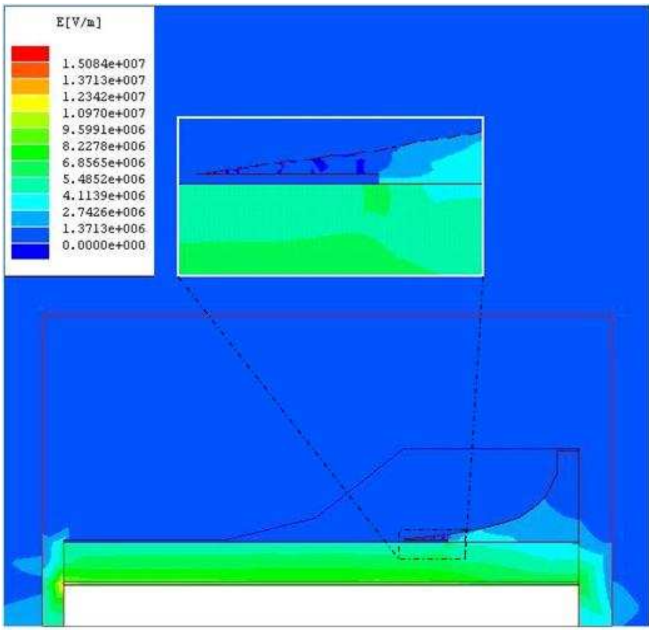

Figure 6.9: Electric field plotting for defect 2 size 20mm at U_0 (122.5 kV_{peak})

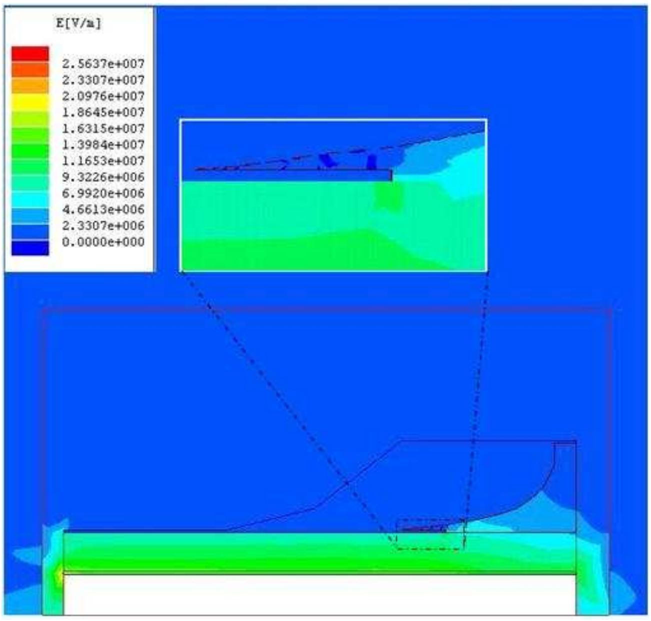

Figure 6.10: Electric field plotting for defect 2 size 20mm at 1.7U_0 (208.2 kV_{peak})

6.1.4 Electric Field Behaviour for Defect 2 Size 30mm

Furthermore, the size of defect 2 is increased to 30mm to see the effect if the defect 2 becomes longer. Figure 6.11 shows the simulation result for defect 2 size 30mm at applied voltage stress 30 kV_{peak}.

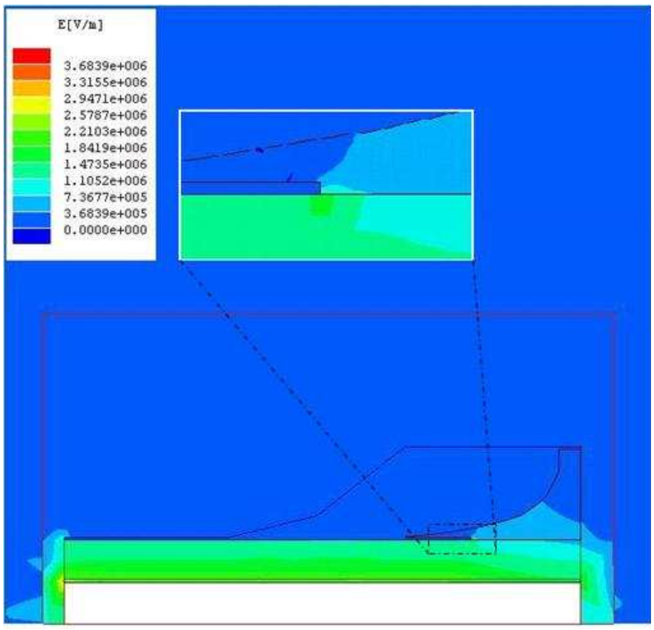

Figure 6.11: Electric field plotting for defect 2 size 30mm at 30 kV_{peak}

It can be seen that the extension of defect 2 results in higher electric field enhancement at the edge of extra semi-conductive screen where it reaches 1.84 kV/mm for voltage stress 30 kV_{peak}. Figure 6.12 and 6.13 show the field plotting simulation for voltage applied $1U_0$ (122.5 kV_{peak}) and $1.7U_0$ (208.2 kV_{peak}).

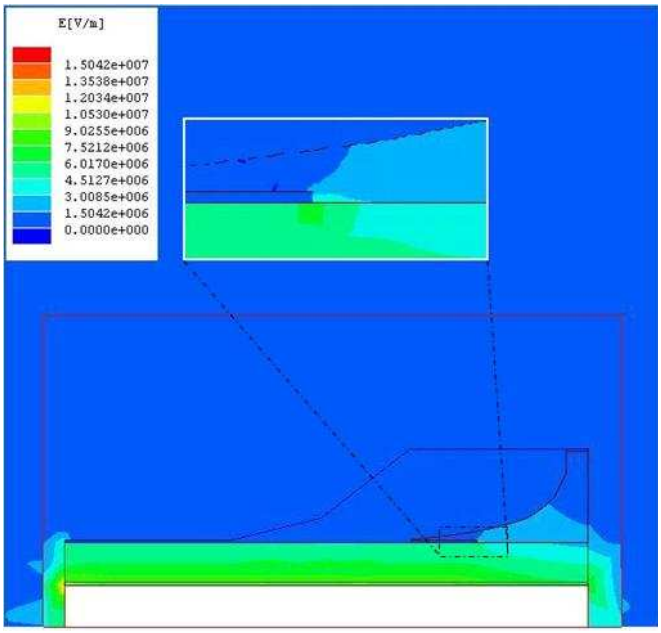

Figure 6.12: Electric field plotting for defect 2 size 30mm at U_0 (122.5 kV_{peak})

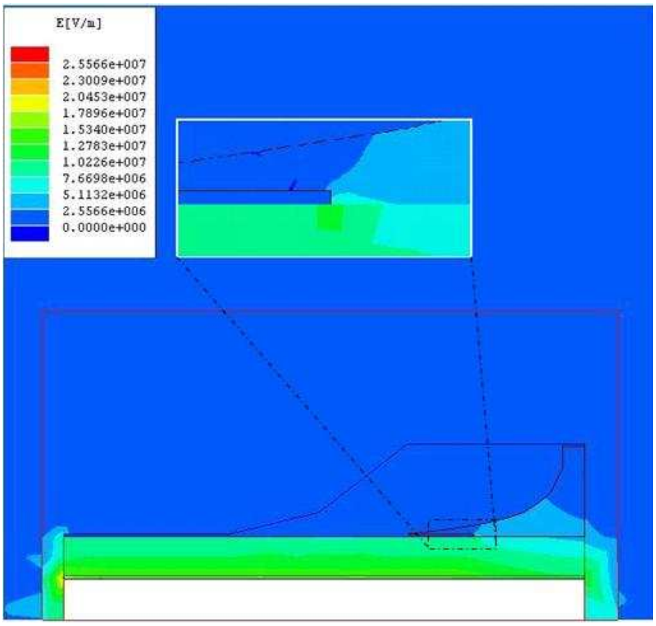

Figure 6.13: Electric field plotting for defect 2 size 30mm at $1.7U_0$ (208.2 kV_{peak})

6.1.5 Electric Field Behaviour for Defect 2 Size 40mm

The last size of defect 2 for investigation is 40mm. The field enhancement due to this size of defect 2 for voltage stress 30 kV_{peak} is shown in Figure 6.14.

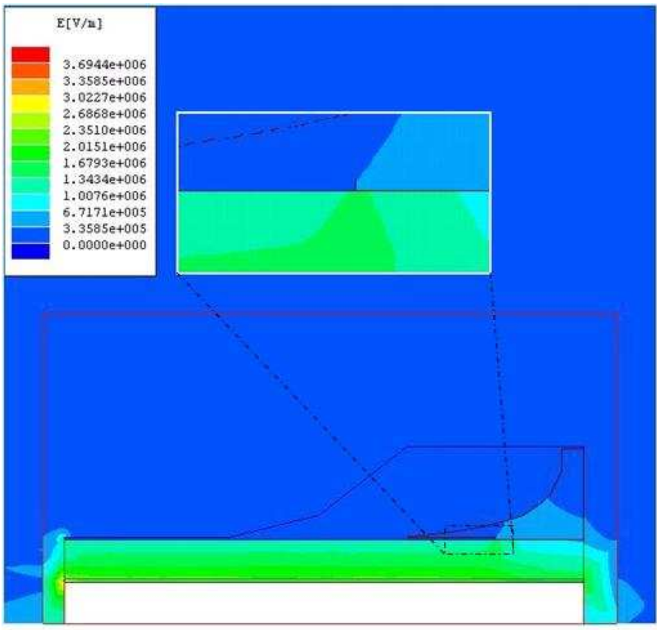

Figure 6.14: Electric field plotting for defect 2 size 40mm at 30 kV_{peak}

The simulation result shows similar trend as previous simulation that the increase of the size of defect 2 results in the higher field enhancement at the edge of extra semi-conductive screen. Figure 6.15 and 6.16 show simulation results of defect 2 size 40mm for voltage applied $1U_0$ (122.5 kV_{peak}) and $1.7U_0$ (208.2 kV_{peak}).

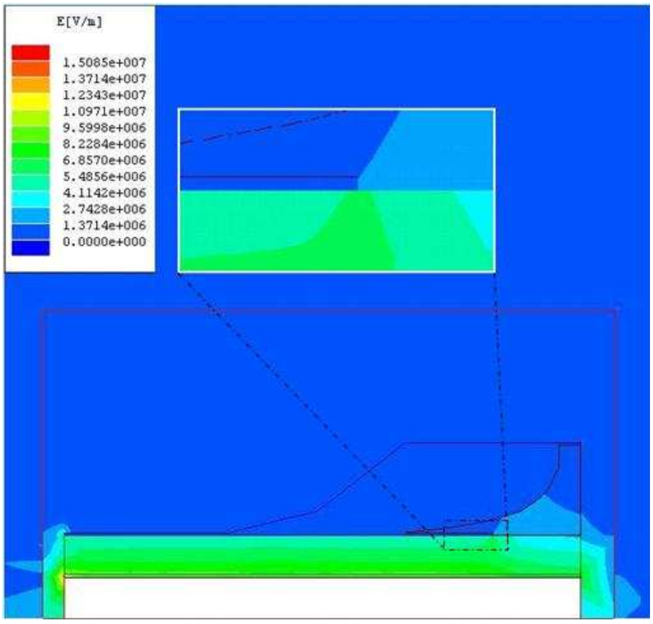

Figure 6.15: Electric field plotting for defect 2 size 40mm at U_0 (122.5 kV_{peak})

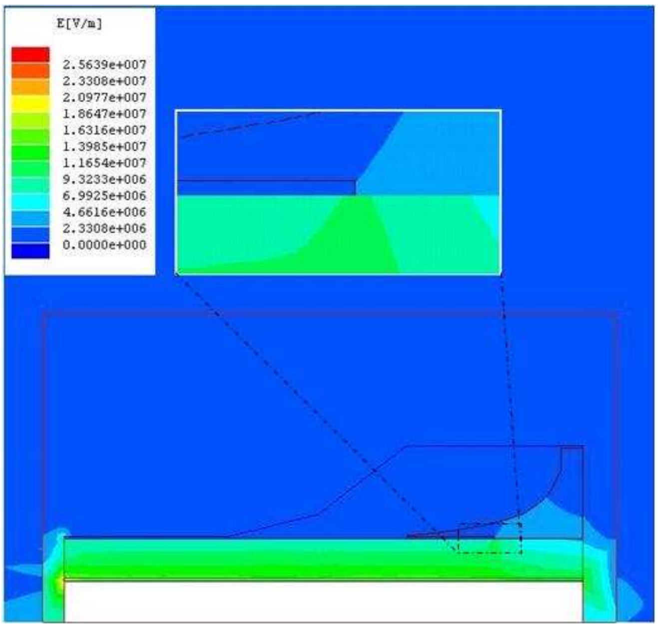

Figure 6.16: Electric field plotting for defect 2 size 40mm at $1.7U_0$ (208.2 kV_{peak})

6.1.6 Comparison of Simulation Result for Four Sizes of Defect 2

Field plotting simulation for different size of defect 2 shows that the size of the defect determines the electric field enhancement at the edge of extra semi-conductive screen. The field enhancement will increase with the size of the defect 2. Table 6.1 shows the result of simulation for different size of defect 2 at several values of voltage stress.

Table 6.1

Electric Field for Different Situation of Defect 2 at Different Voltage Stress

Voltage Stress (kV_{peak})	Electric Field (kV/mm) for Each Condition				
	No defect	Defect 10mm	Defect 20mm	Defect 30mm	Defect 40mm
30	1.24	1.54	1.68	1.84	2.02
122.5 (U_0)	5.06	6.28	6.86	7.52	8.23
208.2 ($1.7U_0$)	8.61	10.68	11.65	12.78	13.98

The plot of electric field as a function of voltage stress up to $1.7U_0$ for different size of defect 2 is shown in Figure 6.17. The value of electric field without the defect 2 is taken from the electric field which occurred at the boundary between the cable insulation and the joint insulation where the defect 2 will be presented. It can be seen that the presence of the defect 2 results in high electric field on the boundary between cable and joint insulation and the field enhancement is higher for bigger size of defect 2. Similar to the defect 1, the increase of electric field as function of voltage applied is steeper for the bigger size of defect 2.

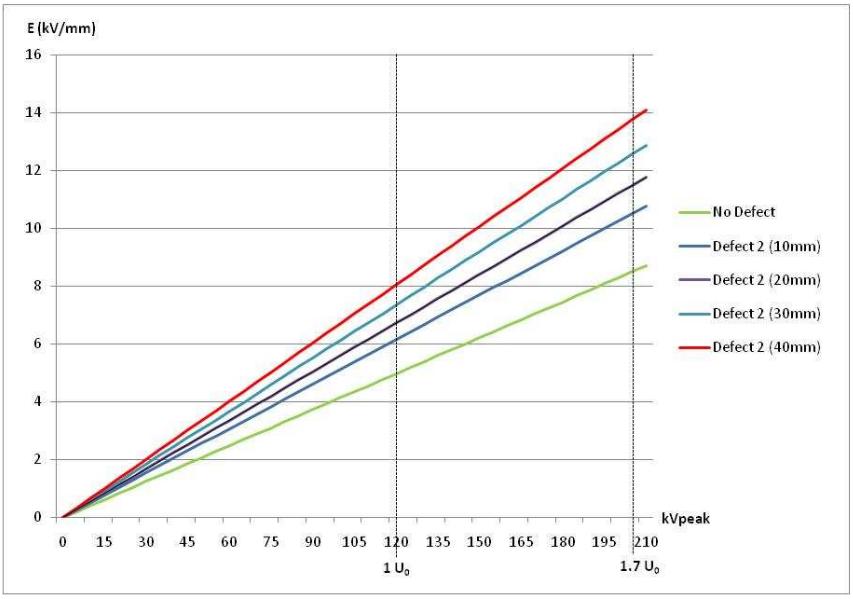

Figure 6.17: Plot of electric field as a function voltage applied for defect 2

It can be concluded from the result of field plotting of defect 2 that the situation will be more critical for longer size of defect 2 due to higher electric field enhancement. Therefore the defect 2 size 40mm is constructed at the test set-up as depicted in Figure 3.13 for the investigation by using different energizing and PD detection methods.

6.2 Measurement Results by Using 50Hz AC Energizing and Conventional IEC 60270 PD Detection

As in the case of defect 1, PD measurement on defect 2 size 40 mm by using TE 571 PD detector is performed by using test set-up as shown in Figure 4.8. Calibration based on IEC 60270 standard is applied before PD measurement is started. PD measurement is performed by slowly increasing the applied voltage stress to find the PDIV where the PD starts to occur.

It was found that no PD occurs in the cable system with voltage stress up to 60 kV_{peak} which is applied for approximately 1 hour and then increased up to 80 kV_{peak} for short duration. The voltage stress is limited due to current limitation in feeding cable of transformer and transformer itself. Plot of PD magnitude in pC as a function of voltage applied up to 80 kV_{peak} is shown in Figure 6.18.

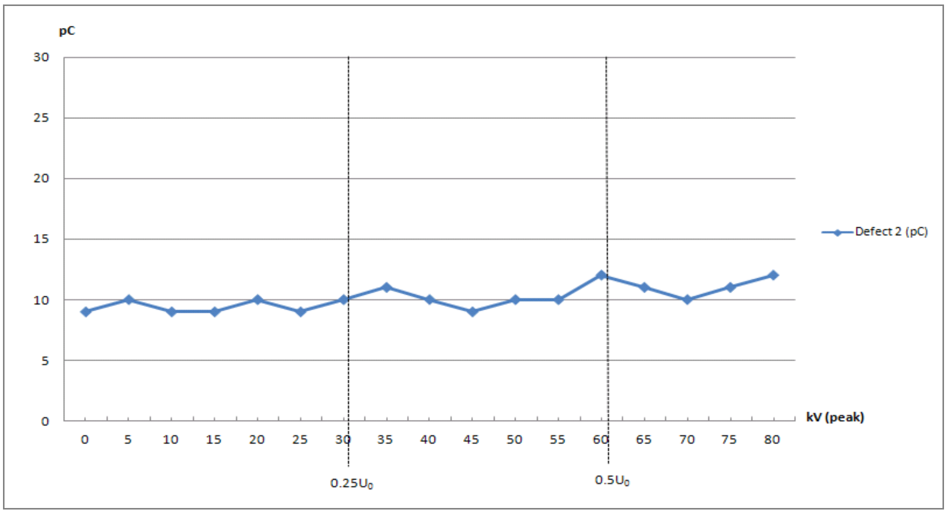

Figure 6.18: PD magnitude – voltage applied for defect 2 by using TE 571

The measurement result for voltage stress 80 kV_{peak} with 2 minutes duration is shown in Figure 6.19.

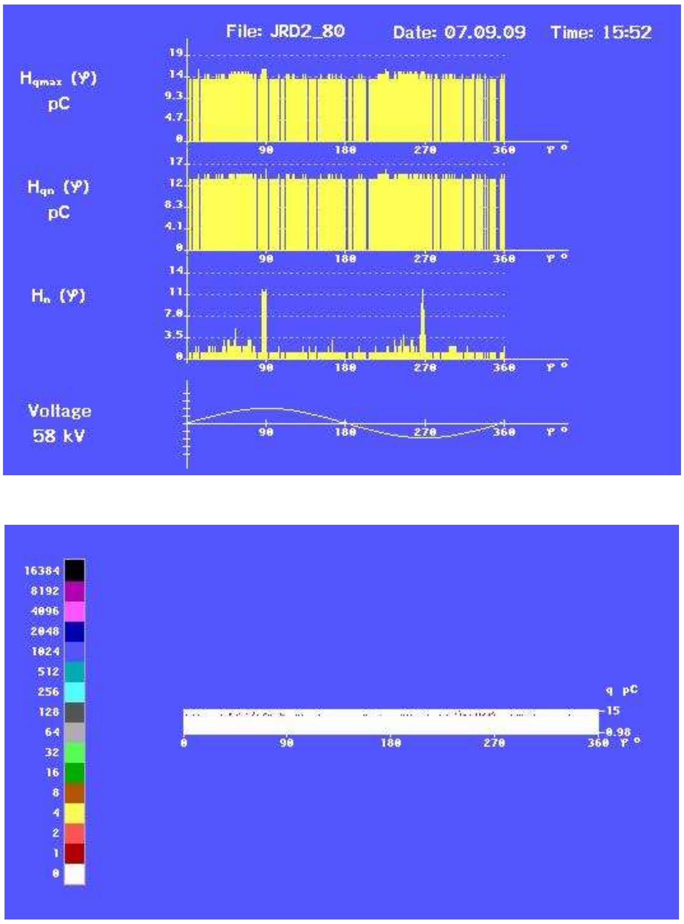

Figure 6.19: Measurement results at 80 kV_{peak} by using TE 571

6.3 Measurement Results by Using 400Hz DAC Energizing and Conventional IEC 60270 PD Detection

PD measurement by using 400Hz DAC energizing and conventional IEC 60270 PD detection is performed by using OWTS HV150 with the test set-up as shown in Figure 4.9. The resonant frequency of the test circuit was around 421Hz. Calibration as mentioned in IEC 60270 standard is applied to the test circuit before the PD measurement is started. By using 0 kV DAC shot, the noise level is measured and reached 10 - 15 pC. The measurement is performed by applying 2 DAC shots for each 5 kV step up to 80 kV_{peak}. Figure 6.20 shows the plot of PD amplitude as a function of voltage applied up to 80 kV_{peak}.

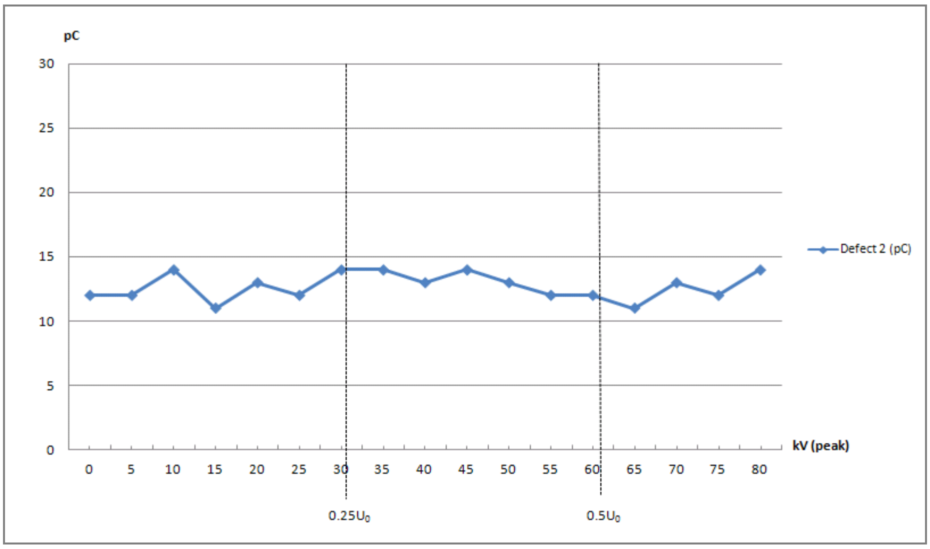

Figure 6.20: Plot of PD amplitude as a function of voltage applied up to 80 kV$_{peak}$

The measurement result shows similar result as in previous measurement with TE 571 PD detector where no PD occurs up to voltage stress 80 kV$_{\text{peak}}$. Figure 6.21 shows PD measurement results at 80 kV$_{\text{peak}}$.

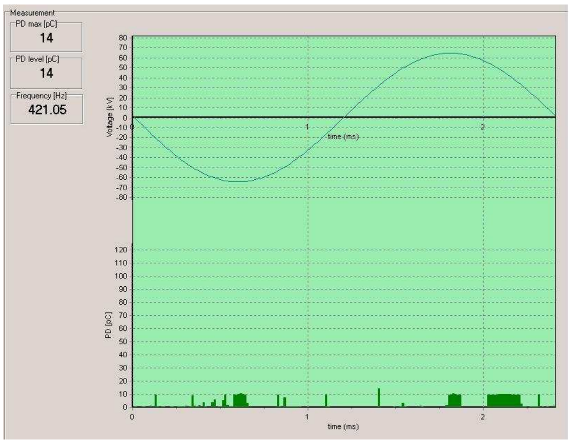

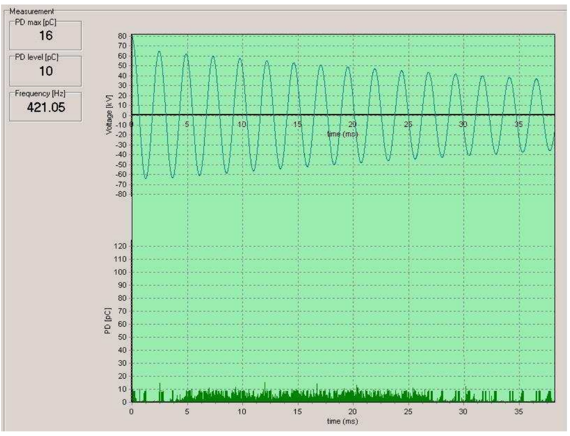

Figure 6.21: PD measurement on defect 2 at 80 kV$_{peak}$

6.4 Measurement Results by Using 50Hz AC Energizing and Un-Conventional PD Detection

The un-conventional measurement is performed by using test set-up as shown in Figure 4.10. Based on the measurement results from TE 571 PD detector and OWTS HV150 that no PD obtained from the defect 2 therefore the un-conventional PD measurement is applied only at the internal sensor S3 which is considered as the most sensitive sensor due to the shortest distance from the defect 2.

Similar to the defect 1 measurement, the “full span” of background noise and PD pulses from the artificial defect 2 are obtained for internal sensor S3 to determine the centre frequency (CF) for PD measurement. Figure 6.12 shows full spectra of background noise and signal for internal sensor S3 up to 500 MHz. Noise spectrums is measured without voltage applied while PD spectrum is obtained by applying 50Hz AC voltage 60 kV_{peak} to the termination 1.

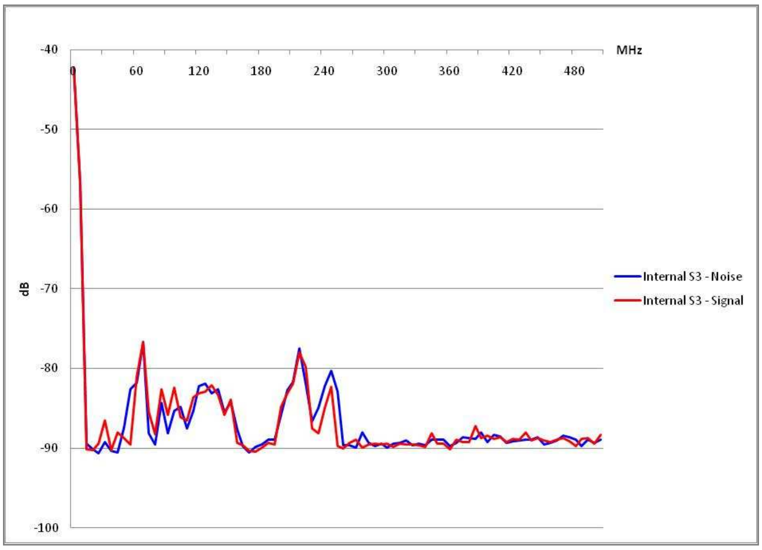

Figure 6.12: Full spectra of noise and signal for internal sensor S3 (at cable joint)

It can be seen that the full spectra of noise and PD signal are relatively same due to no PD occurrence in the cable joint consists of defect 2 size 40mm. Figure 6.13 shows PD pattern obtained at 30 MHz with 500 sweeps measurement.

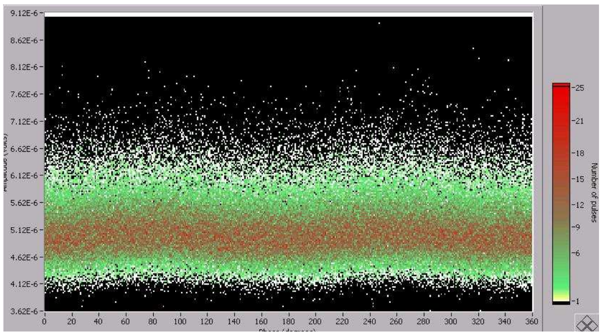

Figure 6.13: PD pattern at 30 MHz for internal sensor S3 at 60 kV$_{peak}$

As in conventional measurement, there is also no PD found by the un-conventional PD detection for the defect 2.

Measurements on defect 2 by using different energizing and PD detection methods show that the presence of the defect 2 does not produce PD up to relatively high voltage stress applied. This phenomenon is completely different than the defect 1 which produces relatively intensive PD for low voltage stress applied. The difference is related to the higher breakdown strength of dielectric combination in the case of defect 2 than in the case of defect 1. In the case of defect 1, there is solid-air dielectric interface which has low breakdown strength than solid-solid dielectric interface in the case of defect 2. Furthermore, the presence of air in the interface between cable insulation and joint insulation in case of defect 2 is restricted by the elastic properties of synthetic rubber of joint insulation and the use of vacuum pump when inserting the cable end into the joint body. However, the simulation results show that this defect produce a field enhancement that probably produces PD activities for higher voltage applied. Therefore, PD measurement at higher voltage applied, e.g. 1.7U_0 as in the case of voltage withstand test is necessary.

6.5 Conclusion

1. Field plotting simulation for different size of defect 2 shows that the size of the defect will determine the electric field enhancement which occurs at the edge of extra semi-conductive screen. The field enhancement will increase with the size of the defect 2.

2. PD measurements on defect 2 size 40mm by using different energizing and PD detection methods show that no PD occur up to relatively high voltage stress applied.
3. The defect 2, extra semi-conductive screen, is indicated as less critical than the defect 1 due to the higher breakdown strength of dielectric combination in the case of defect 2. In the case of defect 2, the presence of air in the interface between cable insulation and joint insulation is restricted by the elastic properties of synthetic rubber of joint insulation and the use of vacuum pump when inserting the cable end into the joint body.
4. Even though there was no PD activity up to 80 kV_{peak}, the simulation results show that the defect 2 produces field enhancement that probably results in PD activities for higher voltage applied, therefore PD measurements at higher voltage applied, e.g. $1.7U_0$ as in the case of voltage withstand test for after-laying test is necessary.

CHAPTER 7

Field Plotting Simulation and Experiment Results for Electrode-Bounded Cavity Defect

The last artificial defect for the investigation is electrode-bounded cavity between cable insulation and outer semi-conductive screen on the area close to the cable joint as shown in Figure 3.15. This artificial defect is considered as defect 3 for further discussion. In this chapter the result of field plotting simulation for condition without and with the presence of defect 3 in the cable system and the PD measurement results by using different energizing and PD detection methods are presented.

7.1 Field Plotting Simulation Results for Defect 3

Similar to the defect 1 and 2, the Ansoft version 9.0 of Maxwell 2D Student Version (SV) is used to investigate the electrostatic field behaviour due to the presence of defect 3 in the cable system. Figure 7.1 shows the cross-section of cable part consists of defect 2 which modelled in the RZ plane similar to the case of defect 1 and 2.

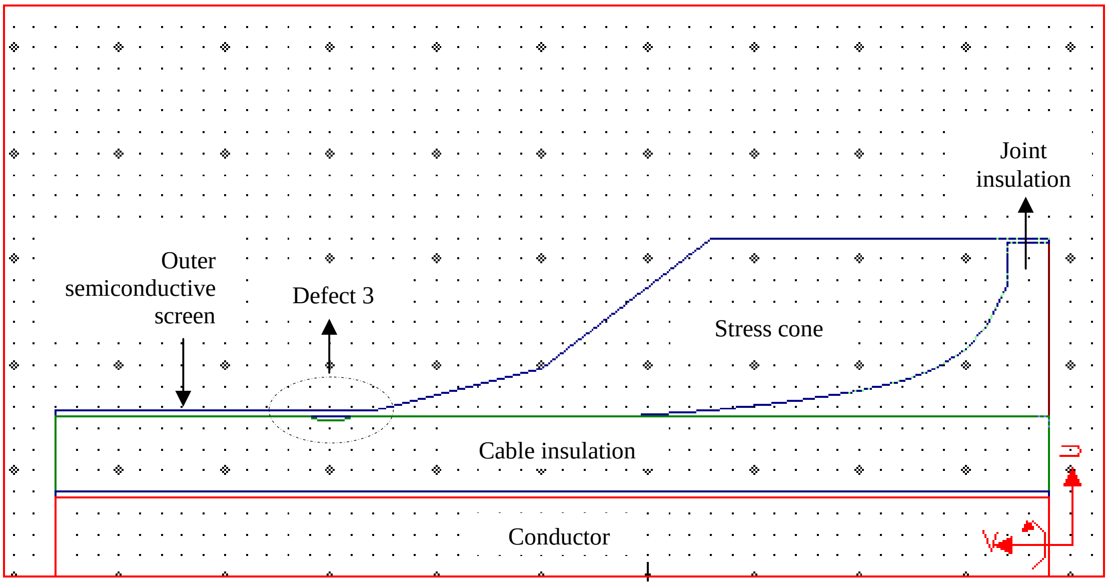

Figure 7.1: The cross-section of cable part which consist of defect 3

The simulation model for the defect 3 has equal material properties as used in model for the defect 1 and 2. The defect 3, electrode-bounded cavity, is assumed filled by air with the relative permittivity (ε) equal to 1 and has a dimension of 10mm length and

1mm depth. In real test set-up, the defect 3 is much more complicated in dimension since it made by scratching the cable insulation and then covering it with the copper tape.

Investigation the effect of electric field behaviour in the cable system due to the presence of the defect 3 is applied by making a comparison of electric field plotting for normal situation without the defect 3 and the situation with the presence of defect 3.

7.1.1 Electric Field Behaviour without Defect 3

As already discussed in section 5.1.1, the radial electric field behaviour in the cable system is not uniform and the highest electric stress will be located in the area close to the high-voltage conductor while the lower stress will be located in area close to the outer semi-conductive screen as depicted in Figure 7.2. The PDIV for defect 3 was found at 50 kV_{peak} from the PD measurement by using TE 571 PD detector. Therefore this voltage stress is used for the comparison of field plotting simulation for both situations, normal and with the presence of defect 3. The field plotting result for simulation without the defect 3 at voltage applied 50 kV_{peak} is shown in Figure 7.2. Simulation for normal situation shows radial field distribution as described by equation (2.1).

Figure 7.3 and 7.4 show the electric field behaviour for voltage applied $1U_0$ (122.5 kV_{peak}) and $1.7U_0$ (208.2 kV_{peak}). When the defect occurs in the form of electrode-bounded cavity, the electric field distribution changes and the electric field inside the cavity will much higher than the electric field in rest part of cable insulation. If this field enhancement is higher than the breakdown strength of gas inside the cavity then the breakdown of gas will occur and produce PD pulses that can be measured by PD detector.

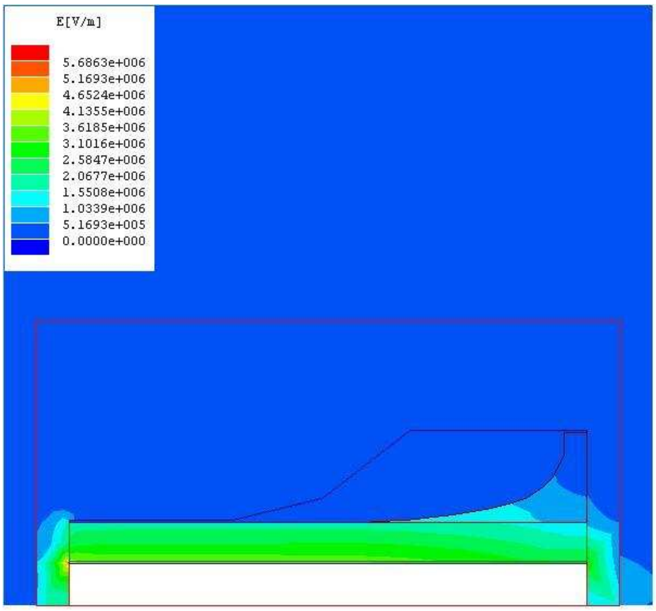

Figure 7.2: Electric field plotting for condition without defect 3 at 50 kV_{peak}

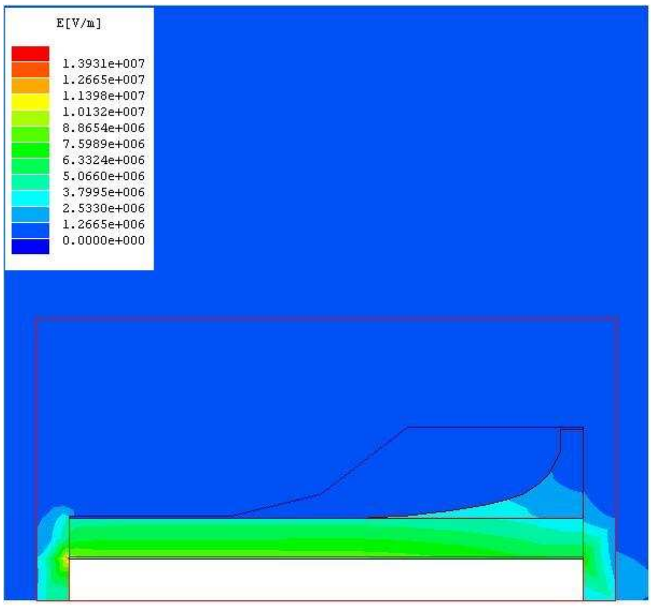

Figure 7.3: Electric field plotting for condition without defect 3 at U_0 (122.5 kV_{peak})

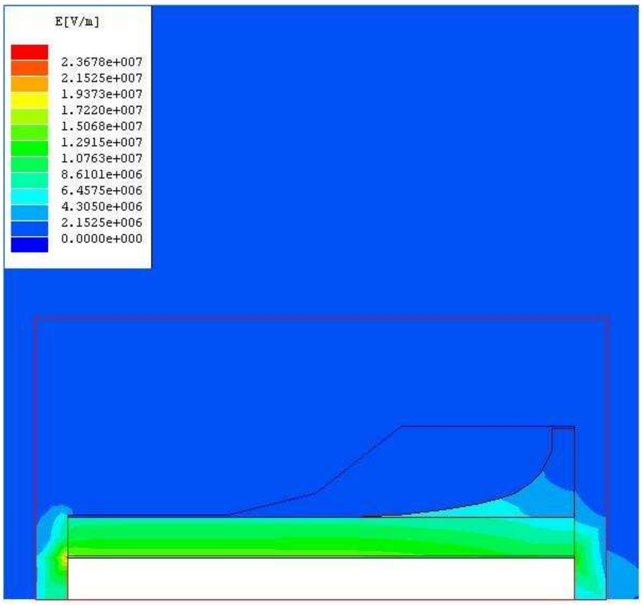

Figure 7.4: Electric field plotting for condition without defect 3 at 1.7U_0 (208.2 kV_{peak})

7.1.2 Electric Field Behaviour with the Presence of Defect 3

The presence of air-filled cavity in the cable insulation will change the normal electric field distribution in the cable insulation. As already described in chapter 3, the electric field inside the cavity will be higher than the surrounding cable insulation due to lower dielectric constant of air inside the cavity than the dielectric constant of cable insulation. The result of electric field plotting simulation for voltage stress 50 kV_{peak} is shown in Figure 7.5.

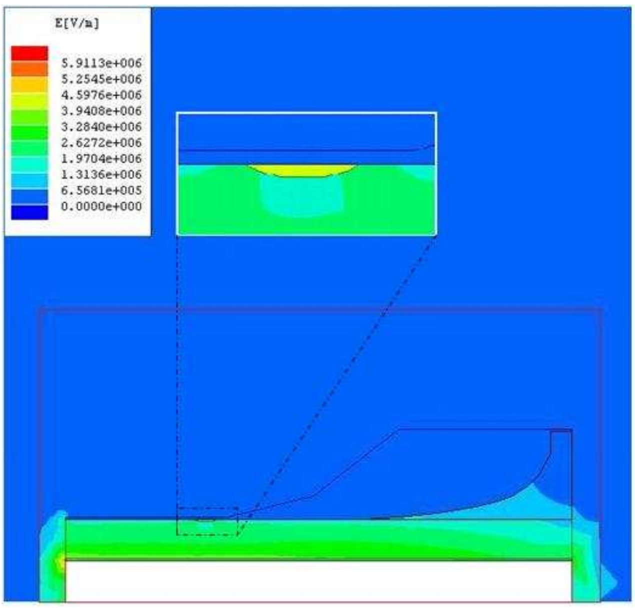

Figure 7.5: Electric field plotting for defect 3 at 50 kV_{peak}

The simulation result at voltage stress 50 kV_{peak} (PDIV) where the PD starts to occur, shows that the presence of defect 3 changes the normal electric field distribution in the cable insulation and the highest electric field enhancement occurs inside the cavity in the range of 3.94 - 4.59 kV/mm.

According to [3], the Paschen curve as shown in Figure 3.3 is valid to describe the breakdown strength of small cavities in solid insulation with pressure times distance, (p.d) up to 5 atm.mm. By using Paschen curve, the breakdown strength of air-filled cavity with 1mm distance between electrodes and assumed has pressure 1 atm will be around 3 kV_{rms}/mm or 4.24 kV_{peak}/mm. This value verifies the result of electric field enhancement in the simulation at voltage stress 50 kV_{peak} (PDIV).

The Townsend breakdown mechanism will play a role for the case of defect 3 with the condition of pressure times distance less than 5 atm.mm [3]. In this mechanism, the cathode material will play an important role for releasing new electrons from feedback mechanism by positive ions or photons. Furthermore, the transition from Townsend to Streamer mechanism in electrode bounded cavities will occur which controlled by the overvoltage where the space charge that determines the streamer mechanism is prevailed [26].

A closed cavity has a special PD characteristic as a function of time where the PD pulses tend to decrease or disappear with long duration of voltage stress applied. This phenomenon related to the reduction of overvoltage due to sufficient supply of initial electrons [27] and the increase of conductivity of the cavity surface that shield the cavity interior from the electric field [28]. Figure 7.6 and 7.7 show the electric field plotting simulation for voltage stress $1U_0$ (122.5 kV_{peak}) and $1.7U_0$ (208.2 kV_{peak}).

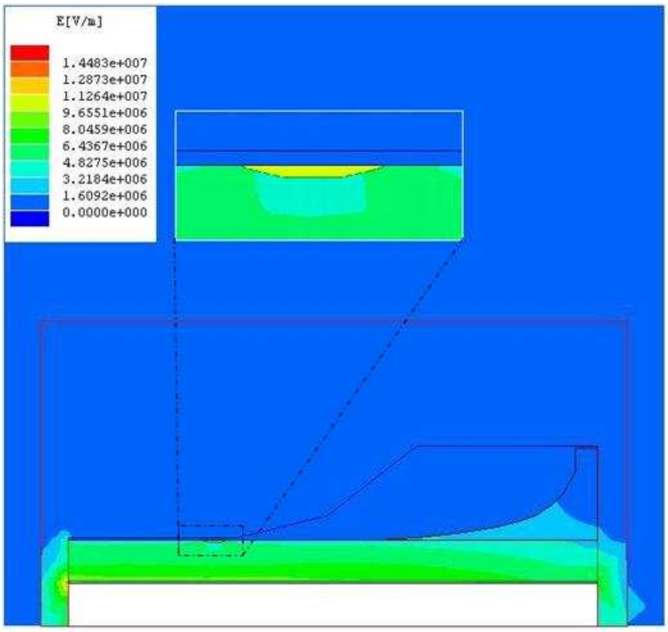

Figure 7.6: Electric field plotting for defect 3 at U_0 (122.5 kV_{peak})

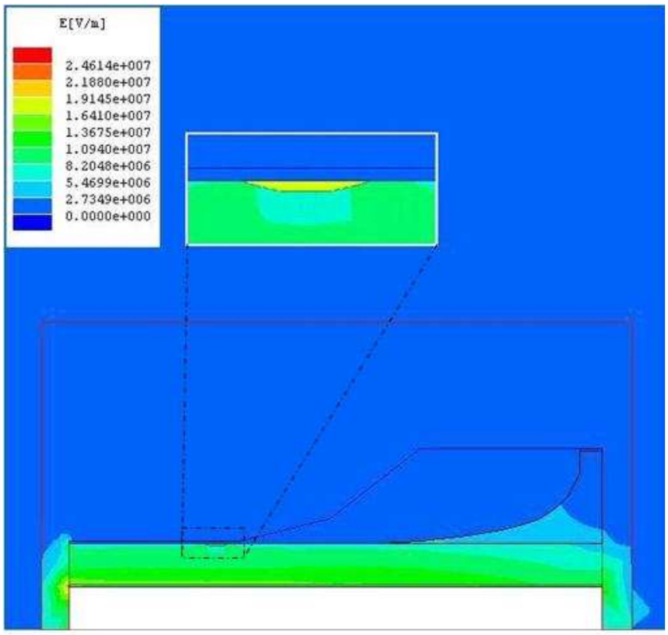

Figure 7.7: Electric field plotting for defect 3 at $1.7U_0$ (208.2 kV_{peak})

The plot of electric field as a function of voltage applied up to $1.7U_0$ for both situations, with and without defect 3, is shown in Figure 7.8. It can be seen from this plot that the field enhancement in the cavity is equal to ε times higher than the normal field in the dielectric.

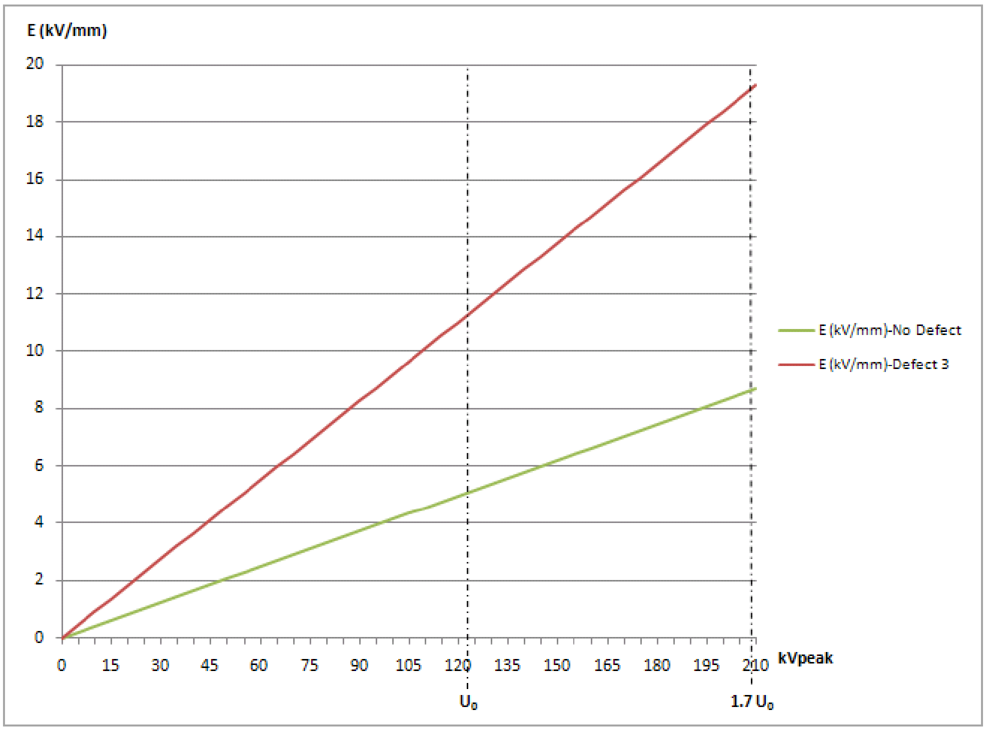

Figure 7.8: Plot of electric field as a function voltage applied for defect 3

7.2 Measurement Results by Using 50Hz AC Energizing and Conventional IEC 60270 PD Detection

Similar to the case of defect 1 and 2, PD measurements by using TE 571 PD detector are performed with the test set-up as shown in Figure 4.8. Calibration as described in IEC 60270 standard is applied to the test set-up before the PD measurement. The noise level is measured without voltage applied and it reached the value of 5 pC. Measurement is done by slowly increasing the voltage start from 0 kV to get the PD inception voltage (PDIV) and then PD measurement is applied for 2 kV voltage step with 2 minutes duration for each voltage up to 60 kV_{peak}. Voltage stress is limited to 60 kV_{peak} due to current limitation in feeding cable of transformer. Plot of PD magnitude in pC as a function of voltage applied up to 60 kVpeak is shown in Figure 7.9.

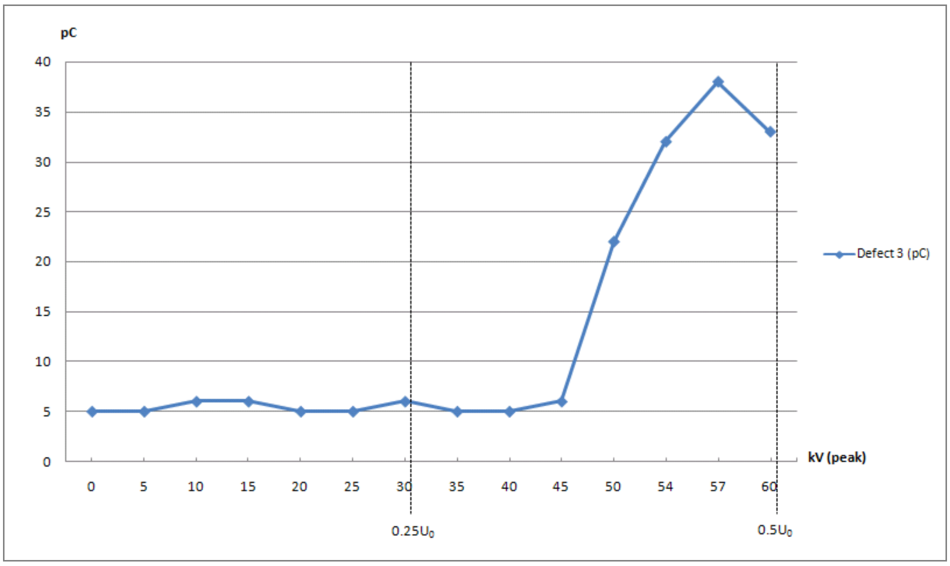

Figure 7.9: PD magnitude – voltage applied for defect 3 by using TE 571

The PDIV from TE 571 PD detector measurement was found at 50 kV_{peak}. PD measurement is done by increasing the voltage up to 60 kV_{peak}. In the early stage, the PD amplitude is increasing by increasing the voltage stress but at 60 kV_{peak} the PD amplitude was decreasing. This phenomenon is related to the PD characteristic of the closed cavity where the PD pulse tends to decrease or even disappear by long duration of voltage applied.

Similar to the measurement of defect 1 and 2, PD phase-resolved patterns for defect 3 are obtained by measuring at PDIV up to 60 kV_{peak} with 2 kV step for 2 minutes duration for each step. Figure 7.10 until 7.12 show PD phase-resolved patterns which observed at PDIV, 54 kV_{peak} and 60 kV_{peak} for defect 3.

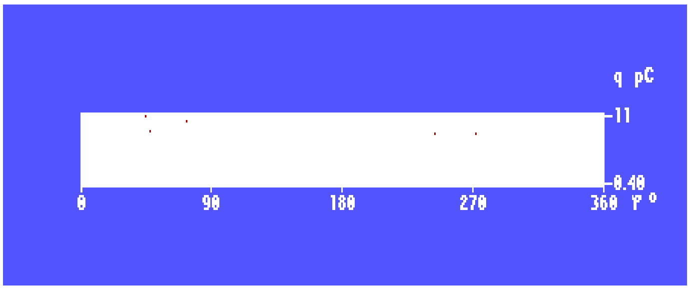

Figure 7.10: PD pattern at 50 kV_{peak} (PDIV) for defect 3

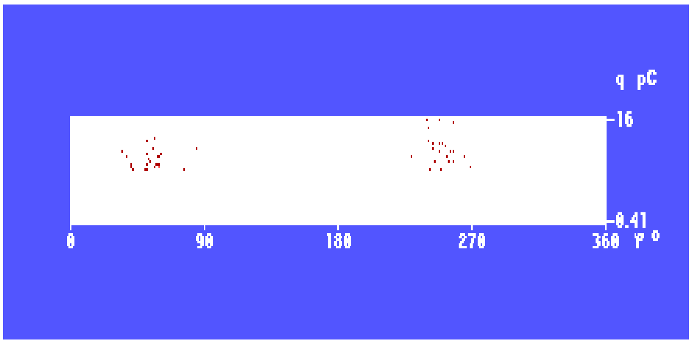

Figure 7.11: PD pattern at 54 kV$_{peak}$ for defect 3

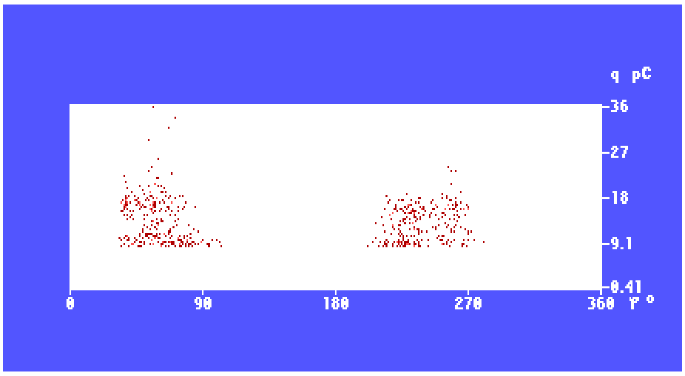

Figure 7.12: PD pattern at 60 kV$_{peak}$ for defect 3

PD phase-resolved patterns for defect 3 show that at PDIV and higher voltage applied, the symmetric PD phase-resolved patterns occur at both positive and negative period of the 50Hz AC voltage cycle.

7.3 Measurement Results by Using 400Hz DAC Energizing and Conventional IEC 60270 PD Detection

PD measurements by using OWTS HV150 are performed by using test set-up as shown in Figure 4.9. The resonant frequency of the PD measurement will be around 412Hz. Calibration as mentioned in IEC 60270 standard is applied to the test circuit before the PD measurement is started. By using 0 kV DAC shot, the noise level is measured and reached 15 pC. Figure 7.13 shows the plot of PD amplitude as a function of voltage applied up to 150kV$_{peak}$.

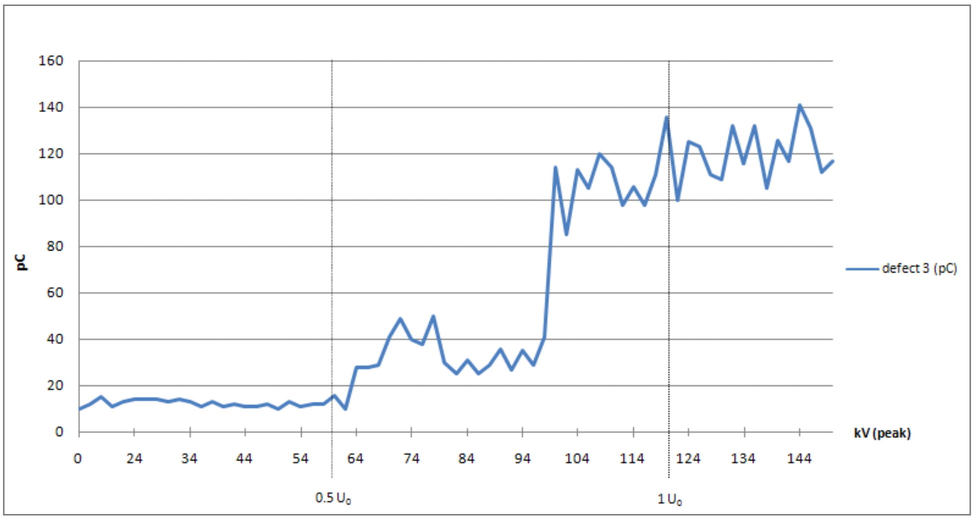

Figure 7.13: Plot of PD amplitude as a function of voltage applied up to 150 kV$_{peak}$

The measurement is done by applying 2 DAC shots for each voltage with step of 2 kV. The PDIV from OWTS measurement was found at 64 kV$_{peak}$. This value is higher than PDIV found by using TE 571 PD detector. This phenomenon is related to the different type of voltage stress between continuous AC 50Hz and DAC voltages. For DAC voltage, the object is stressed only temporarily during short times. This short and decreasing field stress result in high inception delay time for PD to occur due to restricted of electron avalanche development in cavity. In higher voltage stress applied this phenomenon will less significant for PD occurrence. The high resonant frequency of DAC also influences the increase in PDIV as the probability of PD events is smaller at higher frequency [14]. The short stress of DAC voltage and small number of DAC shots also result in varying of PD amplitude during measurement due to the stochastic process of PD occurrence. Figure 7.14 and 7.15 show PD measurement results at PDIV (64 kV$_{peak}$) and 150 kV$_{peak}$.

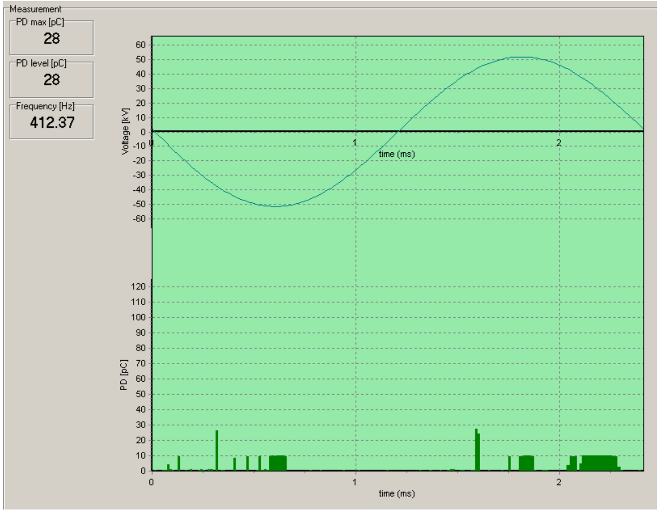

Figure 7.14: PD measurement on defect 3 at 64 kV$_{peak}$ (PDIV)

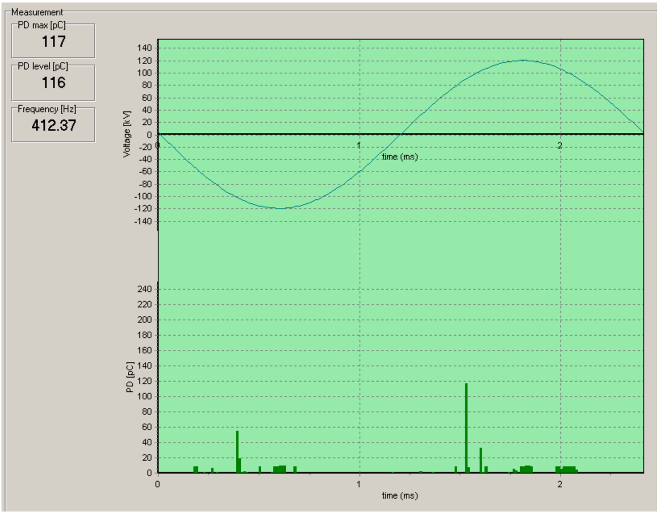

Figure 7.15: PD measurement on defect 3 at 150 kV$_{peak}$

7.4 Measurement Results by Using 50Hz AC Energizing and Un-conventional PD Detection

The measurement set-up used for un-conventional method is shown in Figure 4.10. Similar to the measurement for defect 1 and 2, PD detection and measurement are applied to six sensor positions in the cable accessories. The “full span” of background noise and PD pulses from the artificial defect 3 are measured for all sensors to determine the centre frequency (CF) for PD measurement. Figure 7.16 – 7.21 show full spectra of background noise and signal for all sensors up to 500 MHz. These spectra are obtained by making a single sweep of frequency spectrum from 0 MHz – 3

GHz of noise and PD signal measured for each sensor. Noise is measured without voltage applied while PD signal is obtained by applying 50 Hz AC voltage 60 kV_{peak} to the termination 1.

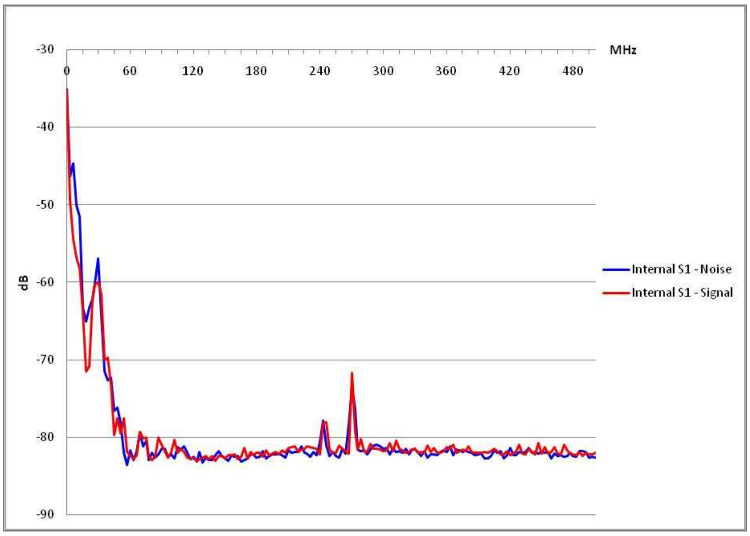

Figure 7.16: Full spectra of noise and signal for internal sensor S1 (at termination 1)

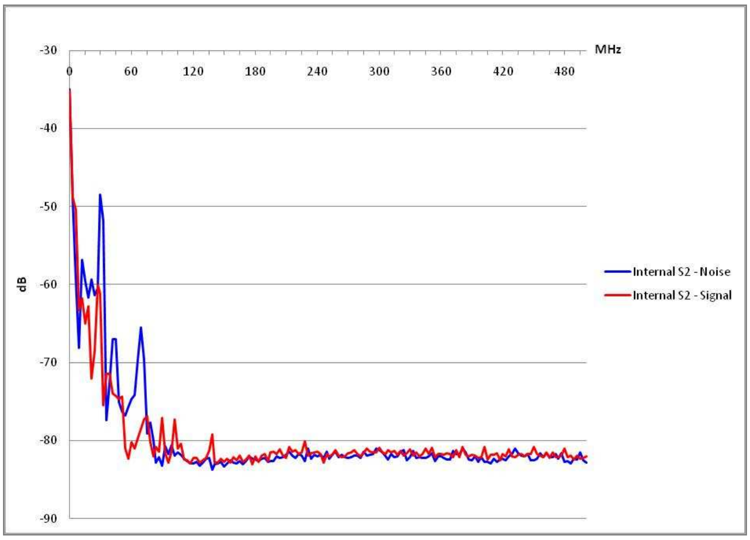

Figure 7.17: Full spectra of noise and signal for internal sensor S2 (at termination 2)

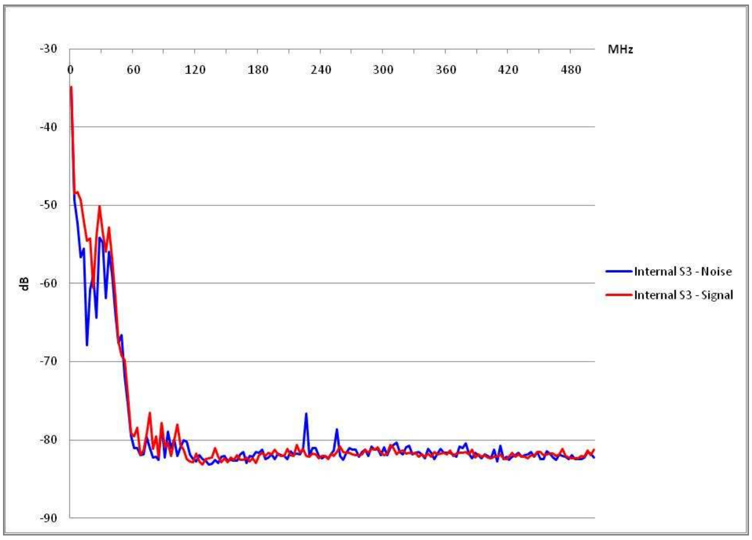

Figure 7.18: Full spectra of noise and signal for internal sensor S3 (at joint)

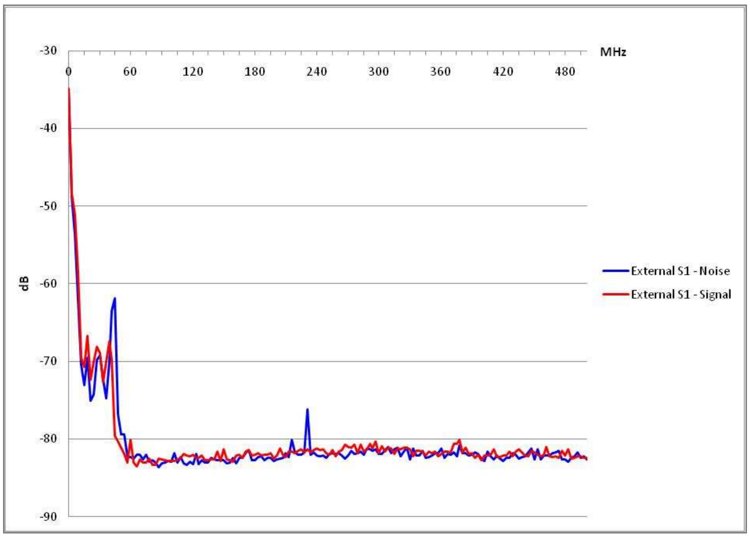

Figure 7.19: Full spectra of noise and signal for external sensor S1 (at termination 1)

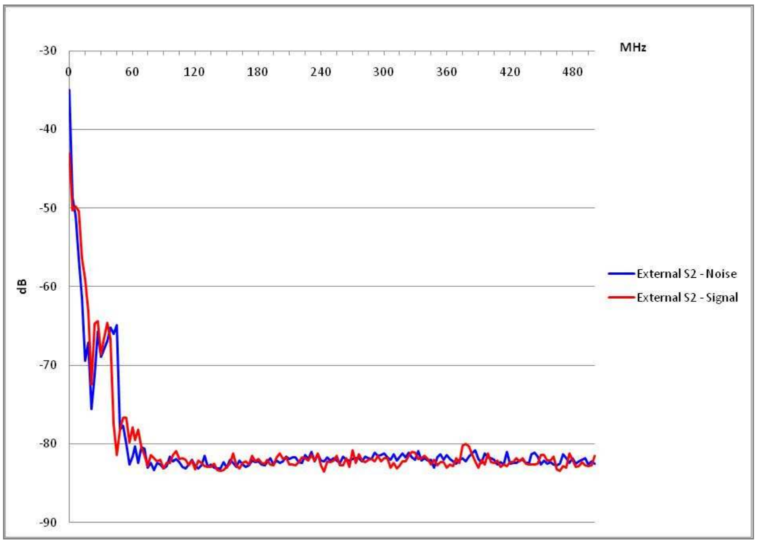

Figure 7.20: Full spectra of noise and signal for external sensor S2 (at termination 2)

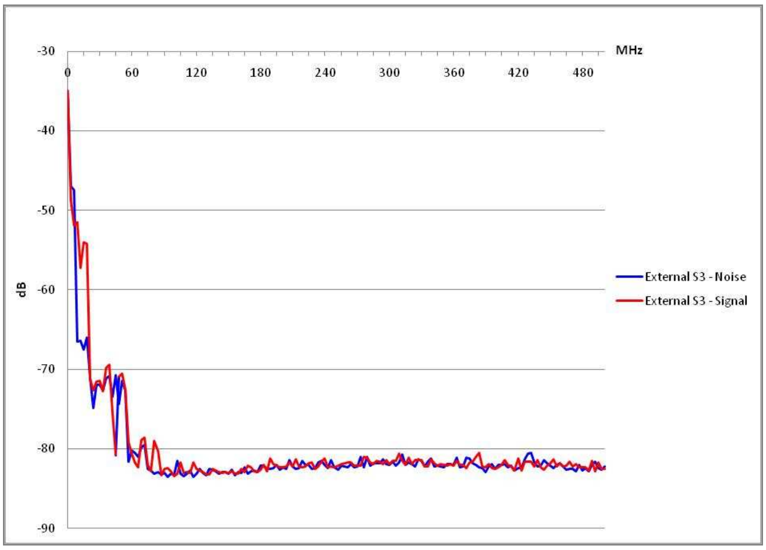

Figure 7.21: Full spectra of noise and signal for external sensor S3 (at joint)

It can be seen from the full spectra of noise and signal that the difference between the noise and signal are relatively small. It relates to the small PD amplitudes that are produced from the defect 3 as measured by TE 571 PD detector. Based on these full spectra three selected frequencies which have high signal-to-noise ratio are selected for each sensor and PD patterns are obtained by measuring with 500 sweeps at 60 kV_{peak}. Figure 7.22 shows PD patterns for sensor S1 which placed at termination 1 (approximately 90m from the defect 3).

Internal ***External***

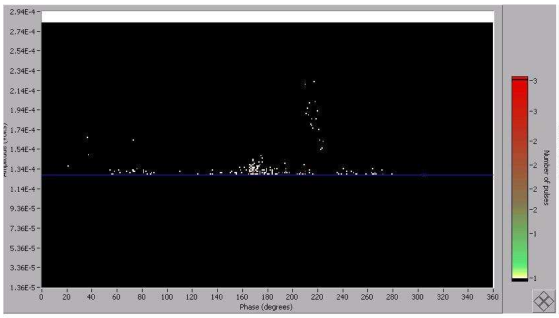
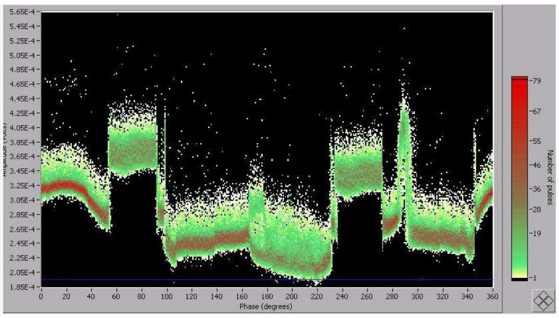

39 MHz 18 MHz

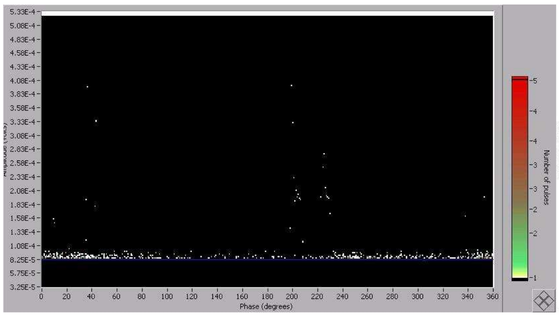
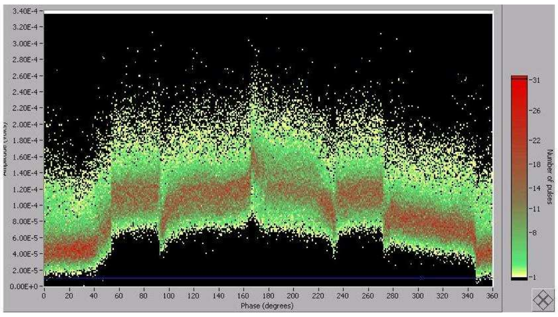

87 MHz 36 MHz

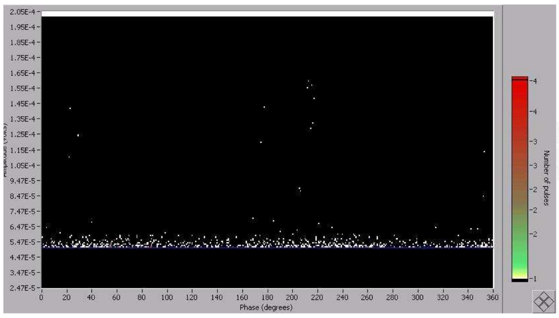
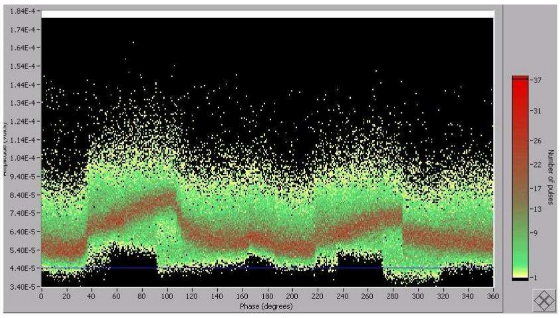

102 MHz 60 MHz

Figure 7.22: PD patterns for sensor S1 (at termination 1) at 60 kV_{peak}

The internal sensors S1 show higher sensitivity than the external sensors. The PD patterns show less PD pulses are measured due to large attenuation of the high frequency PD pulses in distance of 90 m. Figure 6.23 shows PD patterns for sensor S2 at termination 2 (approximately 10m from the artificial defect 3).

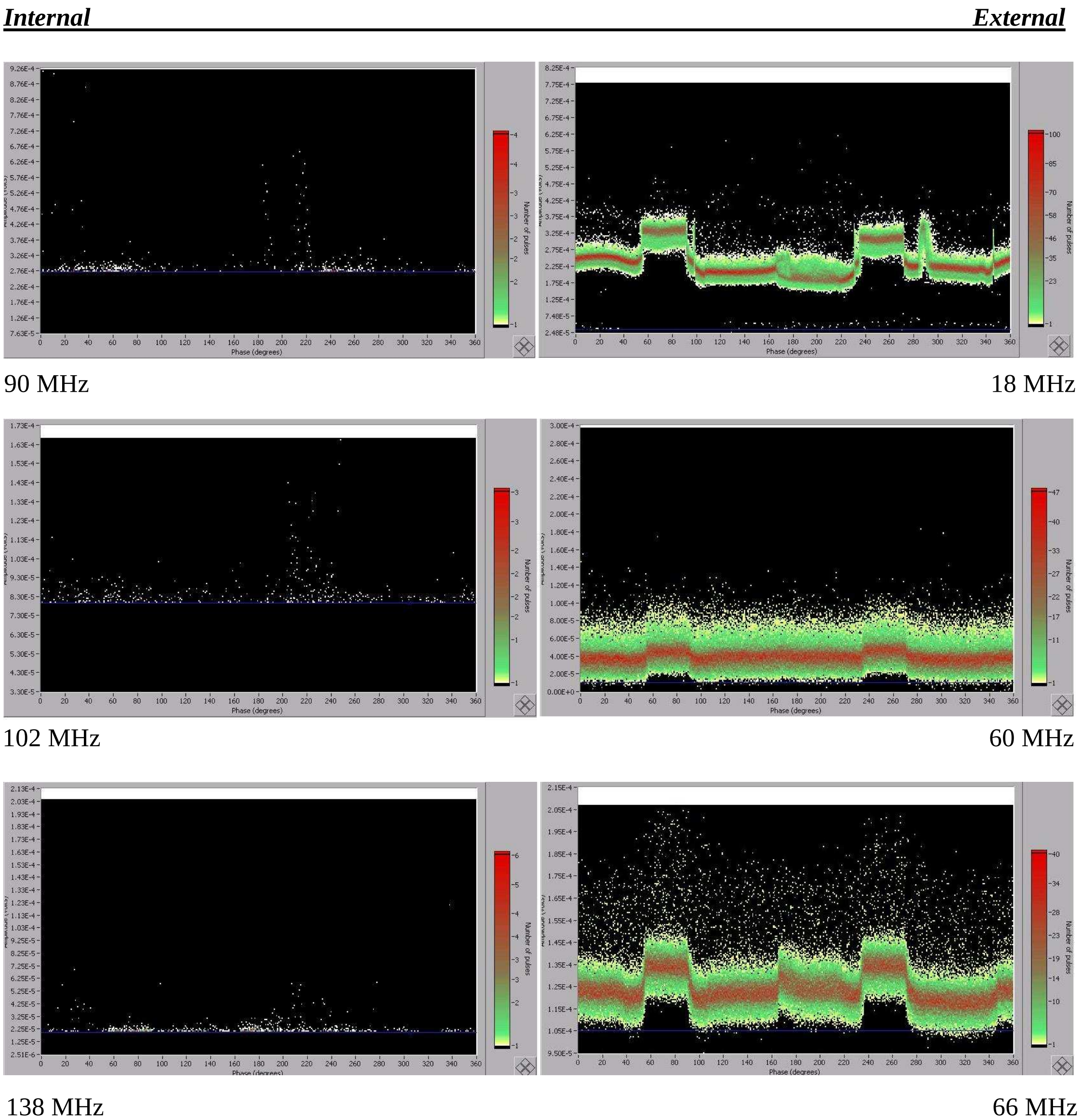

Figure 7.23: PD patterns for sensor S2 (at termination 2) at 60 kV$_{peak}$

Similar to the sensor S1, the internal sensors S2 which placed at the termination 2 show higher sensitivity than the external sensors. The PD patterns obtained from internal sensors S2 show more recorded PD pulses than S1 due to the shorter distance from the PD source to the sensors that results in less attenuation of high frequency PD pulses. Internal sensors of S2 show that the PD pattern occurs at both positive and negative half voltage cycle whereas more PD recorded at negative half cycle of AC voltage. Figure 7.24 shows results of PD patterns for sensor S3 which located close to the cable joint.

Internal ***External***

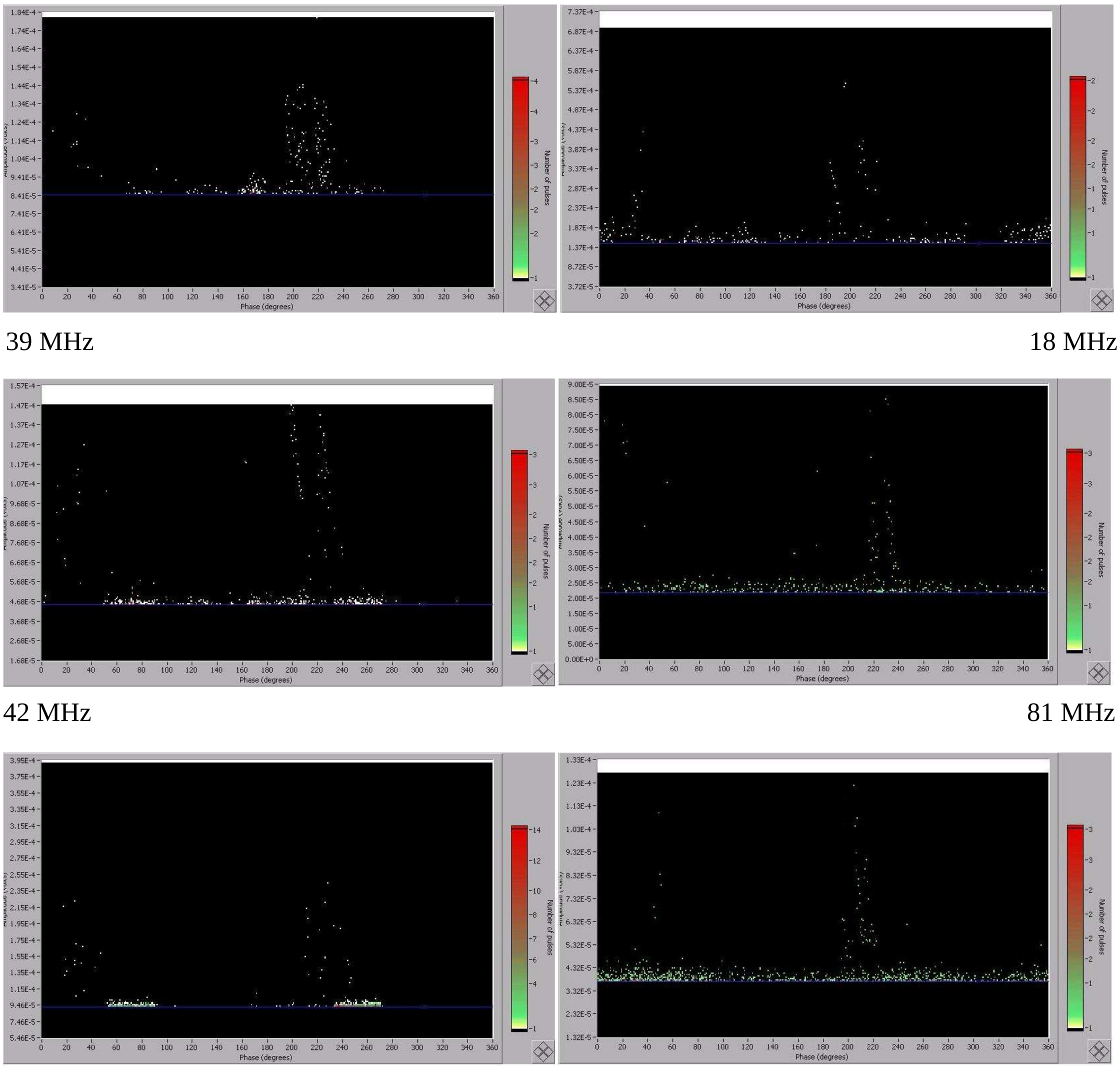

39 MHz 18 MHz

42 MHz 81 MHz

75 MHz 84 MHz

Figure 7.24: PD patterns for sensor S3 (at joint) at 60 kV$_{peak}$

PD patterns from sensor S3 show that sensor S3 has higher sensitivity than sensor S1 and S2 where PD patterns from sensor S3 are obtained for both internal and external ones due to close distance between the sensors and the PD source that results in less attenuation of high frequency PD pulses. Similar to the defect 1, in the case of after-laying test where the main interest is the cable accessory, the sensor should be placed as close as possible to the accessories due to large attenuation of the high frequency PD pulses with the distance. Similar to the other sensors, PD pattern occurs at both half period of voltage cycle and more PD recorded at negative half of voltage cycle.

7.5 Conclusion

1. The field plotting simulation for defect 3 shows that the presence of electrode-bounded cavity results in field enhancement inside the cavity which is equal to ε times higher than normal field. In the case of cavity with 10mm length and 1mm depth, the breakdown voltage of gas inside the cavity follows the Paschen curve where PD starts to occur in voltage stress 50 kV_{peak}.

2. PD measurements by using 50Hz AC energizing and conventional IEC 60270 PD detection results in low PD amplitude. The PD amplitude was increasing by increasing the voltage but it tends to decrease for longer voltage application due to the PD characteristic of the closed cavity where the PD pulse tends to decrease by long duration of stress voltage applied. PD phase-resolved patterns for defect 3 show that at PDIV and higher voltage applied, the symmetric PD phase-resolved patterns occur at both positive and negative period of the 50Hz AC voltage cycle.

3. PD measurements by using 400Hz DAC energizing and conventional IEC 60270 PD detection found that the PDIV was higher than the value obtained by using 50Hz AC energizing and conventional IEC 60270 PD detection. This phenomenon is related to the shorter stress duration and higher frequency resonant of the DAC voltage. The short stress of DAC voltage and small number of DAC shots also result in varying of PD amplitude during measurement due to the stochastic process of PD occurrence.

4. It was quite difficult to determine the best centre frequency for un-conventional PD measurement duo to the relatively small difference between the full spectra of background noise and PD signal. It relates to the small PD amplitudes that are generated from the defect 3.

5. The internal sensors have higher sensitivity than external ones and the distance of the sensor from the PD source determines the attenuation of the high frequency PD pulses. Therefore in the after-laying test where the main interest is the cable accessories due to the probability of the installation defect, the sensor should be placed as close as possible to the cable accessories.

CHAPTER 8

Measurement Issues for Un-conventional Partial Discharge Detection Method

The use of un-conventional PD detection becomes more interesting due to its advantage on on-site PD measurement with the presence of high external noise. Unlike the conventional PD detection which already standardized in IEC 60270, there is no standard available for the use of un-conventional PD detection. There are many factors that can influence the un-conventional PD measurement due to the complex situation which can determine the PD signal propagation and detection. In this chapter the effect of external sensor position and the grounding configuration of cable earth connection in un-conventional PD detection are presented.

8.1 Different Position of External Sensor

The first measurement issue is the effect of external sensor position in the cable earth wire. In practical situation it will be difficult to put the external sensor as close as possible to the cable accessories due to construction reasons. Regarding this investigation, the earth wire of each accessory in the test set-up shown in Figure 4.1 was extended up to 6m as depicted in Figure 8.1.

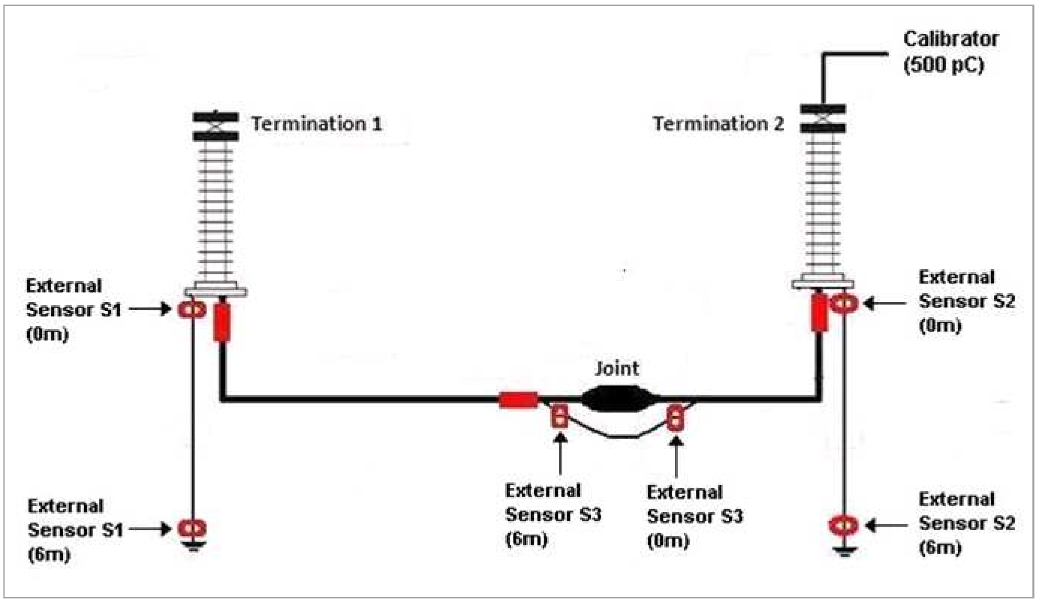

Figure 8.1: Test set-up with different position of external sensor

Measurement was done by applying charge injection 500 pC from the calibrator to the termination 2 and then full spectra are obtained from 2 positions (0m and 6m) for each external sensor of cable accessory as shown in Figure 8.1. Noise for each position of external sensor also measured and then plot of full spectra of noise and charge are made up for frequency 6 - 200 MHz as shown in Figure 8.2 – 8.4. Figure 8.2 shows full spectra of noise and injected charge obtained by external sensor S1.

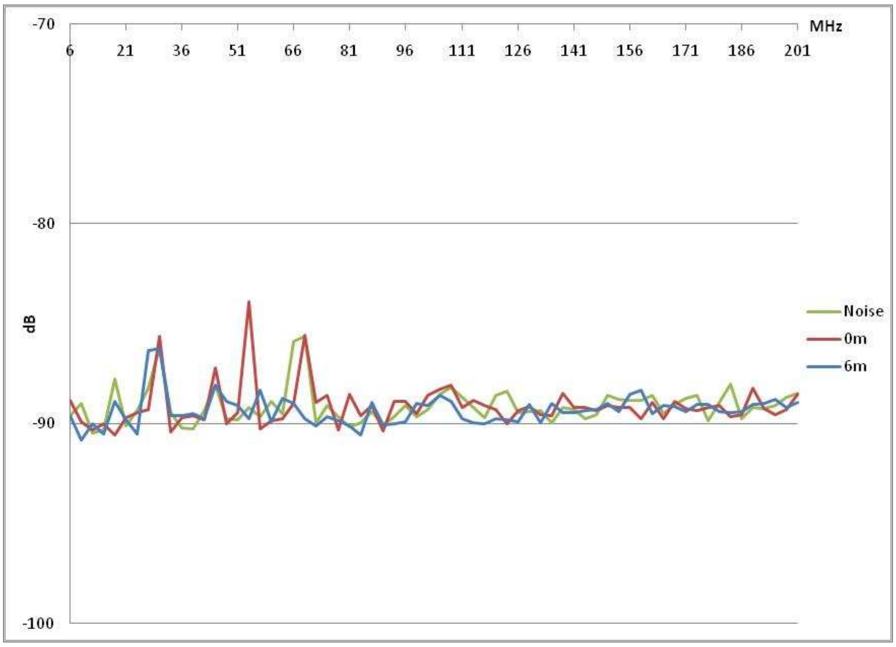

Figure 8.2: Full spectra of noise and injection signal for sensor S1 (at termination 1)

It can be seen that for external sensor S1 which placed about 100m from the injection terminal, there are not many significant difference between the spectrum of signal measured by sensor position 0m and 6m. Figure 8.3 shows the full spectra of noise and signal from calibrator for external sensor S2.

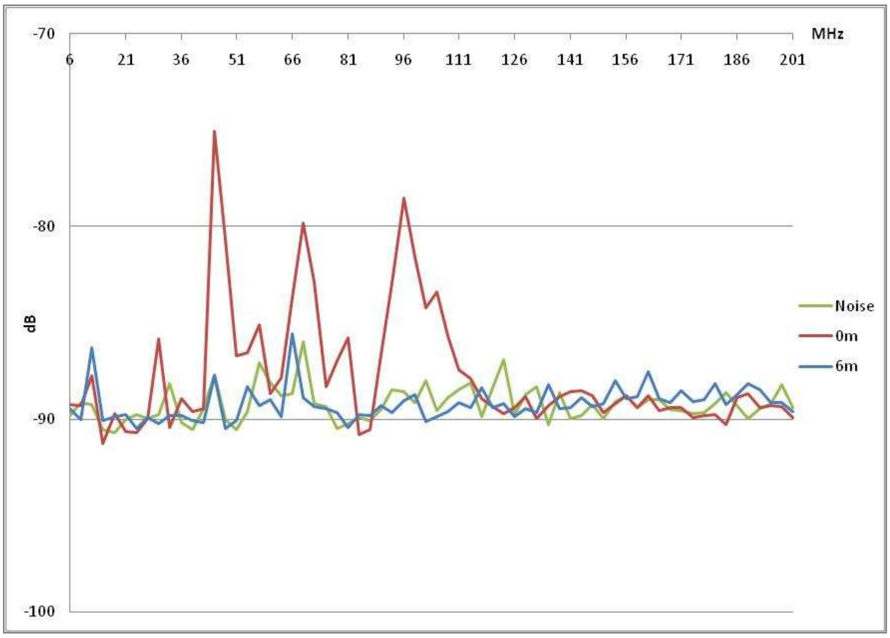

Figure 8.3: Full spectra of noise and injection signal for sensor S2 (at termination 2)

The full spectra of injected charge from calibrator shows that for external sensor S2 which placed at termination 2 where the calibrator is connected, at certain range of frequency (30 MHz – 120 MHz) there are significant different for the signal amplitude between 0m and 6m of external sensor position. Figure 8.4 shows full spectra of noise and signal for sensor S3 which placed at cable joint.

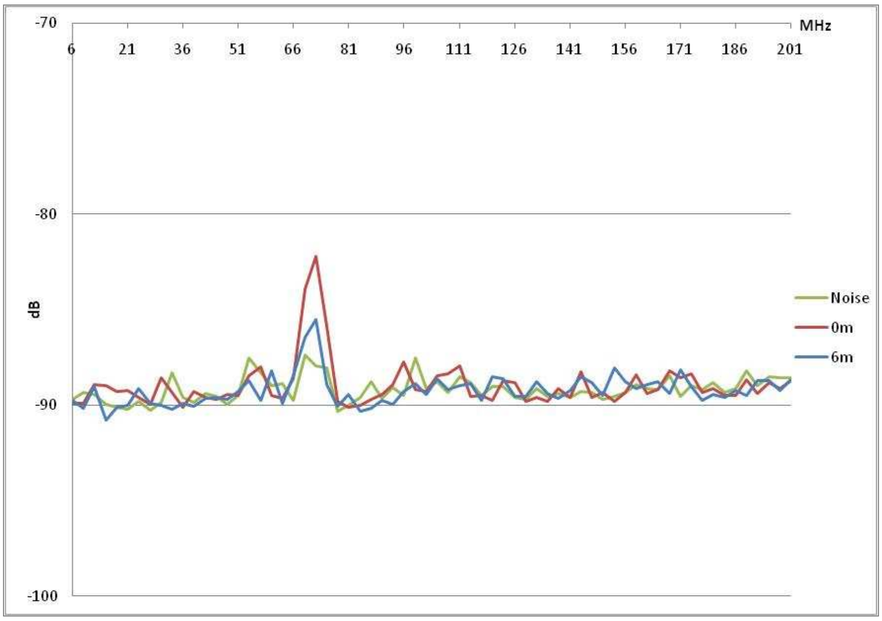

Figure 8.4: Full spectra of noise and injection signal for sensor S3 (at joint)

The spectrum obtained from external sensor S3 at cable joint shows different behaviour than other spectrum obtained from terminations. However, the effect of external sensor position can be seen at small range of frequency (60 MHz – 80 MHz).

By comparing these three spectra from all sensors, it can be seen that the presence of power cable has a large influence on the signal attenuation starting from frequency 80 MHz and the external sensor S3 has different more selective coupling as external sensor S1 and S2. Furthermore, the different position of external sensor at earth wire of cable accessory has an influence in the signal attenuation, the longer the distance the higher the attenuation. This fact becomes important for on-site measurement where the access for the earth wire is at the link boxes which can have quite long distance from the accessory itself that results in less sensitivity of un-conventional PD measurement.

8.2 Different Configuration of Earth Wire Connection in Cable Joint

The second measurement issue for the investigation is the effect of different configuration of earth wire connection in the cable joint. Regarding this investigation, the calibrator is connected to termination 2 and full spectra of 1 nC charge injection from the calibrator are obtained for four different configurations of the cable earth wire connection in the cable joint.

8.2.1 Configuration A

First configuration is shown in Figure 8.5. This is the standard configuration for the cable earth wire connection in the cable joint. Figure 8.6 shows the full spectra of noise and charge injection up to frequency 500 MHz.

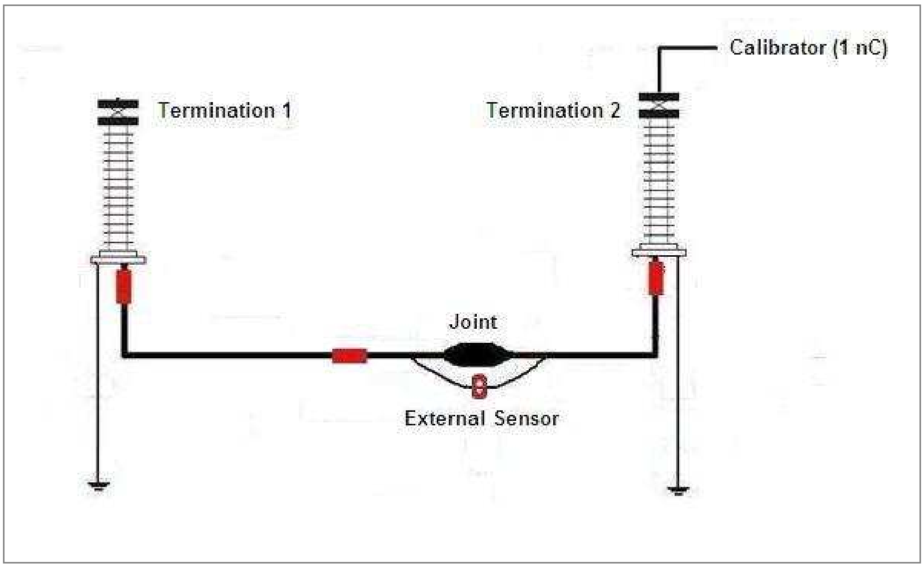

Figure 8.5: Configuration A for earth wire connection in the cable joint

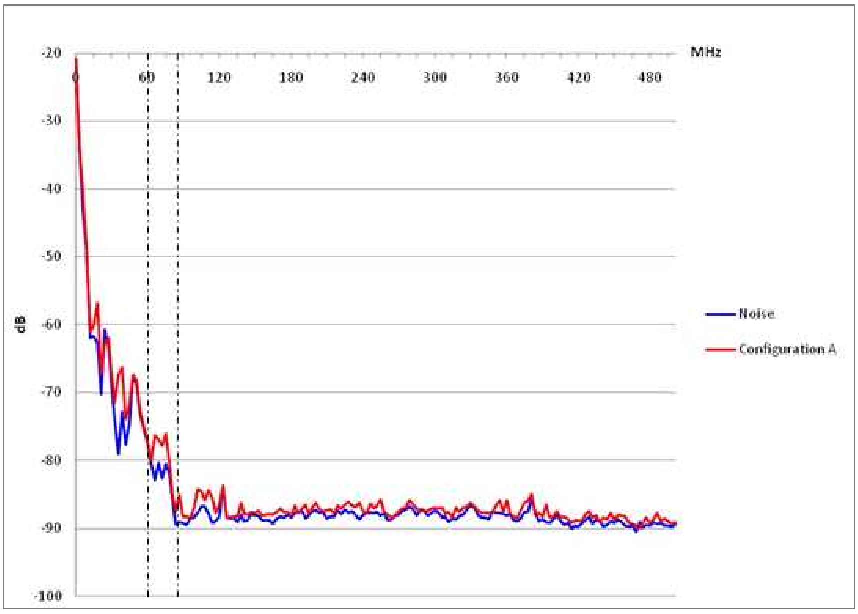

Figure 8.6: Full spectra of noise and injection signal for configuration A

8.2.2 Configuration B

Figure 8.7 shows the configuration B. In this configuration the connection of earth wire from both sides of joint was disconnected and then one of the cable earth wires where the external sensor was placed is grounded while the other is left floating.

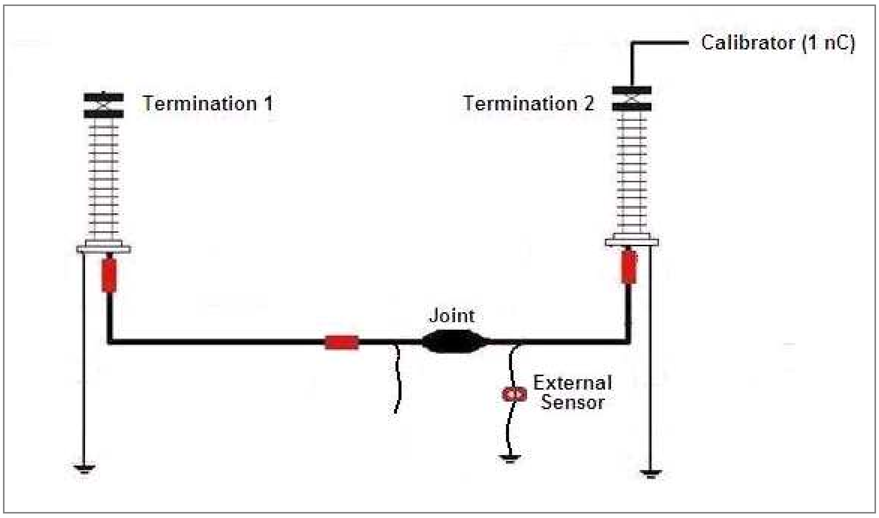

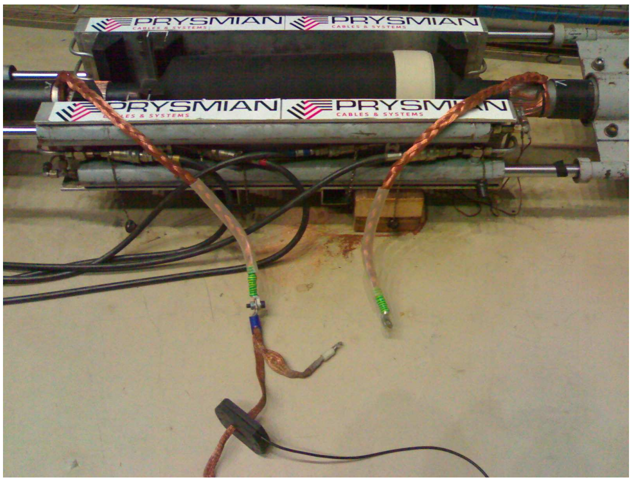

Figure 8.7: Configuration B for earth wire connection in the cable joint

Figure 8.8 shows the full spectra of noise and charge injection obtained from external sensor in configuration B up to frequency 500 MHz.

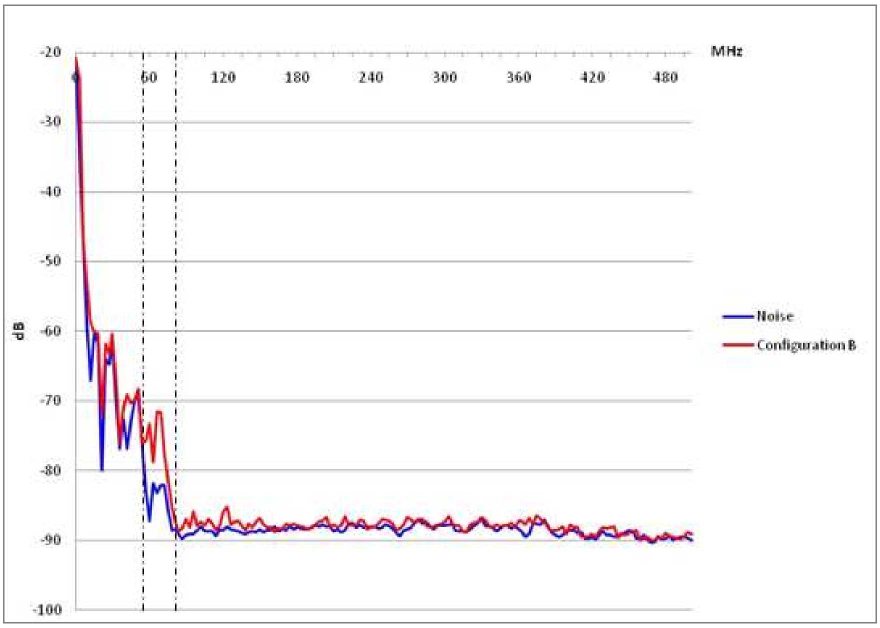

Figure 8.8: Full spectra of noise and injection signal for configuration B

8.2.3 Configuration C

The configuration C is similar to the configuration B where the difference is that the grounding of cable earth wire and the external sensor were applied at opposite position of the cable joint as shown in the Figure 8.9.

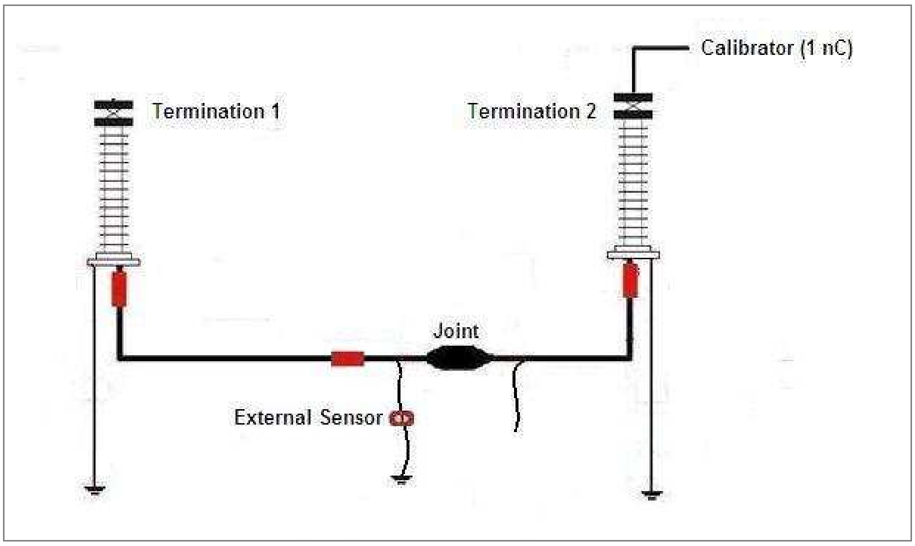

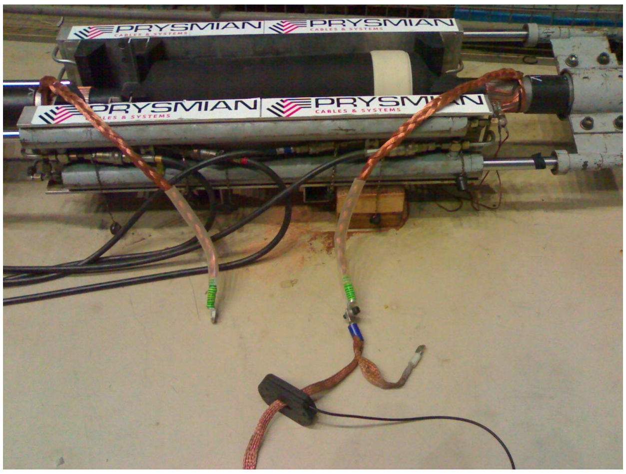

Figure 8.9: Configuration C for earth wire connection in the cable joint

Figure 8.10 shows the full spectra of noise and charge injection obtained from external sensor in the configuration C up to frequency 500 MHz.

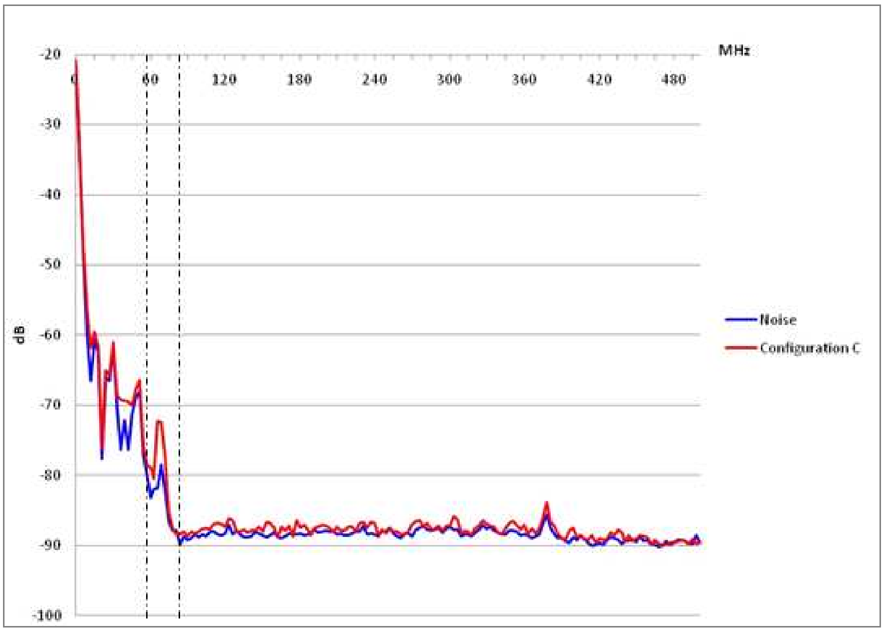

Figure 8.10: Full spectra of noise and injection signal for configuration C

8.2.4 Configuration D

The last configuration of earth wire connection was applied by connecting the standard configuration A to the earth as shown in Figure 8.11.

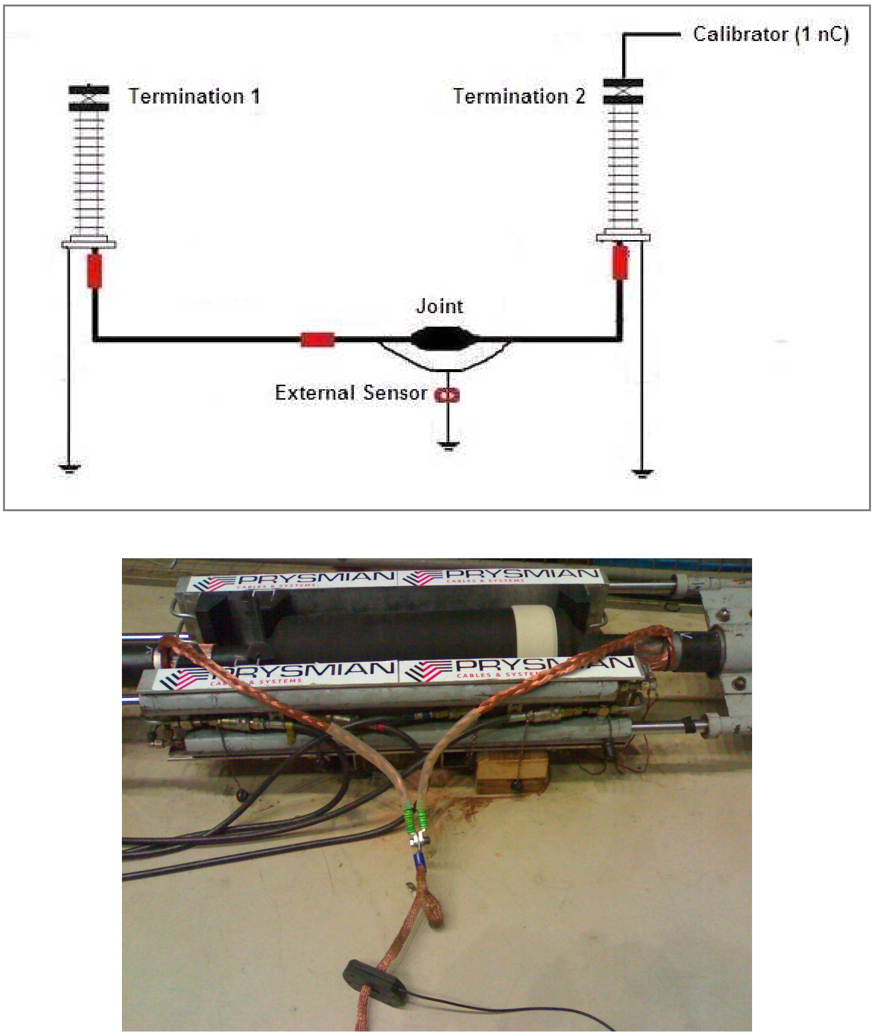

Figure 8.11: Configuration D for earth wire connection in the cable joint

Figure 8.12 shows the full spectra of noise and charge injection obtained from external sensor in configuration D up to frequency 500 MHz.

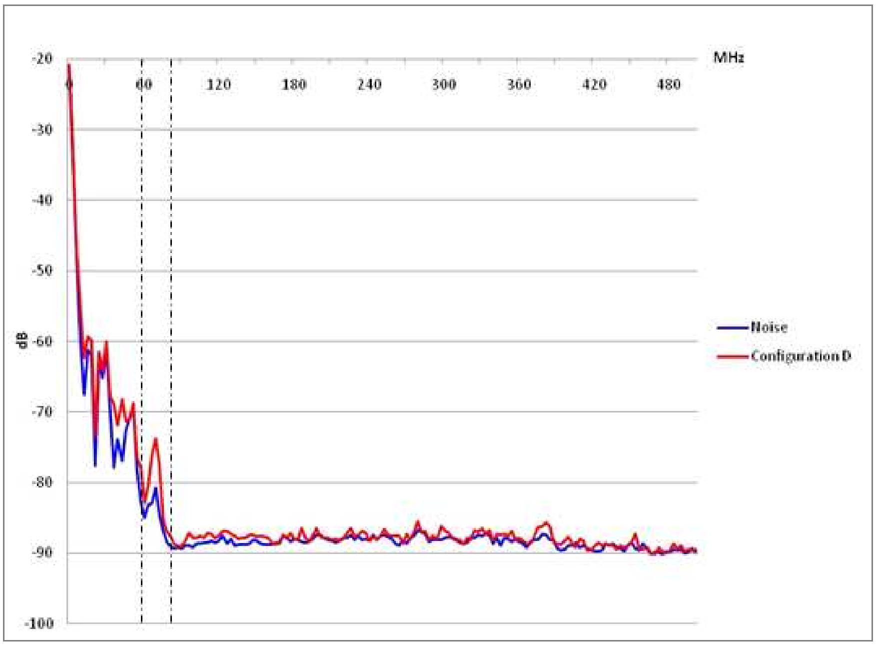

Figure 8.12: Full spectra of noise and injection signal for configuration D

The full spectra of different configurations of earth wire connection in the cable joint shows a similar pattern in the full spectra of the injected charge. The grounding of the earth wire connection in the cable joint (configuration B, C and D) results in higher frequency spectra in the frequency range 60 – 75 MHz.

8.3 Capacitive Coupling between External Sensor and Earth Wire

In this issue the effect of the capacitive coupling that presents between the external sensor and the earth wire while the sensor is not attached around the earth connection of the power cable accessory is investigated. The investigation is applied on the earth connection of the termination 2 while the calibrator is connected at the same termination and then the comparison between the normal connection when the sensor is attached around the earth wire and the situation when the sensor is not attached around is analysed. Figure 8.13 and 8.14 show two positions of external sensor related to the earth connection of the termination.

Figure 8.13: The sensor which attached around the earth connection of the termination

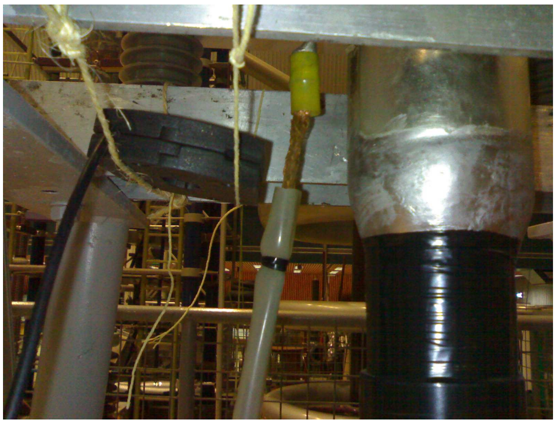

Figure 8.14: The sensor which not attached around the earth connection of the termination

Figure 8.15 and 8.16 show the full spectra which obtained from two positions of the external sensor by using 500 pC charge injection from the calibrator that connected to the termination 2.

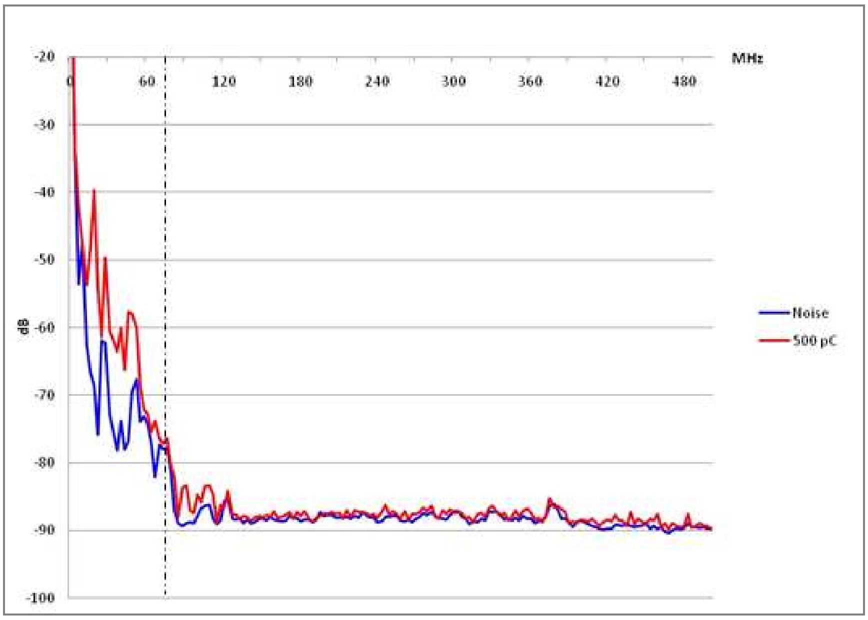

Figure 8.15: The full spectra of noise and signal obtained from the sensor that attached around the earth connection of the termination

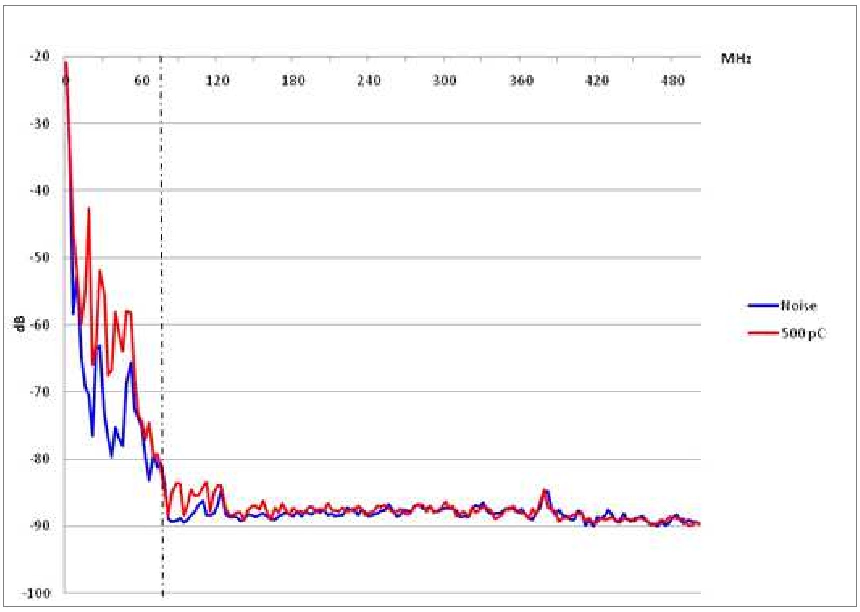

Figure 8.16: The full spectra of noise and signal obtained from the sensor that not attached around the earth connection of the termination

It can be seen from two full spectra obtained from different position of external sensor that the patterns of these two spectra are similar. The difference occurs at low frequency below 75 MHz that the full spectrum from the unattached around situation has lower signal response than the attached around situation. Therefore the coupling capacitance between the external sensor and the earth connection performs like a high-pass filter for the injected pulse due to high impedance of the capacitive coupling.

8.4 Conclusion

1. The presence of power cable has a large influence on the signal attenuation starting from frequency 80 MHz.

2. The different position of external sensor has an influence in the signal attenuation, the longer the distance the higher the attenuation. This fact becomes important for on-site measurement where the access for the earth wire is at the link boxes which can have quite long distance from the accessory itself that results in less sensitivity of un-conventional PD measurement.

3. The full spectra of injected charge for different configurations of earth wire connection in the cable joint shows a similar pattern. The grounding of the earth wire connection in the cable joint (in case of configuration B, C and D) results in higher frequency spectra in the frequency range 60 – 75 MHz.

4. The coupling capacitance between the external sensor and the earth connection performs a high-pass filter for the injected pulse due to high impedance of the capacitive coupling.

CHAPTER 9

Conclusions and Recommendations

Due to the fact that the improper on-site installation of HV cable accessories may produce defects that can result in the cable system failure in short-long term operation, the understanding of typical installation defects and their effects for the after-laying test of HV cable system becomes very important. In this chapter, the conclusions and few additional ideas for further investigation will be presented.

9.1 Conclusions

Based on the field plotting simulation and PD measurement on artificial defects and the investigation of several issues on un-conventional PD detection, there are several important aspects will be discussed.

1. The missing semi-conductive screen defect results in the field enhancement at the edge of semi-conductive screen. The field enhancement will decrease with the size of the defect and the increase of electric field as function of voltage applied is steeper for the bigger size of the defect.

2. PD measurements by using 50Hz AC and 400Hz DAC energizing and conventional IEC 60270 show that the size of missing semi-conductive screen does not give significant influence on PDIV and the increase of PD amplitude as a function of voltage applied is steeper for the bigger size of the defect.

3. PD measurements by using 50Hz AC energizing with conventional IEC 60270 and un-conventional detection show that at low voltage, the asymmetric PD phase-resolved patterns for missing semi-conductive screen occurred at negative half of the 50Hz AC voltage cycle while at higher voltage became symmetrical, occurred at both positive and negative period of the 50Hz AC voltage cycle.

4. The extra semi-conductive screen in the cable joint produces field enhancement at the end of semi-conductive screen and the field enhancement will increase with the size of the defect.

5. The extra semi-conductive screen is considered as less critical defect due to no PD occurrence up to 80 kV_{peak} stress voltage applied by using different energizing and PD detection methods for critical size of the defect (40mm). It related to the higher breakdown strength of dielectric combination in the case of the extra semi-conductive defect. However, the simulation results show that this defect produce a field enhancement that probably produces PD activities for higher voltage applied. Therefore, PD measurement at higher voltage applied, e.g. $1.7U_0$ as in the case of voltage withstand test for after-laying test is necessary.

6. The presence of electrode-bounded cavity defect results in field enhancement inside the cavity which is equal to ε times higher than the normal field in the dielectric. In the case of cavity with dimension 10mm length and 1mm depth, the breakdown voltage of gas inside the cavity follows the value which described by the Paschen curve where PD starts to occur in voltage stress 50 kV_{peak}.

6. PD measurements by using 50Hz AC energizing and conventional IEC 60270 show that the electrode-bounded cavity results in low PD amplitude and the PD phase-resolved patterns are symmetric, occur at both positive and negative period of the 50Hz AC voltage cycle at PDIV and higher voltage applied.

7. PD measurements on electrode-bounded cavity by using 400Hz DAC energizing and conventional IEC 60270 result in higher PDIV than the value obtained by using 50Hz AC energizing and conventional IEC 60270. This occurrence is related to the shorter stress duration and higher frequency resonant of the DAC voltage.

8. For un-conventional PD detection, the distance of the sensor from the PD source determines the attenuation of the high frequency PD pulses. Therefore in the after-laying test where the main interest is the cable accessories due to the probability of the installation defect, the sensor should be placed as close as possible to the cable accessories.

9. The presence of power cable has a large influence on the signal attenuation starting from frequency 80 MHz and the different position of external sensor has an influence in the signal attenuation, the longer the distance the higher the

attenuation. The latter fact is important for on-site measurement where the access for the earth wire is at the link boxes which can have quite long distance from the accessory itself that results in less sensitivity of un-conventional PD measurement.

10. The different configurations of earth wire connection in the cable joint shows a similar pattern in full spectra of charge injection. The grounding of the earth wire connection in the cable joint (in case of configuration B, C and D) results in higher frequency spectra in the frequency range 60 – 75 MHz.

11. The coupling capacitance between the external sensor and the earth connection performs a high-pass filter for the injected charge due to high impedance of the capacitive coupling.

9.2 Recommendations

1. In this thesis only three typical installation defects are investigated. Further study and investigation on different typical installation defects is necessary to provide information and knowledge about their characteristics. One most critical defect which is important for the investigation is the protrusion on the semi-conductive screen as described in section 3.2.1. This artificial defect can be constructed by making a small scratch on cable insulation and then covering the scratch by using semi-conductive paint. Another case is conductive particles on the surface of cable insulation inside the joint as described in section 3.2.4 that can results in surface discharge on the interface between cable and joint insulation.

2. The un-conventional PD detection method can be used to detect the presence of PD from the defect in the cable. However, this method is very sensitive to particular ground wire configurations and the sensor positions. The effects of these aspects in triggering part of un-conventional system which is important for picking up the applied voltage are important to be investigated.

References

[1] E. Peschke, R. Von Olshausen, *Cable Systems for High and Extra-High Voltage,* Publicis MCD Verlag, Erlangen and Munich, 1999, ISBN 3-89578-118-5.

[2] Edward Gulski, Piotr Cichecki, Frank Wester, Johan J. Smit, Riccardo Bodega, Theo J.W.H. Hermans, Paul P. Seitz, Ben Quak, Frank de Vries, *On-site Testing and PD Diagnosis of High Voltage Power Cables*, Electrical Insulation 2008**,** ISEI 2008**.**

[3] F.H. Krueger, *Industrial High Voltage Part I, Fields, dielectrics and constructions*, Delft University Press, 1991.

[4] H. M. Ryan, *High Voltage Engineering and Testing*, 2nd edition, The Institution of Electrical Engineer, 2001, ISBN 0-85296-775-6.

[5] William A. Thue, *Electrical Power Cable Engineering*, Marcel Dekker, Inc, 1999, ISBN 0-8247-9976-3.

[6] Aucourt, Boone, Kalkner, *Recommendations for a New After Laying Test Method for High Voltage Extruded Cable Systems*, Cigré paper 21-105, August 1990, Paris.

[7] *Recommendations for Electrical Tests (type, special and routine) on Extruded Cables and Accessories at Voltage > 150 (170) kV and < 500 (525) kV*, CIGRE, Elektra 151, December 1993.

[8] Th. Heimann, Th. Aschwanden, H. Hahn, M. Laurent, L. Ritter, *On-Site Partial Discharge Measurements on Premoulded Cross-Bonding Joints of 170 kV XLPE and EPR Cables*, IEEE Transactions on Power Delivery, Vol. 13, No. 2, April 1998.

[9] F.H.Kreuger, *Partial Discharge Detection in High-Voltage Equipment,* Butterworths & co Ltd, London, United Kingdom, 1989.

[10] Edward Gulski, *Computer-Aided Recognition of Partial Discharges Using Statistical Tools,* Ph.D Thesis, Delft University Press, The Netherlands, 1991.

[11] Nezar Ahmed, Nagu Srivinas, *Partial Discharge Severity Assessment in Cable System*, IEEE 2001.

[12] F.H.Kreuger, *Industrial High Voltage 4, 5 ,6,* Delft University Press, Delft, The

Netherlands, 1991.

[13] Steven Boggs, John Densley, *Fundamentals of Partial Discharge in the Context of Field Cable Testing*, IEEE Electrical Insulation Magazine, Vol.16, No.5, Sept/Oct, 2000.

[14] Frank J. Wester, *Condition Assessment of Power Cable using Partial Discharge Diagnosis at Damped AC Voltages*, Ph.D. dissertation, Delft Univ. Tech., Delft, The Netherlands, 2004.

[15] Junhua Luo, Jikang Shi, Jian Yuan, *Study on Surface Discharge on Composite Dielectric in XLPE Power Cable Joint*, Electrical Insulation Conference and Electrical Manufacturing & Coil Winding Conference, 2001.

[16] F. Farneti, F. Ombello, E. Bertani, and W. Mosca, *Generation of Oscillating Waves for After-Laying Test of HV Extruded Cable Links*, CIGRE Session Paris, 1990, paper 21-10.

[17] P. Schikarski, M. Gamlin, J. Rickmann, P. Peeters, P. v.d. Nieuwendijk, R. Koning, *Two Years of Experience with a Mobile Resonant Test System for Testing of Installed Medium and High Voltage Power Cables.*

[18] Riccardo Bodega, Peter H. F. Morshuis, Massimo Lazzaroni, and Frank J. Wester, *PD Recurrence in Cavities at Different Energizing Methods*, IEEE Transactions on Instrumentation and Measurement, Vol. 53, No. 2, April 2004.

[19] IEC Publication 60270, *Partial Discharge Measurements*, 3rd Edition, 2000.

[20] *Guide for Electrical PD Measurement in Compliance to IEC 60270*, CIGRE Technical Brochure.

[21] E. Gulski, S. Meijer, P.Cichecki, J.J. Smit, P.P. Seitz, F. Petzold, F. de Vries, *Insulation Diagnosis of High Voltage Power Cables*, 2007 International Conference on Solid Dielectrics, Winchester, UK, July 8-13, 2007.

[22] E. Gulski, F.J. Wester, J.J. Smit, P.N. Seitz and M. Turner, *Advanced PD Diagnosis of MV Power Cables using Oscillating Wave Test System*, IEEE Electr. Insul. Magazine, Vol. 16, No. 2, pp. 17_25, 2000.

[23] Ruben C. Laddé, *Partial Discharge Diagnosis of High-Voltage Power Cable Accessories,* MSc Thesis, January 2007, Delft.

[24] S. Meijer, R.A. Jongen, J.J. Smit, P.P. Seitz, T.J.W.H. Hermans, L. Lamballais, *On-site VHF Partial Discharge Detection on Power Cable Accessories*, Proceedings Jicable 2007.

[25] S. Meijer, R. C. Laddé, R.A. Jongen, J.J. Smit, T.J.W.H. Hermans, L. Lamballais, *Sensitivity Verification Procedure of VHF PD Detection Systems*, Proceedings Jicable 2007.

[26] P. H. F. Morshuis, F. H. Krueger, *The Evolution of Discharge Mechanism in a Dielectric Bounded Cavity due to the Surface Effect*, Proceedings of the 3rd International Conference on Properties and Applications of Dielectric Materials, July 8-12, 1991 Tokyo, Japan.

[27] T. Tanaka, *Internal Partial Discharge and Material Degradation*, IEEE Transactions on Dielectrics and Electrical Insulation EI-21, No. 6, 1986, p.899-905.

[28] Lutz Niemeyer, *A Generalized Approach to Partial Discharge Modeling*, IEEE Transactions on Dielectrics and Electrical Insulation Vol. 2 No. 4, August 1995.

List of Abbreviations

2 D	Two Dimensional
AC	Alternating Current
CF	Centre Frequency
CIGRE	Conseil International des Grands Réseaux Électriques
DAC	Damped Alternating Current
DC	Direct Current
EPR	Ethylene Propylene Rubber
FEA	Finite Element Analysis
HV	High Voltage
IEC	International Electro-technical Commission
IEEE	Institute of Electrical and Electronics Engineers
HDPE	High-Density Polyethylene
HF	High Frequency
OWTS	Oscillating Wave Test System
PD	Partial Discharge
PDIV	Partial discharge inception voltage
PE	Polyethylene
S1	Sensor at Termination 1
S2	Sensor at Termination 2
S3	Sensor at Termination Joint
UHF	Ultra High Frequency
VHF	Very High Frequency
VLF	Very Low Frequency
WG	Working Group
XLPE	Cross-Linked Polyethylene

List of Symbols

C	Capacitance
C_a	Capacitance of test object
C_k	Coupling capacitance
$E(x)$	Electric field strength at radius x

f_1	Lower limit of frequency
f_2	Upper limit of frequency
f_{res}	Resonant frequency
i_C	Current wave of cable
I_{load}	Maximum load current of DC supply
L	Inductance
M_i	Measuring instrument
q	Discharge magnitude
R	External radius of insulation
r	Internal radius of insulation
t_{ch}	Charging time
t_i	Time instant of PD occurrence
u_i	Test voltage at t_i
U	Operating Voltage
U_m	The maximum allowed line-to-line voltage
U_0	The rated voltage between line and earth
v_a	Voltage over the insulation system
v_c	Voltage over the defect
Z_n	Noise blocking impedance
Z_m	Measuring impedance
ΔV	Voltage drop as a result of a discharge
ε	Permittivity of insulation material
ψ_i	phase angle at t_i

List of Units

C	Coulomb
F	Farad
H	Henry
Hz	Hertz
m	Meter
s	Second
V	Volt